AD NUMBER

AD888489

NEW LIMITATION CHANGE

TO

Approved for public release, distribution unlimited

FROM

Distribution authorized to U.S. Gov't. agencies only; Administrative/Operational Use; SEP 1971. Other requests shall be referred to Naval Air Systems Command, Washington, DC.

AUTHORITY

USNASC ltr, 27 Oct 1976

GENERAL DYNAMICS
Electro Dynamic Division

AD 888 489

STRUCTURAL DYNAMIC PROPERTIES OF
TACTICAL MISSILE JOINTS - PHASE 2

Final Report

(June 1970 to August 1971)

September 1971

CR-6-348-945-002

By

J. G. Maloney
M. T. Shelton

Prepared Under Contract N00019-70-C-0296

for the

Naval Air Systems Command

by

Electro Dynamic Division

Pomona Operation of the General Dynamics, Inc.

FOREWORD

This study has been conducted by the Pomona Operation of General Dynamics Corporation for the Naval Air Systems Command under Contract N00019-70-C-0296.

The principal investigator for the study has been Mr. John G. Maloney. The experimental work and much of the analytical work was performed by Mr. Michael T. Shelton. Dr. George Lasker and Mr. Richard F. Sholtis served as staff consultants providing guidance for the finite element analysis. Mr. David O. Rife provided assistance in developing the joint compliance extraction technique. The direct technical supervisor has been Mr. David A. Underhill, Structural Dynamics Section Head.

Mr. George P. Maggos has been the Naval Air Systems Command technical monitor.

The joint compliance extraction technique discussed in Section 3, which was developed in the Phase 1 study, has been restructured in Phase 2 to take advantage of the more general approach developed by Messrs. Bert M. Hall and E. D. Calkin and Dr. M. S. Sholar (Reference 3). The authors wish to acknowledge the contributions of Hall, Calkin and Sholar to the Phase 2 study.

Acknowledgement is made to Messrs. W. J. Werback, E. L. Jeter and J. W. Onstott of the Naval Weapons Center, China Lake for providing part of the experimental data used in Section 4 of the study.

TABLE OF CONTENTS

LIST OF FIGURES

LIST OF FIGURES - Cont'd.

LIST OF FIGURES - Cont'd.

LIST OF TABLES

Section 1.0

SUMMARY

The work performed and the results accomplished during the second phase of a study of the structural dynamic properties of tactical missile joints are presented in this report. The joint compliance extraction technique evaluated in the Phase 1 study was extended, and the major restrictions were overcome during the Phase 2 effort. A vibration test program was performed to determine structural dynamic characteristics of several actual tactical missile joints, with the unknowns in the test being minimized to improve the quality of the data obtained. The joint compliance extraction technique was then used to obtain joint compliance information from the measured modal data. Also an investigation was performed which demonstrates the possibility of predicting mechanical joint properties using finite element methods. In addition, the finite element analysis also demonstrated analytically that the number of load paths and their spacing around the circumference of a joint are major factors in determining joint compliance. The proposed Phase 3 objectives are listed in the conclusions section along with the major conclusions of the Phase 2 study.

1

Section 2.0

INTRODUCTION

The study described in this report represents the second phase in a basic investigation of the structural dynamic properties of tactical missile joints being undertaken for the Naval Air Systems Command by the Pomona Operation of General Dynamics.

The Phase 1 study, Reference 7, included the preliminary evaluation of a method of extracting joint compliances from measured missile modal response data. The method is further developed in Section 3 of this study to the point that all of the significant restrictions and limitations of the original method have now been removed.

A test method for isolating the structural dynamic characteristics of joints using full scale actual missile joint hardware is developed in Section 4. The effective flexural and shear compliances of several different joints are derived from the test data collected in the experimental portion of the study using the joint compliance extraction technique of Section 3.

Finite element analyses of three configurations of one of the joints tested are presented in Section 5. A correlation analysis between the measured and predicted flexural joint compliances is accomplished using a two step finite element analysis. The test specimen is modeled first using solid elements of revolution and the deflections due to axial loading are computed. Then a conical shell element model is developed which matches the axial deflections of the solid element model. The conical shell element model is then used to compute the deflections due to a moment loading and the effective flexural compliances of the joints are determined.

Section 6 presents a status review of the Phase 2 effort and outlines the scope of the study planned for Phase 3.

Section 3.0

JOINT COMPLIANCE EXTRACTION TECHNIQUE DEVELOPMENT

A joint compliance extraction technique was developed during Phase 1 of the study of structural dynamic properties of tactical missile joints (Reference 7). It utilized a steepest-descent method to solve for variable unknown spring rates based upon a weighted best fit match between experimental and theoretical mode shapes and natural frequencies. The method was tailored specifically to beam representations of missile structures. Unfortunately, the method as implemented had several limitations. One of the restrictions was that the number of modes used had to equal or exceed the number of unknown joints to obtain meaningful results. Also, only bending cases with free-free boundary conditions could be run, and no method of handling appendages had been devised.

Late in the Phase 1 study, a general method for estimating structural parameters from dynamic test data appeared in Reference 3 which looked promising for use in the extraction of missile airframe joint compliances. Subsequently this method was applied in Phase 2 to simple test cases with encouraging results. As confidence was gained in the optimization method, the method was programmed for use with a Control Data Corporation 6400 computer. Originally only first order gradient terms were used. The first order gradient method worked well with a small (two degree of freedom) system, but was inadequate for larger systems. Next a second order gradient method in which the second order terms were approximated by differences was tried. This method as implemented would work for certain initial conditions, but not for all initial conditions. Therefore, techniques were developed to improve convergence of the method. The resulting computer program is called program JOINTS.

Section 3.1 presents the theory that program JO..TS is based upon, and section 3.2 presents the test cases used in the development of JOINTS. Program JOINTS has been employed to obtain airframe joint compliances from experimental data. These results are included in Section 4.

3.1 METHOD OF ANALYSIS

The joint compliance extraction technique optimizes a linear lumped parameter mathematical model of an elastic missile structure by determining the joint compliances of the model which can not be directly measured from dynamic test data. It is, therefore, a tool which optimizes a semi-empirical model by essentially a least square fit to the experimental data. The dynamic test data to be used consists of a few of the lowest mode frequencies and shapes. Therefore, the joint compliances yielding the best fit are found by minimizing a quadratic function of the differences between corresponding theoretical and experimental eigenvalues and

3

eigenvectors. The function which is the sum of weighted squares of the differences is referred to as the cost function:

$$F = \frac{1}{2} \sum_{i=1}^{N_i} \left\{ W_{if} \left(\omega_{ie}^2 - \omega_{it}^2 \right)^2 + \left(\underline{X}_{ie} - \underline{X}_{it} \right)^T W_{ix} \left(\underline{X}_{ie} - \underline{X}_{it} \right) \right\} \quad (1)$$

The frequencies and mode shapes are denoted by ω and $\underline{X}$, respectively. The weighting factor matrix is W and the index i is the mode number. If the mode shape slopes are used, they are treated as additional components of the $\underline{X}$'s. The subscripts e and t denote experimental and theoretical values, respectively. The minimization of the cost function constitutes a nonlinear programming problem which is the subject of this section. Optimization problems not amenable to standard methods are more the rule than the exception. In this case the optimization is accomplished by a steepest descent method especially developed for this study. The basic concept originally appeared in Reference 3. Before proceeding with a detailed discussion of the method, the structural mathematical model utilized will be described. The third section will deal with the proper selection of the weighting factors.

    3.1.1 **System Model.** The fundamental structural dynamic considerations of a tactical missile are often handled with a linear lumped parameter mathematical model. The one used in this study is typical. More expressly, the mathematical model simulates a beam-like body with a series of lumped masses connected by weightless beams. Discrete shear, compressive, torsional, and flexural springs may be included at any point in the model. The model can be used to analyze bending, torsion, and longitudinal motion. The model contains provisions for including appendages attached to the main body at arbitrary angles with arbitrary attachment springs. The appendages are modeled similarly to the main body. The boundary value problem that results from this representation can be expressed as an eigenvalue problem:

$$\left[K - \omega_{it}^2 M \right] \underline{X}_{it} = 0 \qquad i = 1, 2, \cdots N \qquad (2)$$

where M and K are mass and stiffness matrices, respectively. The subroutine within the computer program which solves the eigenvalue problem uses the Holzer-Myklestad method. This numerical method utilizes transfer matrices from point to point on the model and finds the eigenvalues by satisfying the boundary conditions using an iterative procedure. A complete description of the method is found in Reference 9. Limitations of the method and of economy preclude extraction of all N modes where N is typically 50 to 200. It will be seen later that the lack of a complete set of modes introduces approximations into the steepest descent algorithm and necessitates modifications.

3.1.2 <u>Optimization Method</u>. The optimum values of the joint com-
pliances, defined in a least square error sense, are determined by mini-
mizing the cost function which is accomplished with a modified steepest
descent method. Figure 3-1 shows a simplified flow diagram of the
computer program, JOINTS, which has been developed from this method.
Steepest descent or gradient methods as they are also known, iteratively
converge on the location of the minimum, since an analytical solution
of the condition for an extremum, $\nabla F = 0$, is not possible. The
successive estimates of the minimizing values of the independent variables,
in this case a vector the components of which are the unknown spring
rates of the structural joints $\underline{k}$, are

$$\underline{k}^{(n+1)} = \underline{k}^{(n)} - \Theta \nabla F \Big|_{\underline{k}^{(n)}} \tag{3}$$

The superscript indicates the number of the estimate. If the quantity
Θ is a constant, the algorithm is a first order method commonly referred
to as the steepest descent method. It is based on the intuitive notion
that if one proceeds in the direction of steepest descent, which Equation
(3) does, in small steps one must arrive at a local minimum. It can also
be proven rigorously (Reference 4). A very efficient second order method
may be derived by applying the Newton-Raphson algorithm to the gradient
of the cost function which yields the successive approximation,

$$\underline{k}^{(n+1)} = \underline{k}^{(n)} - S \left[\frac{\partial^2 F}{\partial k_i \partial k_j} \right]^{-1} \nabla F \Big|_{\underline{k}^{(n)}} \tag{4}$$

The matrix of second partial derivatives must be non-singular. Theoreti-
cally, the step size, S, is a scalar. However, in this study, it was
necessary to generalize its definition. Equation (4) serves as the basis
for the algorithm developed. The reasons for the modifications that were
necessary will be explained as they are encountered.

The jth component of the gradient of the cost function is

$$\frac{\partial F}{\partial k_j} = \sum_{i=1}^{N_I} \left\{ W_{if} \left(\omega_{it}^2 - \omega_{ie}^2 \right) \frac{\partial \omega_{it}^2}{\partial k_j} + \left(\underline{X}_{it} - \underline{X}_{ie} \right)^T W_{ix} \frac{\partial \underline{X}_{it}}{\partial k_j} \right\} \tag{5}$$

where k_j is the <u>jth</u> unknown spring rate. In order to calculate the
partial derivatives of the eigenvalues and mode displacement with respect
to the k_j's, a departure was made from Reference 3. Here the modes were
normalized to unity with respect to the generalized mass M,

$$\underline{X}_{it}^T M \underline{X}_{jt} = \delta_{ij} \tag{6}$$

5

Also a joint compliance positioning matrix, K^j, is introduced which locates the unknown spring rates within the full spring matrix -

$$K = \overline{K} + \sum_{j=1}^{N_S} K^j k_j \tag{7}$$

$\overline{K}$ is the matrix of known spring elements. Because of the peculiarities of the method used to solve the eigenvalue problem, the spring matrix, K, is not directly available and so neither are the variable spring positioning matrices, the K^j's. However, they can be derived by considering the strain energy stored in the $\underline{jth}$ spring. For simplicity, assume that a separate spring rate is assigned to each joint. Then the strain energy associated with the $\underline{jth}$ spring is:

$$U_j = \frac{1}{2} k_j \left({}'x_j - x_j' \right)^2 \tag{8}$$

where ${}'x_j$ and x_j' are the slopes to the left and to the right of the joint for the case of a rotational spring. The strain energy is also $U_j = 1/2 k_j {}_x'^T K j_x'$. Equating the two expressions and then the coefficients of like terms, it can be deduced that the matrix, K^j, must be the null matrix except for a submatrix,

$$\begin{pmatrix} 1 & -1 \\ -1 & 1 \end{pmatrix} \tag{9}$$

corresponding to the coordinates on either side of the joint. Then according to Reference 2 the partial derivatives are

$$\frac{\partial \omega_{it}^2}{\partial K_j} = \underline{X}_{it}^T K^j \underline{X}_{it} \tag{10a}$$

$$\frac{\partial \underline{X}_{it}}{\partial K_j} = \sum_{\ell \neq i}^{N} \frac{\underline{X}_{\ell t}^T K^j \underline{X}_{it}}{\omega_{it}^2 - \omega_{\ell t}^2} \underline{X}_{\ell t} \tag{10b}$$

6

Equations (10a) and (10b) can be expanded in terms of components of the normal coordinates by utilizing the strain energy relationship for each joint.

$$\frac{\partial \omega_{it}^2}{\partial K_j} = X_{it,mj}\left(X_{it,mj} - X_{it,mj+1}\right) + X_{it,mj+1}\left(-X_{it,mj} + X_{it,mj+1}\right)$$

$$= \left(X_{it,mj} - X_{it,mj+1}\right)^2 \tag{11a}$$

$$\frac{\partial \underline{X}_{it}}{\partial K_j} = \sum_{\substack{\ell=1 \\ \ell \neq i}}^{N} \left(\omega_{it}^2 - \omega_{\ell t}^2\right)^{-1}\left\{X_{\ell t,mj}\left(X_{it,mj} - X_{it,mj+1}\right)\right.$$

$$\left. + X_{\ell t,mj+1}\left(-X_{it,mj} + X_{it,mj+1}\right)\right\}\underline{X}_{\ell t} \tag{11b}$$

where the indices mj and $mj+1$ refer to the components of the normal coordinates to the left and right of the jth joint respectively. The partial derivatives of the mode shapes were derived using the second formulation of Reference 2 which requires a complete set of theoretical modes. As pointed out previously the sum has to be truncated for reasons of accuracy and economy. This is usually the case in dynamic problems. Here the justification is a posteriori. The number of theoretical modes used in the computation of their derivatives is always the same as the number of experimental modes available.

$$\frac{\partial \underline{X}_{it}}{\partial K_j} \cong \sum_{\substack{\ell=1 \\ \ell \neq i}}^{N_i} \frac{\underline{X}_{\ell t}^T K^j \underline{X}_{it}}{\omega_{it}^2 - \omega_{\ell t}^2}\underline{X}_{\ell t} \tag{12}$$

The second partial derivative of the cost function with respect to the unknown spring rates, k_q and k_j, is

$$\frac{\partial^2 F}{\partial K_q \partial K_j} = \sum_{i=1}^{N_i}\left\{W_{if}\left[\frac{\partial \omega_{it}^2}{\partial K_q}\frac{\partial \omega_{it}^2}{\partial K_j} + \left(\omega_{it}^2 - \omega_{ie}^2\right)\frac{\partial^2 \omega_{it}^2}{\partial K_q \partial K_j}\right]\right.$$

$$\left. + \frac{\partial \underline{X}_{it}^T}{\partial K_q} W_{ix} \frac{\partial \underline{X}_{it}}{\partial K_j} + \left(\underline{X}_{it} - \underline{X}_{ie}\right)^T W_{ix} \frac{\partial^2 \underline{X}_{it}}{\partial K_q \partial K_j}\right\} \tag{13}$$

7

The second partials of the eigenvalues and mode shapes are

$$\frac{\partial^2 \omega_{it}^2}{\partial K_q \partial K_j} = \frac{\partial X_{it}^T}{\partial K_q} K^j \underline{X}_{it} + X_{it}^T K^j \frac{\partial \underline{X}_{it}}{\partial K_q} \tag{14a}$$

$$\frac{\partial^2 \underline{X}_{it}}{\partial K_q \partial K_j} \cong \sum_{\ell \neq i}^{N_i} (\omega_{it}^2 - \omega_{\ell t}^2)^{-1} \left\{ \left[-(\omega_{it}^2 - \omega_{\ell t}^2)^{-1} \left(\frac{\partial \omega_{it}^2}{\partial K_q} - \frac{\partial \omega_{\ell t}^2}{\partial K_q} \right) \underline{X}_{\ell t}^T K^j \underline{X}_{it} \right. \right.$$

$$\left. + \frac{\partial \underline{X}_{\ell t}^T}{\partial K_q} K^j \underline{X}_{it} + \underline{X}_{\ell t}^T K^j \frac{\partial \underline{X}_{it}}{\partial K_q} \right] \underline{X}_{\ell t}$$

$$+ \underline{X}_{\ell t}^T K^j \underline{X}_{it} \frac{\partial \underline{X}_{\ell t}}{\partial K_q} \right\} \tag{14b}$$

The maximum number of second partial derivatives of the eigenvalues that is desired to be considered is a few hundred. However, the maximum number of second partial derivatives of all the mode displacements that may have to be computed is of the order of ten thousand. This fact and the number of intermediate calculations for the evaluation of the analytical expressions for the second partials made computer memory and machine time requirements prohibitive for the intended use of the computer program.* Therefore, the second partials were computed approximately by taking differences of the first partials. Such a numerical process tends to be accuracy sensitive and demands careful monitoring. Without resorting to double precision arithmetic, the step size must be large enough to yield a sufficient number of significant figures. On the other hand, too large a step size may enclose a region too large for the cost function to be represented by a quadratic. The procedure settled upon was the following. Using the current estimate $\underline{k}^{(n)}$, the gradient of the cost function is computed with Equations (5), (11a) and (12). The current estimates of the unknown springs are successively incremented one at a time in the direction dictated by the corresponding component of the gradient:

$$K_j'^{(n)} = K_j^{(n)} \left[1 - r \cdot SGN\left(\frac{\partial F}{\partial K_j}\bigg|_{K^{(n)}} \right) \right] \tag{15}$$

*Late in the Phase 2 study it was realized that direct calculation of the second partials is very likely feasible since many of the terms are zero. Direct calculation of the second partials is potentially faster than approximating the second partials by taking differences.

The relative increment, r, is the same for all the unknown spring rates and fixed for a particular problem. The gradient is calculated at $\underline{k}'^{(n)}$ and the ratios of the differences of the respective components and the spring rate increments are computed. In order to improve the estimates of the second partial derivatives, corresponding off-diagonal estimates which theoretically should be equal are averaged as indicated below.

$$\frac{\partial^2 F^{(n)}}{\partial K_i \partial K_j} = \frac{\partial^2 F^{(n)}}{\partial K_j \partial K_i} \approx \frac{1}{2} \left\{ \left(K_i'^{(n)} - K_i^{(n)} \right)^{-1} \left[\frac{\partial F^{(n)}}{\partial K_j} \right]_{K_i}^{K_i'} \right.$$

$$\left. + \left(K_j'^{(n)} - K_j^{(n)} \right)^{-1} \left[\frac{\partial F^{(n)}}{\partial K_i} \right]_{K_j}^{K_j'} \right\} \qquad (16)$$

The Hessian, the matrix of second partial derivatives, is then inverted. The correction terms in Equation (4) are computed using a value of 1.0 for S. The sign and magnitude of each correction component are compared to those of the increment used to estimate the second partials. If the signs agree or if the magnitude is less than 2-1/2% of the current spring rate, the second order correction is utilized. If not, equation (15) is used. If the new spring rates, $\underline{k}^{(n+1)}$, result in an increase in the cost function, the correction terms to $\underline{k}^{(n)}$ are halved repeatedly until a decrease in the cost function is obtained. In any case, each variable spring rate is kept within prespecified limits. These procedures which taken together may be considered a complicated method of selecting a varying step size, S, evolved heuristicly. Modifications which can be made to improve them and put them on a more rigorous basis are possible.

3.1.3 <u>Selection of Weighting Coefficients</u>. Ideally the weighting coefficients in the cost function should reflect the relative accuracy of the experimental data and the relative importance of the information to be obtained from applications of the mathematical model. The values of the weighting coefficients relative to each other also can affect the rate of convergence. The first two requirements can be satisfied qualitatively by decreasing the coefficients with increasing mode number. Generally, the quality of the experimental data will deteriorate in progressively higher modes. Also the contribution of the higher modes to dynamic responses of the structure will be less significant. Therefore, in order to construct the weighting coefficients, each one was divided into two multiplicative factors. One factor, the relative weighting factor, is used in both the frequency and mode shape weighting coefficients to weight the importance of each mode with respect to all other modes. In cases run to date, the relative weighting factor has usually

been decreased by an order of magnitude for consecutively higher modes. The other multiplicative factor in the frequency weighting coefficients was made inversely proportional, to the fourth power of the experimental frequency. The corresponding factor in the mode shape weighting coefficients was made a constant, the reciprocal of the number of components in the mode shape. The mode shape weighting coefficients, which were originally defined to be full matrices, are now equal to a constant times the identity matrix. It might have been tempting to weight some mode components more than others, but such a procedure if not carefully used could distort the resulting mathematical model limiting its applications. In conclusion, the sets of weighting coefficients selected according to these guide lines resulted in error terms in the cost function of about the same order of magnitude. This was observed to enhance the rate of convergence.

3.2 TEST CASE RESULTS

The purpose of the analytical test cases was to exercise program JOINTS, to aid in its development, to uncover flaws and help debug the program, to point out areas where improvements might be implemented, and to prove the program functions as desired. The test cases were developed as required - beginning with a simple test case and progressing to more complicated systems.

Figure 3-2 shows a simple system composed of two masses with three compressive springs constraining their motion (Case 1). The test case was used to check out program JOINTS beginning with its earliest form (consisting solely of a first order gradient method). The program functioned very well for the simple case in which the unknown springs represented the total compliance of the system. Figures 3-3 and 3-4 show two examples of the use of Case 1. In Figure 3-3, all three spring rates were started low, and after eight iterations the program converged on the correct solution. Figure 3-4 shows an example in which the initial estimates for the three spring rates were selected high. For this situation, the correct solution was arrived at within fourteen iterations. Encouraged by these results, non-uniform beam systems were then investigated.

A non-uniform bending beam test case is shown in Figure 3-5 (Case 2). It consists of five beam sections connected by four flexural joints. The first order gradient method developed with the aid of Case 1 was insufficient to solve the more complex problem of Case 2. Because of the limitations uncovered by Case 2, a second order gradient method was incorporated into program JOINTS. Even with a second order gradient method, only limited success was achieved for Case 2. If the initial estimates for the joint compliances were close to the correct values, the second order gradient method would converge. However, if large initial deviations for the joint compliances were assumed, the program

10

diverged away from the correct solution. Therefore additional altera-
tions to the program were required to alleviate this problem. The
resultant method is that discussed in Section 3.1.

A change incorporated into program JOINTS based upon Case 2 was to
make use of a first order gradient method when far from convergence, and
to make use of a second order gradient method when near a cost function
minimum. Here, the phrase 'far from convergence' is defined as a region
which is determined by the directions indicated for changes in individual
spring rates from the first order and the second order gradient methods.
If the two methods indicate opposite directions should be taken for the
change in spring rate, the first order method is used. As the cost func-
tion minimum is approached, the first and second order methods agree in
sign for the change in spring rate and the magnitude determined from the
second order method is used. This choice of either the first or second
order method is considered independently for each spring. Figure 3-6
shows a comparison of using the first order and second order methods to
solve for the spring rates of Case 1. Here the initial step size for the
first order method is different than for the example shown in Figure 3-3.

Figures 3-7 thru 3-11 show the use of program JOINTS with Case 2.
Recall that Case 2 is a non-uniform bending beam with four flexural
joints. For the example shown in Figure 3-7, two of the four joint com-
pliances are assumed known correctly while two are considered unknown.
The compliances of joint numbers two and three are started high by a
factor of 2.0, and the correct joint compliances are converged upon in
five iterations (where the first iteration represents the initial
estimate input by the user). Only two bending modes are utilized in this
solution. It should be pointed out that the partial derivatives of the
eigenvectors with respect to the unknown spring rates (section 3.1, equa-
tion (10b)) are approximated by a single term in what should be a series
expansion when only two modes are used. Despite this possible problem
area, the results shown in Figure 3-7 look very good. It should also be
noted that the value of r (section 3.1, equation (15)) used in this case
was 25%, where r is the increment each spring is altered for the inter-
mediate steps in the computation of the second order gradients.

Figure 3-8 shows the same case as Figure 3-7 with the exception that
three flexural joint compliances are assumed unknown rather than two. In
this example, convergence is much slower than in the previous example
(approximately sixteen iterations). Again the value of r used is equal
to 25%. Other values of r have been considered with interesting
results, Figure 3-9 shows the same example as Figure 3-8 but the value
of r used is only 1%. Here convergence upon the three correct joint
flexural compliances is achieved in five iterations. In both of these
examples three unknown spring rates were solved for, using only two modes.
Figure 3-10 illustrates further the importance of the first order gradient
step size, r, in the convergence of the method. Values of r considered

11

range from 25% to 1%. Very little difference is seen between 1% and 5%, suggesting that both approximate the second order gradients well. For this case, it can be seen that 25% is too large a value of r for the problem with three unknown springs, even though it worked well for the problem with two unknown springs.

The choice of the step size, r, for the intermediate variation in spring rates can cause a problem unless care is taken in the selection of r. The step size must be large enough to prevent incurring computer accuracy problems, yet small enough to adequately estimate second order gradients of the cost function. Factors which enter into the correct choice of r are the joint stiffness ratio, k_r, and the joint location, X/L. In future program modifications, the effect of joint parameters given in Reference 7 should be made use of to guard against an improper choice of step size.

A further example of the use of program JOINTS with Case 2 is shown in Figure 3-11. This figure illustrates the convergence upon three unknown joint compliances using two modes when the initial estimates are low. Here two values of r were used. A value of r equal to 25% was used for the first four iterations, then an r equal to 1% was used for the last four iterations. The reason for the use of a larger value of r in the early iterations is because the initial estimates are "far from convergence". The correct joint compliances are obtained in six iterations.

With the program functioning well for Cases 1 and 2, Case 3 was developed to demonstrate the program's use for a system containing an appendage to the main beam. Case 3, shown in Figure 3-12, consists of a uniform bending beam with a simple appendage. The appendage is connected to the main beam by means of a flexural spring. On the main beam are two joints with flexural springs. Figure 3-13 shows an example of the use of program JOINTS with Case 3. For this example, three modes are utilized in the problem solution. Two of the three initial estimates for the joint flexural compliances are high by 33% and the other is 50% high. Here convergence to the correct answer is obtained in three iterations.

Again going to a more complicated system uncovered additional areas where improvements in program JOINTS could be implemented. For certain initial estimates of joint and appendage attachment compliances, the order of appearance of the appendage dominated modes will vary. Logic needs to be implemented at the present time to safeguard against these problems.

Program JOINTS has been used to analyze a considerable amount of data in Section 4.0. The weighting coefficients discussed in Section 3.1.3 were used in most but not all of these analyses. The weighting coefficients are input by the user and are really quite arbitrary. It is noted that for the 2.75 inch diameter ring joint, reducing the mode shape weighting factor for all modes yielded better results than the normal weighting factors.

3.3 DEVELOPMENT STATUS

The following areas of concern remain in the program at the present time. The eigenvalue problem solution utilized in program JOINTS is the predominant time consuming computational step when large systems are analyzed. An existing eigenvalue routine was used which is known to have certain inefficiencies. Improvements in this routine will significantly reduce the overall computer time used by program JOINTS. Also the eigen- value subroutine will under certain circumstances miss a mode in the frequency range of interest; this can cause many additional problems not discussed fully here. At the present time, mode weighting coefficients are used in the program, and are required to be input by the user. It would be advantageous to have the program generate these coefficients. It is believed that the rate of convergence can be further improved with a few easily implemented programming changes. Among these changes is the consideration of the magnitude of spring rate change relative to other quantities of concern - - the joint stiffness ratio and the joint location along the beam. Methods are also being considered to improve the run time by approximating intermediate changes in eigenvalues and eigenvectors, and hence the gradients themselves.

13

FIGURE 3-1

SIMPLIFIED FLOW DIAGRAM OF PROGRAM JOINTS

PROGRAM JOINTS

READ INPUT DATA

PRINT INPUT DATA

$n = ITERATION = 1$

NORMALIZE EXPERIMENTAL MODES

$k_j' = k_j \quad j = 1, 2, \cdots$ NO. OF SPRINGS

$j = 0$

COMPUTE SECOND ORDER TERMS FROM FINITE DIFFERENCES

COMPUTE INVERSE OF SECOND ORDER TERMS

COMPUTE NEW SPRING RATES FOR EACH UNKNOWN SPRING
$$\underline{k}^{(n+1)} = \underline{k}^{(n)} - S \left[\frac{\partial^2 F}{\partial k_\ell \partial k_m} \right]^{-1} \nabla F \big|_{k^{(n)}}$$

CHECK FOR CONVERGENCE

NO $\rightarrow$ $n = n + 1$

YES $\rightarrow$ STOP

COMPUTE MODES BASED UPON CURRENT k_j'

NORMALIZE THEORETICAL MODES

COMPUTE COST FUNCTION AND FIRST ORDER GRADIENTS

IS $j =$ NUMBER OF UNKNOWN SPRINGS ?

YES

NO $\rightarrow$ $j = j + 1$

$k_j' = (1 \pm r) k_j$
$k_i' = k_i \quad i \neq j$

14

FIGURE 3-2

CASE 1

TWO DEGREE OF FREEDOM SYSTEM

15
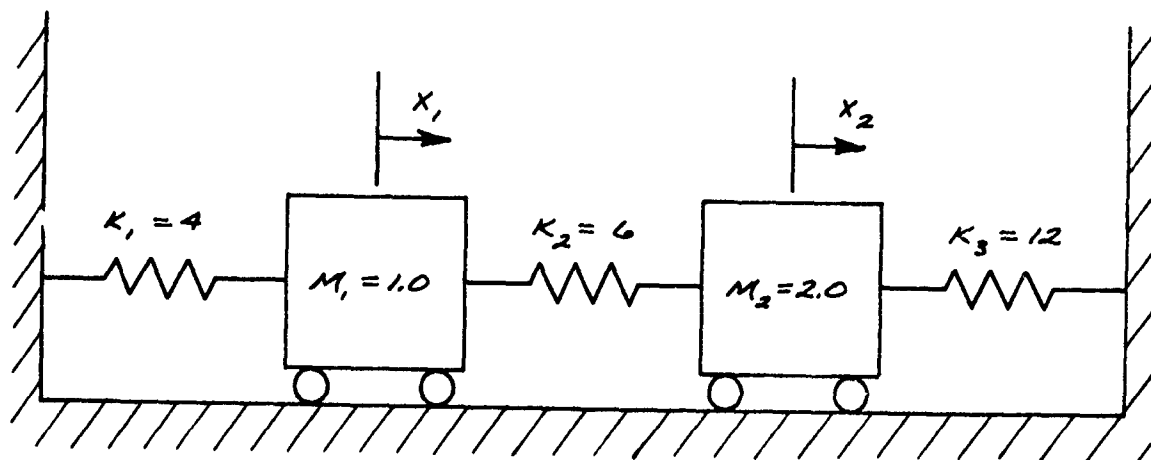
FIGURE 3-3

CASE 1

FIRST ORDER GRADIENT METHOD

INITIAL ESTIMATE OF SPRING RATES LOW
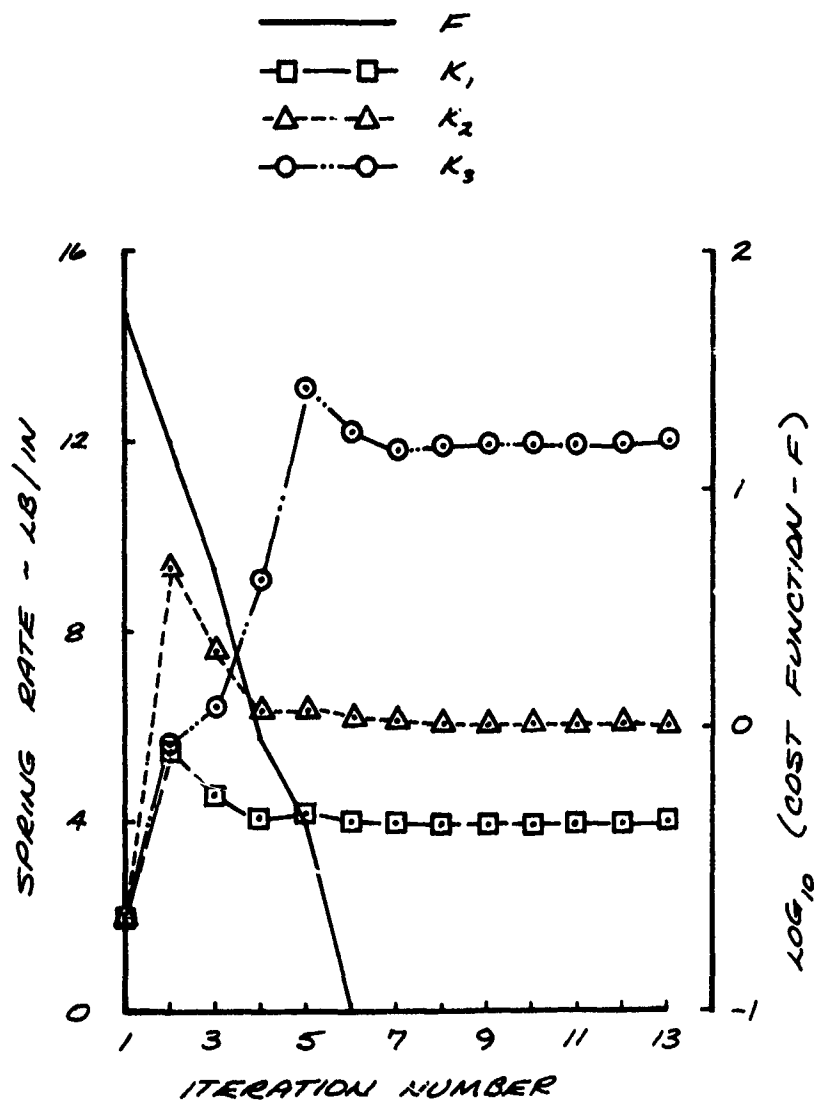
FIGURE 3-4

CASE 1

FIRST ORDER GRADIENT METHOD
INITIAL ESTIMATES OF SPRING RATES HIGH

——————— F

—□——□— K_1

-△---△- K_2

-○---○- K_3

17
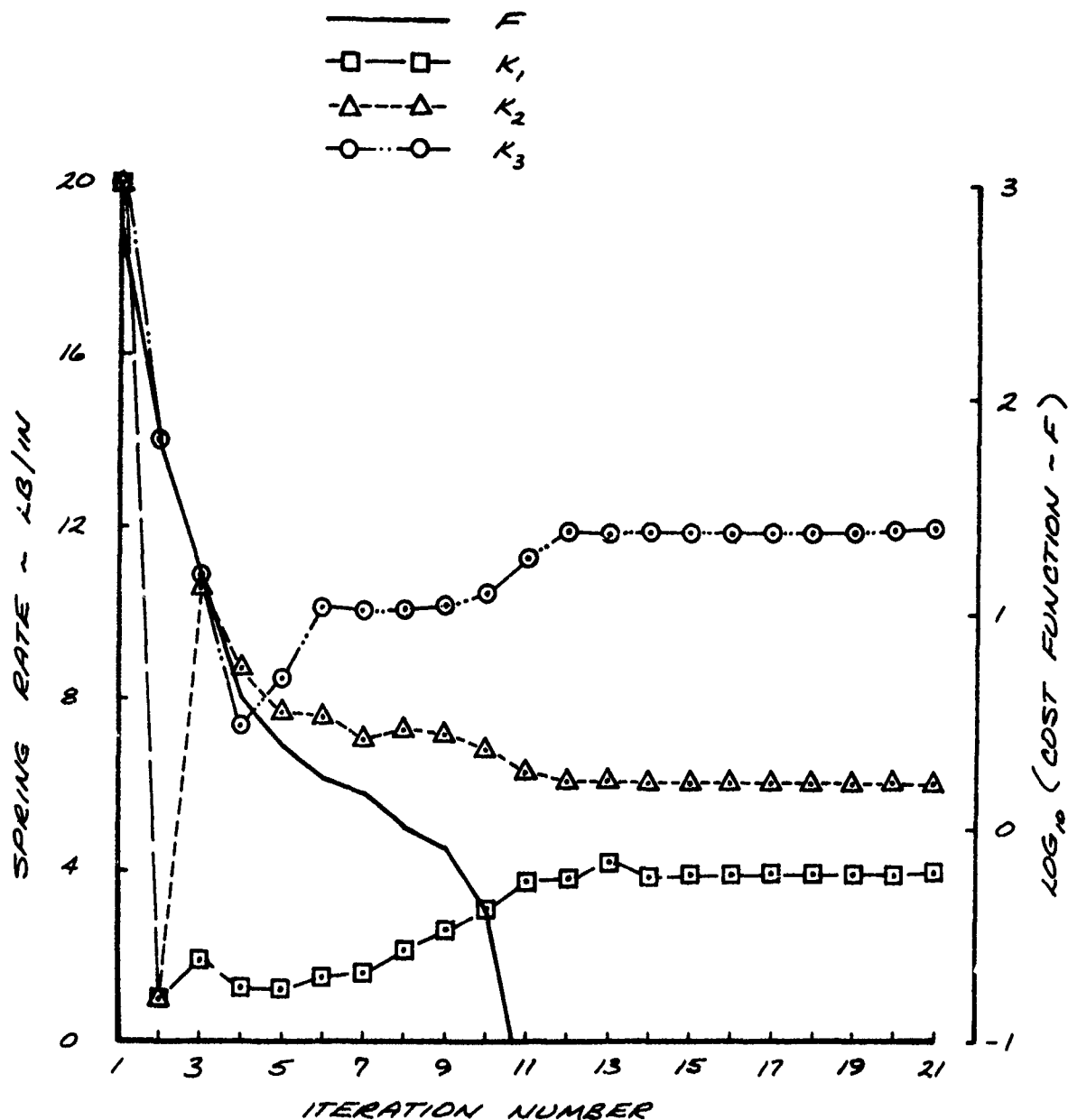
FIGURE 3-5

CASE 2

NON-UNIFORM BENDING BEAM PROPERTIES

BENDING STIFFNESS DISTRIBUTION

WEIGHT DISTRIBUTION
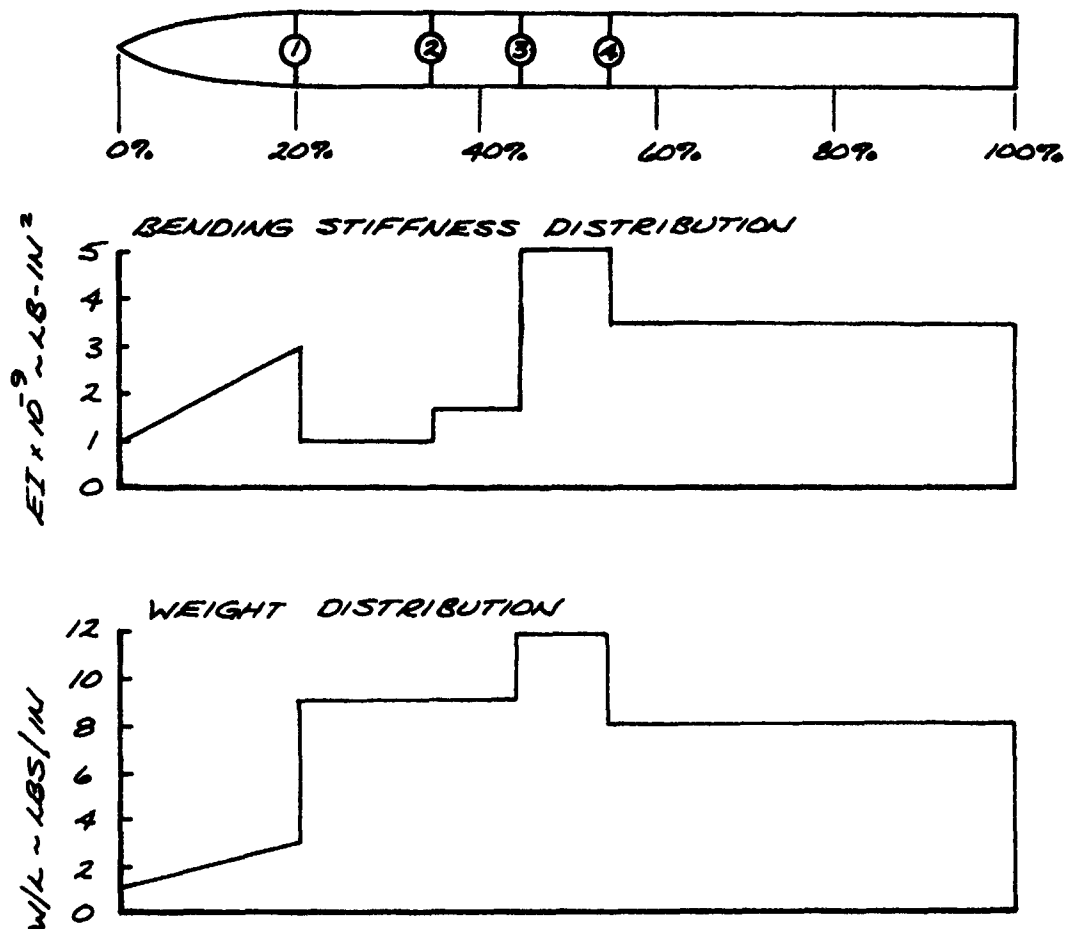
JOINT NO.	COMPLIANCE RAD/IN-LB	
1	.1	-7
2	.1	-7
3	.1	-7
4	.1	-7

18

FIGURE 3-6

CASE 1

CONVERGENCE COMPARISON

FIRST ORDER VS. SECOND ORDER GRADIENT METHODS
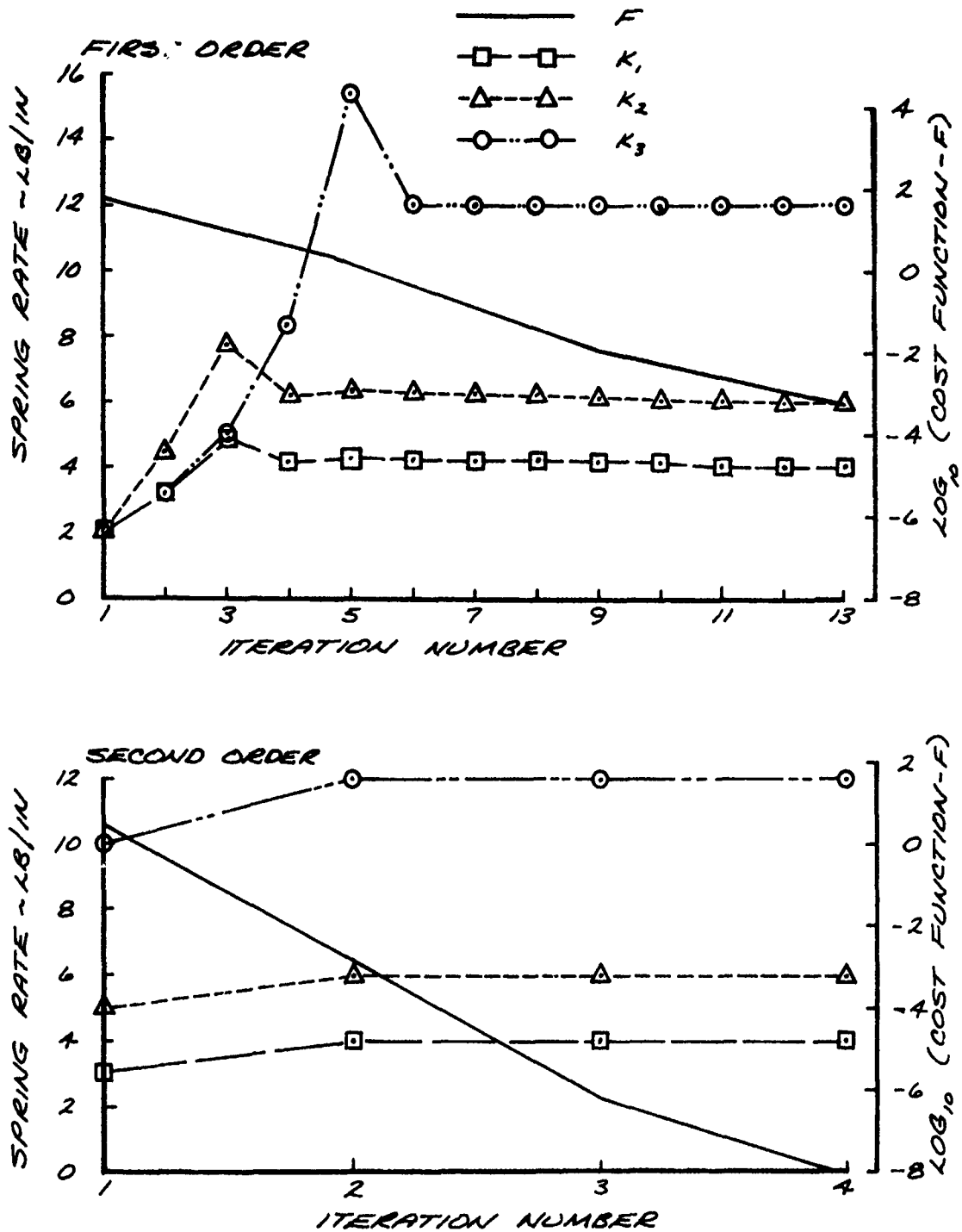
FIGURE 3-7

CASE 2

SOLUTION FOR TWO JOINT COMPLIANCES

USING TWO MODES

20
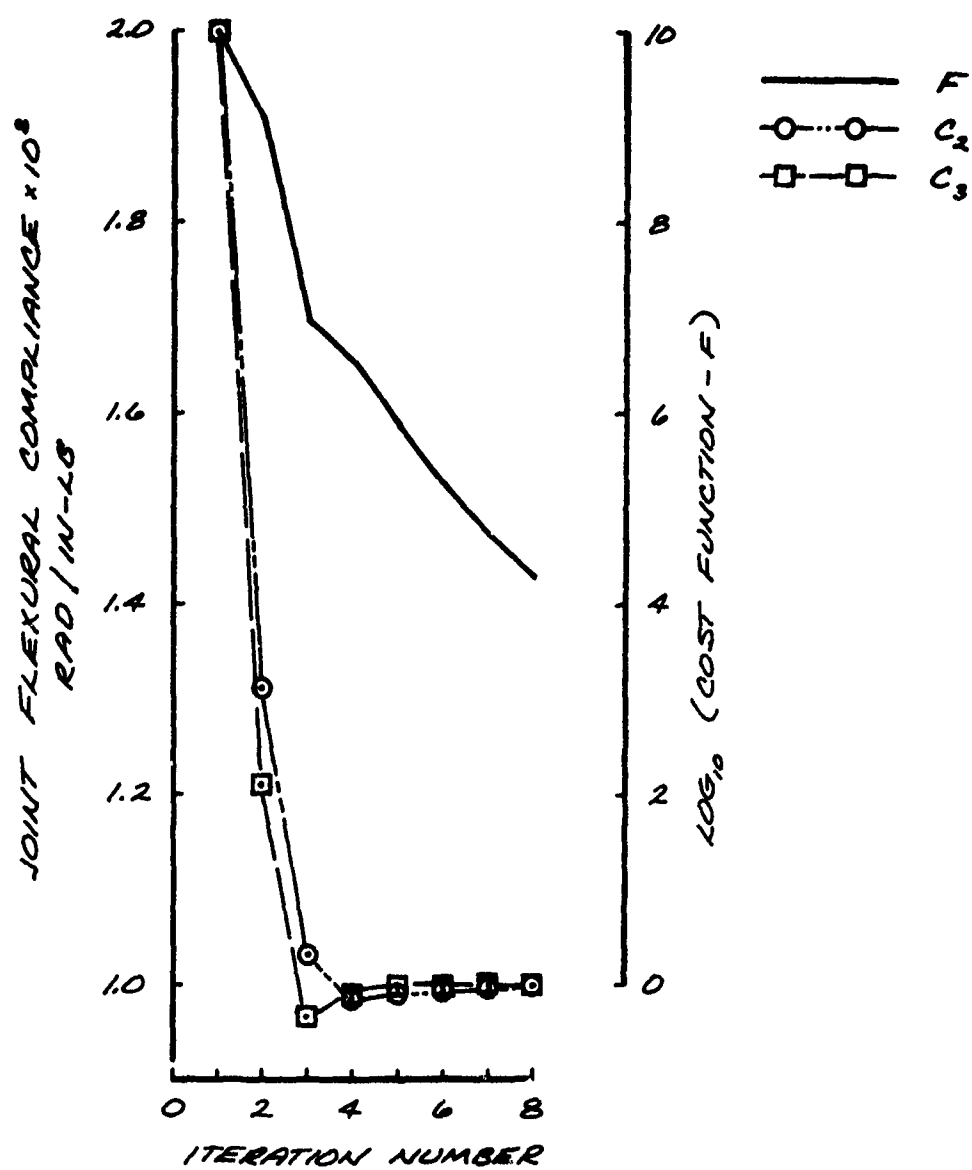
FIGURE 3-8

CASE 2

SOLUTION FOR THREE JOINT COMPLIANCES

USING TWO MODES

$\gamma = 25\%$

21
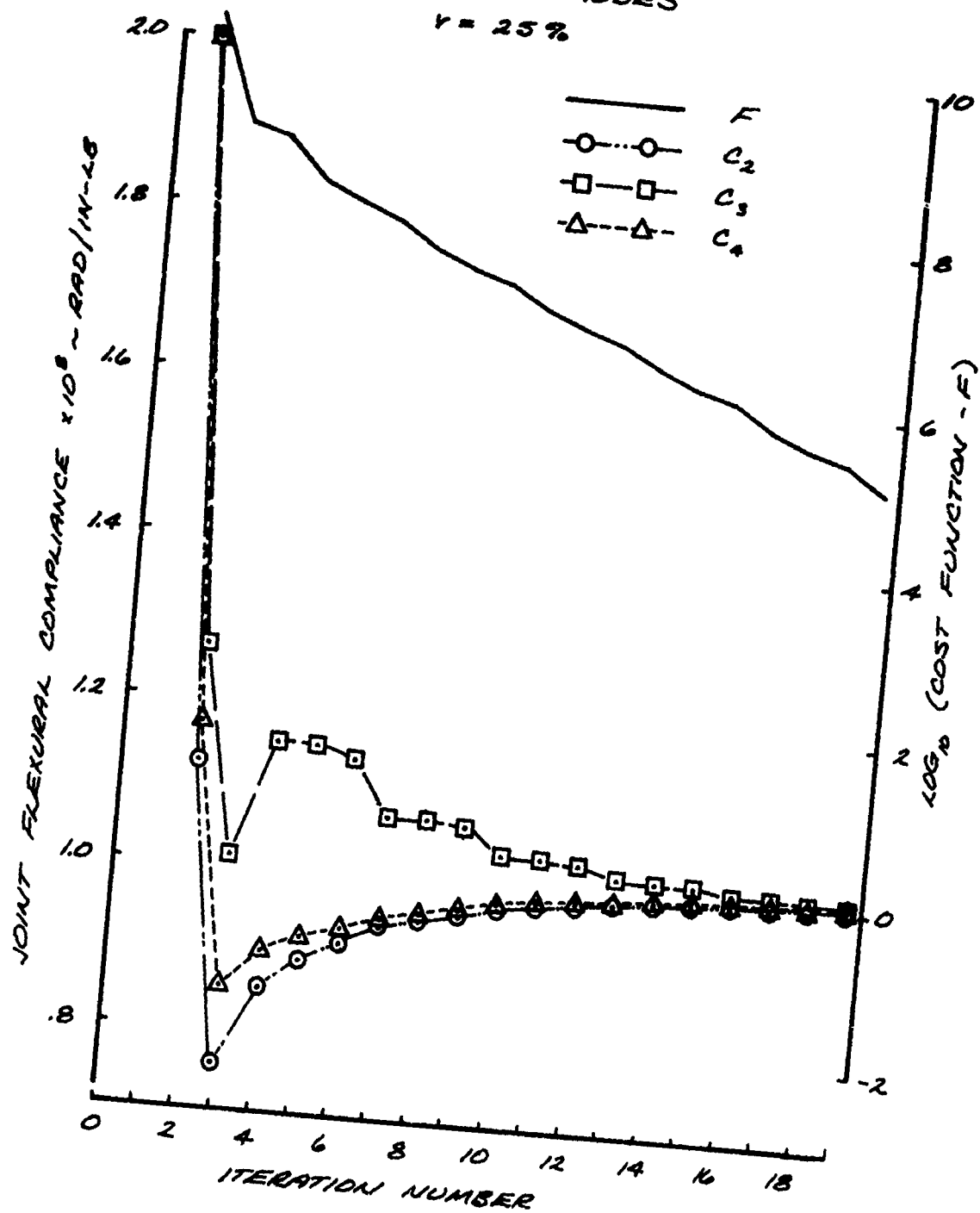
FIGURE 3-9

CASE 2

SOLUTION FOR THREE JOINT COMPLIANCES

USING TWO MODES

$r = 1\%$

22
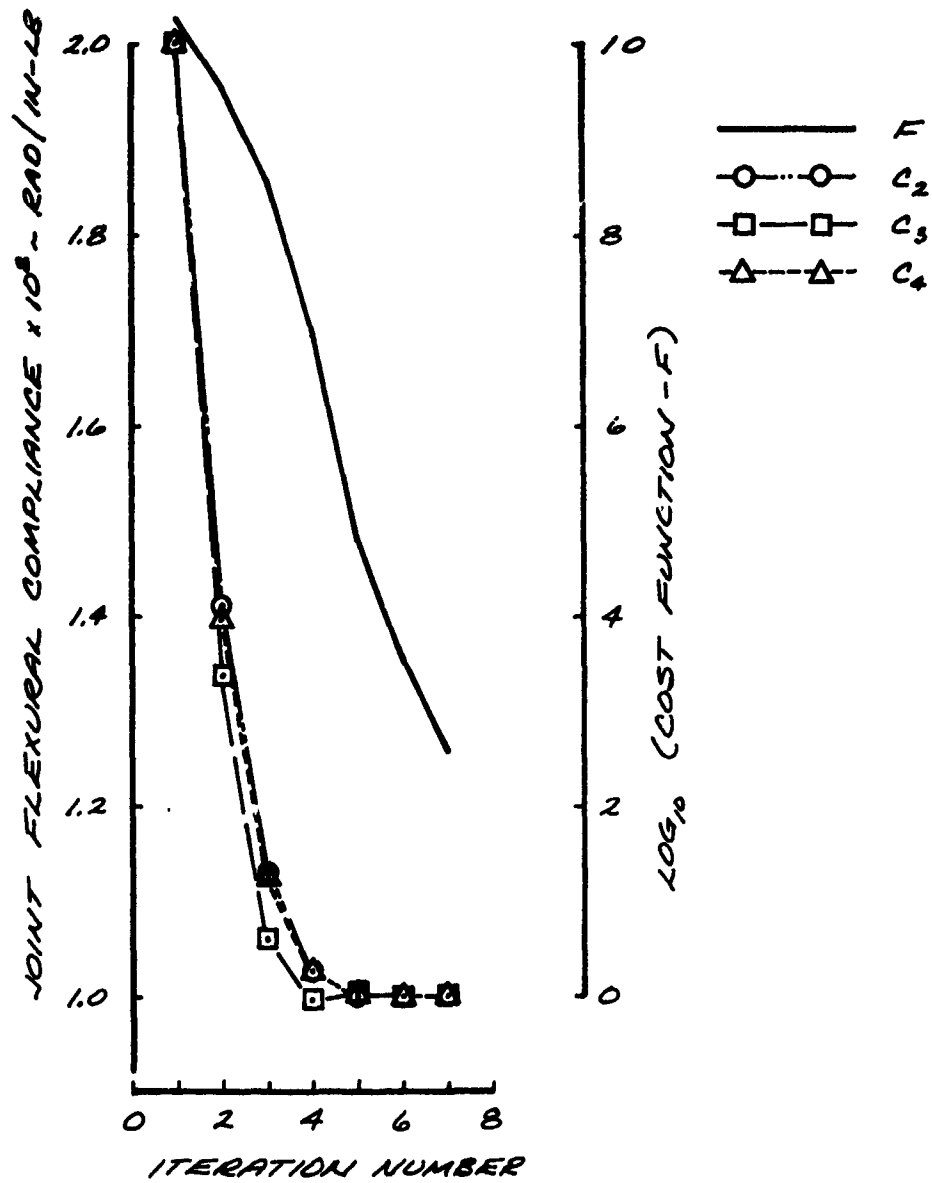
FIGURE 3-10

CASE 2

CONVERGENCE VS. INTERMEDIATE STEP SIZE-r

SOLVING FOR THREE JOINT COMPLIANCES

USING TWO MODES

23
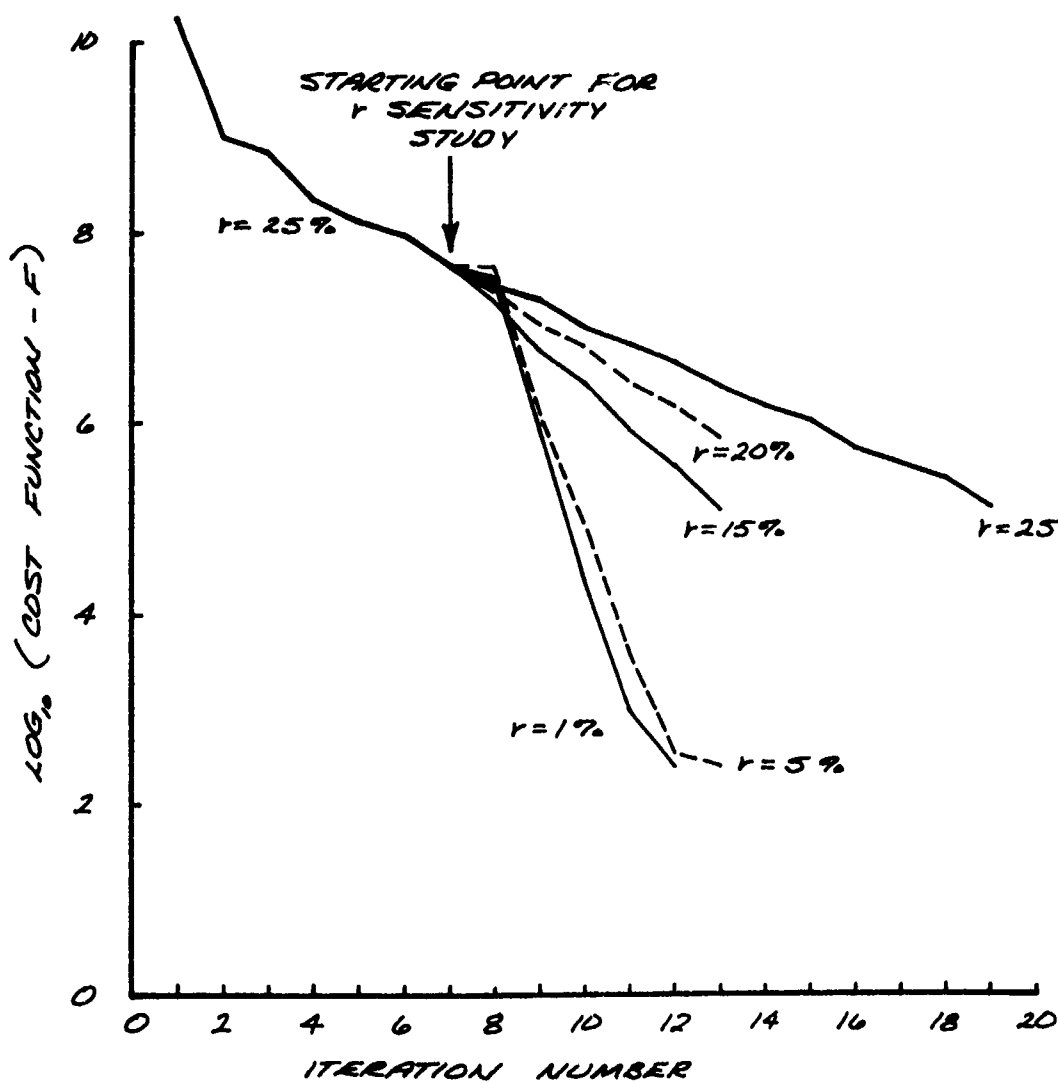
FIGURE 3-11

CASE 2

SOLUTION FOR THREE JOINT COMPLIANCES

USING TWO MODES

INITIAL ESTIMATES LOW

24
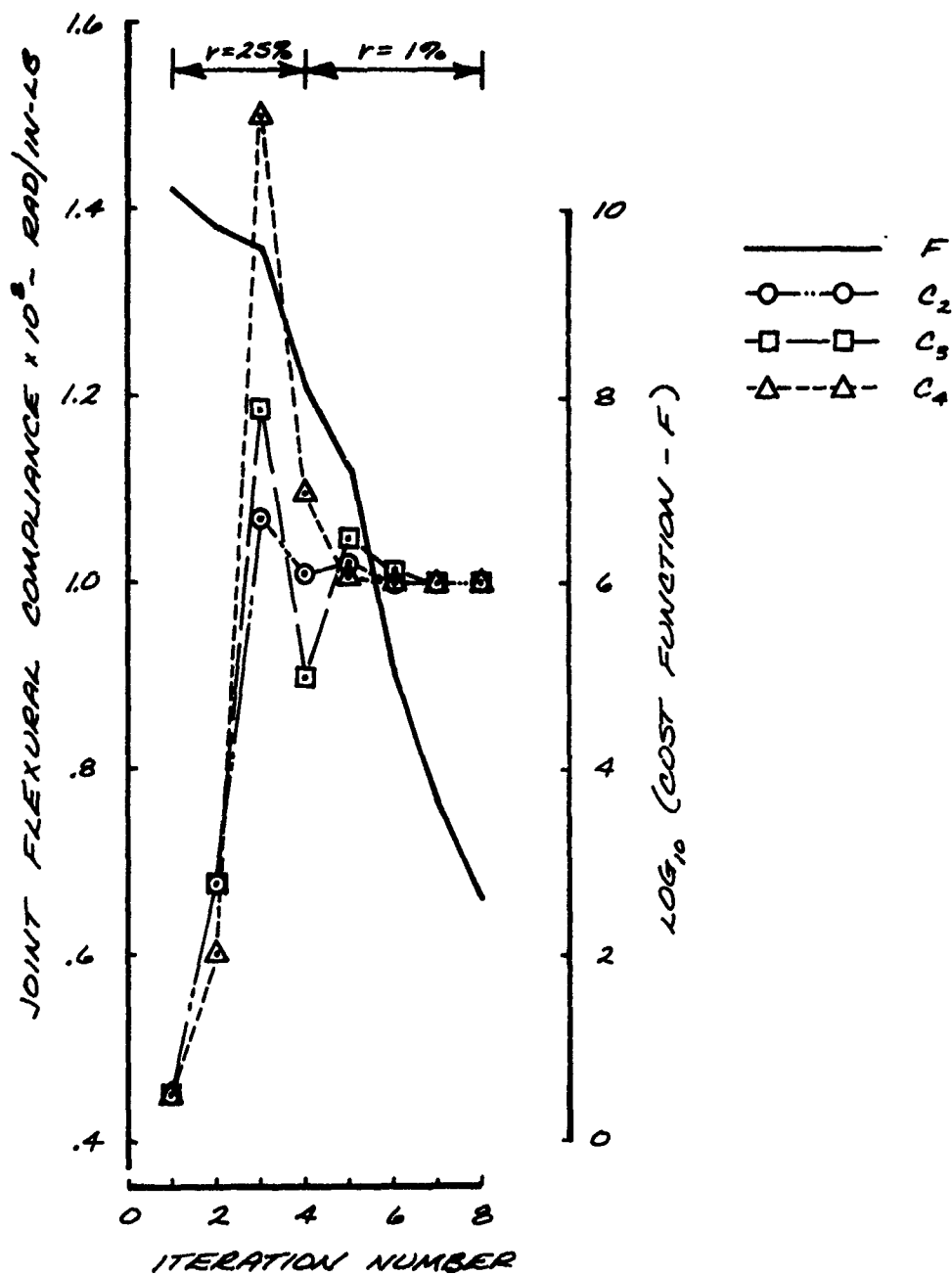
FIGURE 3-12

CASE 3

UNIFORM BEAM WITH APPENDAGE

UNIFORM BEAM

STIFFNESS DISTRIBUTION

WEIGHT DISTRIBUTION

LUMPED MODEL REPRESENTATION
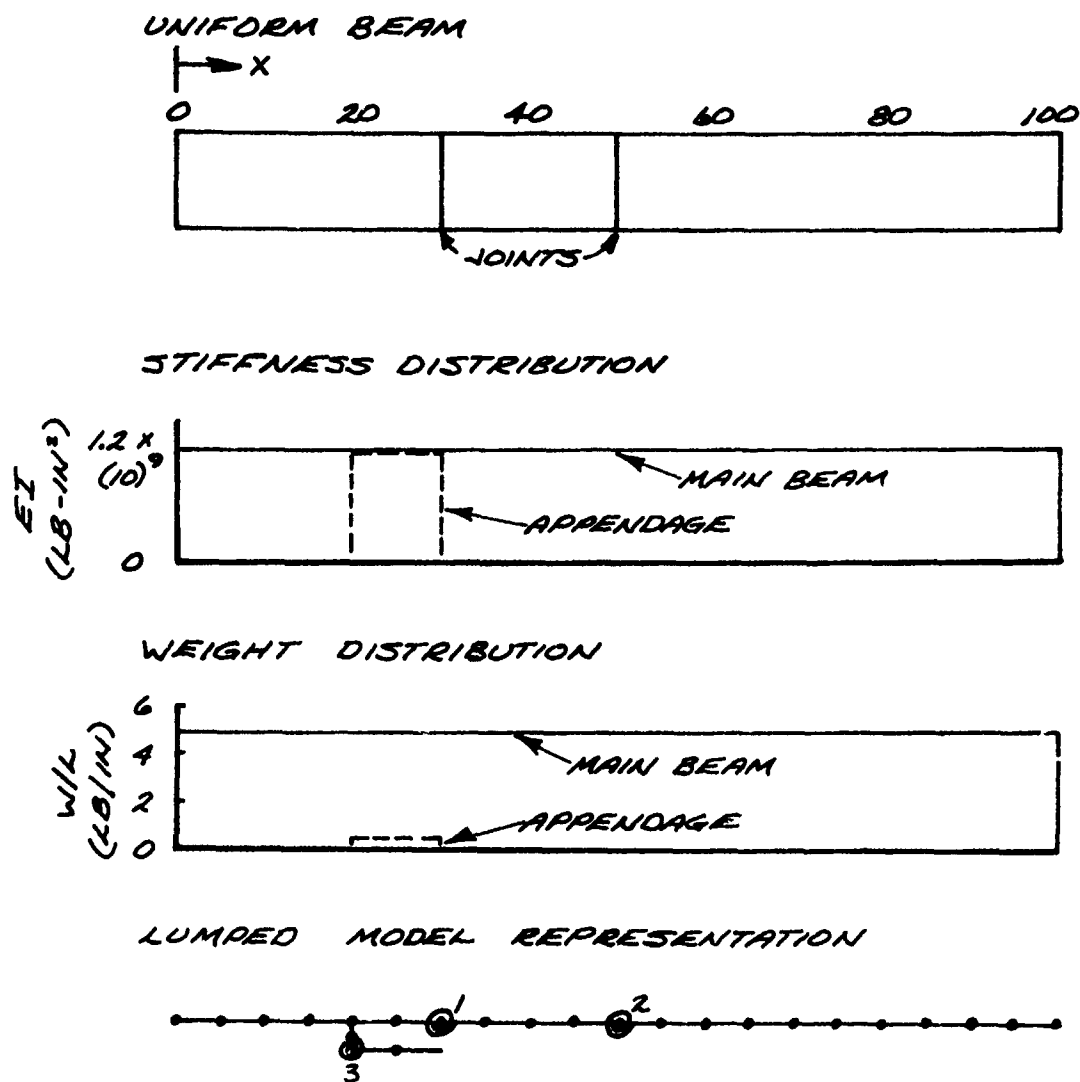
SPRING NO.	COMPLIANCE RAD/IN-LB	
1	.3	-7
2	.3	-7
3	.1	-5

MODE NO.	MODE TYPE	FREQ. (Hz)
1	1ST AIRFRAME	64.4
2	2ND AIRFRAME	203.5
3	APPENDAGE	286.8

25

FIGURE 3-13

CASE 3

CONVERGENCE USING THREE MODES

26
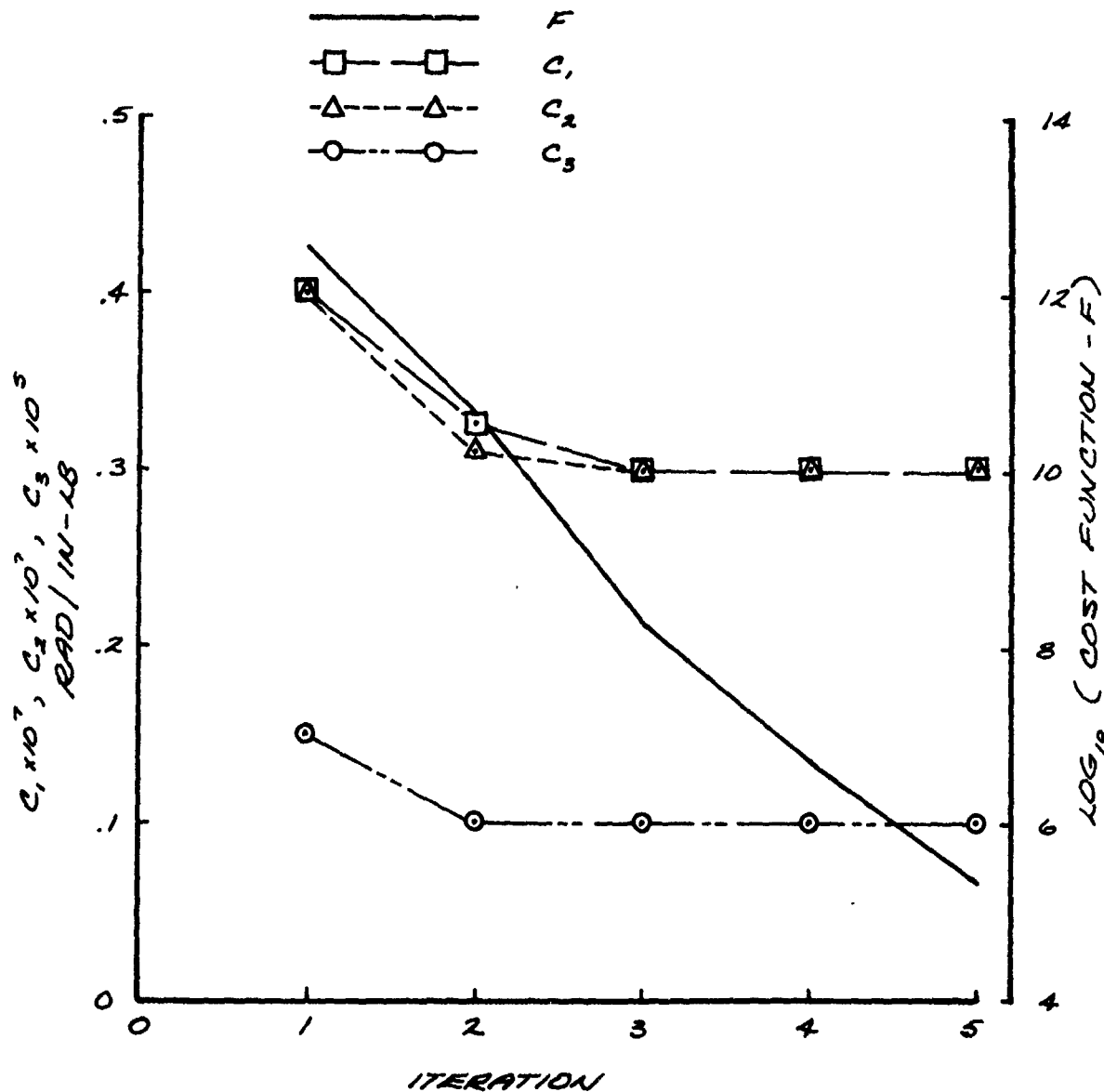
Section 4.0

EXPERIMENTAL PROGRAM

The experimental program was designed to provide selected data on the dynamic characteristics of representative tactical missile airframe joints. A secondary objective of the experimental program was to develop test data which could be used to evaluate practical applications of the joint compliance extraction code described in Section 3. The test specimens were specially configured to achieve design simplicity and to minimize the number of unknowns and thus increase the accuracy with which the joint characteristics of the test specimen might be derived.

The following airframe joints, illustrated in Figures 4-1 thru 4-7, were tested in the experimental portion of this study:

TEST CONFIG.	JOINT TYPE	DIAMETER	MISSILE APPLICATION
1.	Threaded Coupling	2.75"	Redeye
2.	Marmon Clamp	5.0"	Sidewinder
3.	Lapped Shear Bolt	8.0"	(Design Study)
4.	Lapped Shear Bolt	13.5"	Standard ARM
5.	Continuous Land Ring / Tension Bolt (4) / Tension Bolt (8)	13.5"	Standard Missile

Test data on Configurations 2 and 3 were provided by the Naval Weapons Center, China Lake through the cooperation of Messrs. W. J. Werback, E. L. Jeter and J. W. Onstott. The data on the remaining test configurations were obtained in the Structural Test Laboratory at General Dynamics, Pomona Operation. Special pieces of hardware were constructed for the testing of the joints in Configurations (1) thru (4), while Configuration 5 consisted of a portion of a Medium Range Standard Missile airframe which included three of the primary airframe joints but with the control surfaces, dorsal fins, and all internal components removed. The tests consisted of identifying and surveying the first three flexural modes of vibration for each of the test specimens.

The joint compliance extraction computer program discussed in Section 3 was used to analyze the test data obtained for each configuration. The results are shown in this section, along with the measured and

27

computed mode shapes and frequencies of the test specimens. Also, measured damping data are shown where obtained for the test configurations.

4.1 DESIGN OF THE EXPERIMENT

The ideal test configuration for experimental determination of joint compliance (as recommended in the Phase I Study) would consist of uniform well defined structure with the joint in question placed at the midspan. Minimizing the number of unknowns is of primary importance. Midspan symmetry about the joint plane permits the flexural and shear properties of the joint to be isolated since no shear loads would exist at the midspan in the first bending mode, and no bending moment at the midspan would exist in the second bending mode. Additionally of course, the midspan joint has the greatest effect on first mode frequency and thus enhances the accuracy of joint flexural compliance predictions.

Few actual joints in tactical missile airframes lend themselves directly to this ideal test airframe configuration, although close approximations are often possible. In three of the five test configurations, empty rocket motor cases with the desired joint on one end were used to establish the desired relatively uniform well defined primary structure. In each case, comparatively short span adapters were used to join a pair of identical empty rocket motors creating a symmetric configuration with two like joints near the midspan. The required adapters were designed with the same tolerance limits as production missile hardware so that the resulting joints would truly be representative of those on the actual missiles.

Before the test specimens were assembled, weight and center of gravity measurements were made for the individual parts. Also to assist in defining the stiffness of the rocket motor cases, each motor was suspended and vibrated individually to obtain its lower free-free bending mode characteristics. The special hardware was then used to join the rocket motors using production assembly torque specifications.

Figure 4-8 shows a typical test configuration. The specimen is suspended in a soft support system at the two nodes of the first free-free bending mode. Here the type of specimen support system was chosen because of its ease of assembly and because of the well defined boundary conditions of the specimen. The excitation source is provided by an electromagnetic shaker, and the force input is measured with a piezoelectric force gauge. The bending mode shapes were measured using a piezoelectric accelerometer mounted on a permanent magnet. Small flat steel pads were bonded to the test configuration using dental cement, and the accelerometer-magnetic was moved from pad to pad during the modal survey. At each monitoring location the acceleration magnitude and phase were measured using a Weston transfer function analyzer. The acceleration data were then normalized, to obtain convenient scales, and plotted.

28

The structural damping is found from a decay response plot. These plots were obtained by switching off the input to the power amplifier and recording the decaying acceleration trace on a storage oscilloscope. The damping ratio is then computed using the logarithmic decrement

$$\gamma = \frac{\ln(X_0/X_n)}{2\pi n}$$

where γ =   structural damping ratio

X_0 =   peak acceleration response at some time after the amplifier power has been switched off

X_n =   peak acceleration response   n   cycles after X_0.

4.2   TEST RESULTS

The test data on the seven joints under consideration are presented in five sections corresponding to the five test specimens. Comparisons of measured and predicted mode shapes and frequencies are given for each configuration. In addition to the basic data, section 4.2.4 presents parametric studies dealing with the effects of joint fastener number, spacing, and preload on modal response, damping, and effective joint compliance charac'eristics. Section 4.3 presents a comparison of the joint compliances obtained in this study with the compliances presented for similar joints in the Phase 1 study (Reference 7).

4.2.1   Threaded Coupling Ring Joint. The cross section of the threaded coupling ring joint (used in the 2.75 inch diameter Redeye missile) is shown in Figure 4-1. The joint occurs in the missile airframe between a titanium warhead and a steel rocket motor. The test configuration employed a special five inch long spacer fabricated out of aluminum (Figure 4-9). This spacer was designed to have identical joints at both ends so that two Redeye rocket motors could be joined together. The resulting configuration is 54 inches in length and geometrically symmetric about the midspan of the assembly.

The test specimen was light, weighing only 4.37 pounds, and the vibration modes were easily excited by a small induction shaker, which requires no mechanical contact with the test specimen. The mode shapes were measured with a roving miniature accelerometer mounted to the specimen by bees' wax. Also a fixed miniature accelerometer was mounted at one end of the specimen as a reference accelerometer.

The theoretical mode shapes shown on the mode plots were predicted by program JOINTS (Section 3   ) using a lumped parameter mathematical model containing flexural springs at the two joint locations. The weighting factors used in program JOINTS to match the measured data were slightly

different from those discussed in Section 3.1.3. Here the mode shape weighting factors were assumed proportional to the square of the mode frequency rather than to the fourth power of the frequency. The reason for the change was that the fourth power weighting factor on frequency did not yield a quick convergence. Since the weighting factors are completely arbitrary, the effects of different weighting were investigated.

A comparison of the experimental and theoretical modal data for the 2.75 inch diameter threaded coupling ring joint test specimen are shown in Figure 4-10. The measured mode shape data shows little scatter and the predicted mode shapes agree quite well with the measured data. The first theoretical mode frequency agrees exactly with the first experimental frequency and the second mode frequency difference is less than 0.2%. Only flexural springs were considered since the second mode shows virtually no shear deformation across the joints. The resulting flexural joint compliances are

$$C_1 = .196 (10)^{-6} \text{ rad/in-lb} = C_2$$

4.2.2 <u>Marmon Clamp Joint</u>. The dynamic response characteristics of a five inch diameter Marmon clamp joint were investigated at the Naval Weapons Center, China Lake, California (Reference 5). The mode shape and frequency data are presented here. These data were used with program JOINTS to compute joint compliances. Figure 4-2 shows the cross section of the Marmon clamp joint. The test configuration and procedure were quite similar to the tests performed at General Dynamics. Two rocket motors were joined using a simulated warhead case which has identical joints at both ends. The test specimen was suspended by a soft support system at the nodes of the first free-free bending mode. The excitation source and response measurements were made in a manner similar to that discussed in Section 4.1.

The measured test data on the Marmon clamp test specimen are shown in Figure 4-11 together with the theoretical modes obtained using program JOINTS. The theoretical data matches the measured data quite well for all three modes, with the third mode having the largest deviation. Only flexural springs were modeled at the two joints for this configuration. About a 3% frequency difference occurs in the second mode frequency, indicating either a shear spring could have been modeled at the joint or the calculated section properties of the test specimen might be slightly in error. Approximately a 3% error occurs between the third measured and computed bending mode frequencies. Overall, the comparison of experimental and analytical modes looks quite good, with the resulting flexural compliances for the two Marmon clamp joints as follows:

$$C_1 = C_2 = .39 (10)^{-7} \text{ rad/in-lb}$$

4.2.3 <u>Shear Bolt Joint - 8.0 inch Diameter</u>. Data on an additional special test configuration were provided by the Naval Weapons Center,

China Lake, California. The test specimen in this case employed an 8-inch diameter eight fastener shear bolt joint. A cross sectional view of the joint is shown in Figure 4-3, and a sketch of the test specimen is shown in Figure 4-12. The test specimen differs somewhat from the other test configurations in that this specimen contains only a single rather than two joints. Also, the test specimen is not actual missile hardware but was designed and fabricated explicitly to investigate the dynamic characteristics associated with the joint. Since the mechanical joint is formed by joining a male and female section, the assembled specimen is not precisely symmetric about the joint interface when assembled. This feature, however, is not considered to be significant.

In addition to the experimental data, analytical modes were also provided. The modes were obtained by a trial and error selection of the single joint compliance. A comparison of the results obtained is shown in Figure 4-13; a good match of the measured mode shapes is noted. A frequency difference of 3.4% occurs in the first mode, while the second and third mode frequencies are very close. The 3.4% error is obtained when the 90° phase crossing is used to define resonance. However, double peaked first and third modes appeared in the measured frequency response of the 8.0 inch diameter test specimen. If the average frequency between the two peaks near each mode are used, the theoretical first mode frequency matches this frequency quite well. The justification for considering the average frequency of the two first mode peaks is that these two peaks actually represent the bending frequencies in the two principle planes. Neither of these planes are aligned with the plane in which the specimen is being excited, thus both peaks occur in the excitation plane response. Since the predicted first mode frequency lies between two actual first mode frequencies for a single specimen, the predicted frequency should be considered a good match of the measured first mode frequency. The resulting joint flexural compliance for this joint is 4.44 $(10)^{-8}$ radians/(inch-pound).

4.2.4 <u>Shear Bolt Joint - 13.5 Inch Diameter</u>. The second shear bolt joint on which test data were obtained has an outside diameter of 13.5 inches. It is employed in both the Standard ARM and Standard Missile medium range airframes between the aft end of an eighty inch long rocket motor and the forward end of a ten inch long spacer. The joint consists of eighteen one-quarter inch diameter fasteners equally spaced at twenty degree increments around the circumference of the joint*. The cross section of this joint is shown in Figure 4-4.

To accomplish the test objectives, a special ten inch long spacer (shown in Fig. 4-14) was designed and fabricated which would permit two eighty inch long rocket motors to be joined back to back, thus forming two identical joints near the midspan. In addition to the basic eighteen fastener configuration, other configurations were obtained and tested by removing selected fasteners from the same hardware. The additional bolt patterns consisted of twelve, nine, six, and three fasteners. The eighteen,

*For alignment purposes, one fastener does not conform with the twenty degree spacing. It is shifted one degree and five minutes from the twenty degree spacing to insure the two sections mate together only one way.

31

nine, six and three fastener configurations are capable of being symmetric in that they permit uniform spacing of the fasteners around the circumference of the joint. The initially tested twelve fastener case represents a slight but significant deviation from a uniform fastener distribution since every third bolt was removed to obtain this configuration. An additional investigation of non-uniform spacing effects was also accomplished by varying the bolt patterns for the 6 and 9 bolt configurations. Figure 4-15 illustrates the spacing for the five basic configurations, and Figure 4-30 illustrates the non-uniform spacing configurations.

Before the test specimen was assembled, weight and center of gravity measurements were made on the components of the test configuration to insure that the mathematical model developed had the proper weight distribution. Next, to verify the stiffness distribution of the rocket motors, each motor was hung free-free and excited. Mode shapes, resonant frequencies, and damping ratios were measured for the first two bending modes of the individual motors. Then the analytical model of each rocket motor was tuned to achieve a good match with the measured bending mode data. As a result, the two motors are modeled with slightly different weight and stiffness distributions.

The measured mode shapes and frequencies for the basic eighteen, twelve, nine, six, and three fastener configurations are shown in Figures 4-16 thru 4-20, respectively. Also shown in these figures are plots of the predicted mode shapes obtained from the joint compliance extraction technique discussed in Section 3. For these analytical modes, a lumped parameter mathematical model was used containing both a flexural spring and a shear spring at each of the two joints. Shear springs were employed in the model to account for the mode shape discontinuities which were observed in the measured data, denoting shear deformation at the joints. The match of the first mode data was weighted the heaviest in these studies, with the match of the higher modes decreasing by a factor of ten for each consecutively higher mode.

The correlation between measured and predicted mode frequencies and mode shapes is generally good for all of the fastener configurations investigated. Agreement tends to be best for the first mode frequency and shape, deteriorating somewhat in the second and third mode (particularly for the three fastener configuration in which large unsymmetric shear deformations are observed). In other instances also, lack of symmetry in the response about the midspan is evident which is attributed to the slight differences in rocket motor weight and stiffness distribution as well as the joint behavior. An additional characteristic of the response which was exposed in the three fastener configuration was a high frequency distortion as shown in Figure 4-21. High frequency transients (approximately 1200 Hz) occur on one side of the 37 Hz fundamental waveform. This behavior may be attributable to local impacting of the joint

32

surfaces and could be a significant contributor to the relatively high damping measured for this mode.

The variation in first mode frequency with the number of uniformly spaced fasteners is shown in Figure 4-22. The resulting trend appears to be very nearly linear on a semi-log plot and could be closely approximated by an exponential function. The linearity of the structural response was examined from the standpoint of first mode frequency variation with changes in both excitation force and fastener preload. A twenty-five to one variation in excitation force produced a first mode frequency change of only 3.6 percent. Similarly, a factor of 2 reduction in design torque on the fasteners (60 inch pounds to 30 inch pounds) produced a first mode frequency drop of only 3.4 percent. These effects are also shown in Figure 4-22. The joint compliances derived for the basic fastener configurations are listed in Table 4-1. The flexural compliances are plotted in Figure 4-23 against the number of fasteners used in the joint, and the shear compliances are shown plotted versus the number of fasteners in Figure 4-24. Again it is noted that the twelve fastener configuration represents a slight deviation from a uniform fastener distribution, and hence the compliance values are plotted as dashed symbols. Also, it is noted that the joint compliances obtained are not precisely equal in magnitude for the two joints. A difference of 15% exists between the flexural compliances and a difference of 54% exists between the shear compliances. It is felt that the comparatively large difference in shear compliance is due to possible experimental errors in measuring the second mode shape. Generally, shear compliances known to within a factor of two would probably be satisfactory because of the relative unimportance of joint shear compliance in most practical applications. In fact, shear compliances are rarely considered in tactical missile analyses (Reference 7). The variation in flexural compliance with number of fasteners is shown to be remarkably well ordered (Figure 4-23) again being very closely approximated by an exponential function. Doubling the number of fasteners in this configuration increases the joint stiffness by a factor of nearly 3. The predicted trend shown for shear compliance, Figure 4-24, appears to be a more complex function.

In addition to the effect the number of fasteners has on the derived joint compliance, the influence of the bolt preload was also investigated for both the six and the nine fastener configurations. The design assembly torque on the one quarter inch diameter bolts is nominally 60 inch-pounds. For this investigation, the bolt torque was varied from 10 inch-pounds to 80 inch-pounds. Only the first mode frequency was recorded at each value of fastener torque. A curve of estimated flexural compliance versus bolt torque is shown in Figure 4-25. The effect of variations in excitation force on the joint compliances was also briefly investigated, and the results shown in Figure 4-25.

As stated before, the damping measurements were obtained from response decay plots for all five of the bolt patterns. A plot showing the peak

33

amplitude in each cycle versus the number of cycles after the shaker power was switched off was made for the three, six, nine and eighteen fastener configurations. Figure 4-26 shows these plots normalized to a common amplitude at the beginning of the decay. The only configuration exhibiting a significant departure from linear (viscous) damping is the three fastener specimen. The slope of the decay plot changes for this configuration between the fifth and tenth cycles indicating the damping mechanisms affecting the response has changed. One possible explanation is that some form of sliding friction contributes at the higher amplitudes and that beyond the tenth cycle the amplitude has decreased to the point where this mechanism is no longer present. The variation in estimated first mode damping ratio with the number of fasteners is shown in Figure 4-27 along with the damping ratio of the two rocket motors alone. The first mode damping ratio increases in magnitude by a factor of six in going from eighteen fasteners to three fasteners. Figure 4-28 shows the first mode damping ratio versus bolt torque for the six and nine bolt patterns. The damping ratios level out at approximately 40 inch-pounds of torque for the six and nine bolt patterns, as do the joint compliances.

An investigation was also conducted into the effect of non-uniform spacing for a given number of fasteners. The six fastener configuration, for example, could employ equal spacing of 60 degrees around the circumference, or alternate 40° and 80° or 20° and 100° between fasteners. The latter cases lie between the three equally spaced and the six equally spaced fastener configurations as far as joint compliance is concerned. Figure 4-29 shows a plot of the joint flexural compliance versus the number of fasteners for both the equally and the unequally spaced fastener configurations. The bolt patterns associated with these compliances are shown in the sketches of Figure 4-30. It is concluded that fasteners located uniformly around the circumference of the joint will produce the stiffest joint for the number of fasteners.

4.2.5 <u>Standard Missile Airframe</u>. The last test configuration consisted of the primary structure of a Standard Missile (MR) airframe incorporating three separable tactical missile joints (Figures 4-5 thru 4-7). The test configuration was obtained by removing all internal and external components as well as the entire steering control section in order to achieve the simplest possible test airframe with minimum unknowns. The resulting airframe assembly is shown in Figure 4-31.

The excitation source was an electromagnetic shaker attached to the aft end of the airframe. The mode shape data were obtained using a roving accelerometer mounted to a magnet everywhere except on the radome, where a hand held velocity probe was used. Again program JOINTS was used to match the measured modes with theoretical modes and, hence, derive values of joint compliance for the mechanical joints. In this situation only flexural compliances were considered to be significant at the airframe joints. The weighting factors used in matching the measured data are listed below.

34

Mode Number	Weighting Factors	
	Frequency	Shape
1	2	1
2	1/2	1/4
3	1/4	1/16

A comparison of the analytical and experimental bending modes are shown in Figure 4-32. The theoretical first and second mode shapes match the measured data points quite well, while the third computed mode shape exhibits noticeable deviations from the measured data. The frequency differences between the measured and computed frequencies for the three bending modes are 1.4%, 5.1%, and 5.6% respectively. The flexural compliances derived for the three airframe joints are listed below.

Type of Joint	Flexural Compliance (Radians/Inch-Pound)
Continuous Land Ring	$2.7 \ (10)^{-8}$
4 Bolt Tension	$< 0.1 \ (10)^{-8} \left. \vphantom{\begin{matrix}a\\b\end{matrix}} \right\} \cong 1.1 \ (10)^{-8}$
8 Bolt Tension	$1.1 \ (10)^{-8}$

The individual flexural compliances shown for the tension bolt joints are viewed with some suspicion since the estimated values were found to be quite sensitive to assumed weighting factors in the joint compliance extraction code. The problem in this instance may be due to having two relatively stiff joints very close together (less than a body diameter apart). The sum of the two compliances shown, which controls the net effect on airframe response, is believed to be correct but the distribution between the two joints is felt to be not adequately resolved. The code's ability to resolve joint compliance,of course,diminishes with increasing joint stiffness since the effect on airframe response becomes very small.

4.3 EVALUATION OF DERIVED COMPLIANCES

Table 4-2 presents a comparison of the joint flexural compliances obtained during the Phase 2 study with previous estimates of joint flexural compliance given in the Phase 1 final report. In addition, the derived joint compliances are compared with a NASA stiffness rating based upon joint diameter - - shown in Figure 4-33. Substantial differences,

in some instances, between present and previous estimates of joint compliance point out the sensitivity of the answer to test and analysis methods.

The flexural compliance derived for the 2.75 inch diameter threaded coupling ring joint test agrees closely with the compliance value given in the Phase 1 report. In this case, the previous compliance estimate was based upon a simplified vibration test where the number of unknown variables could be minimized (similar to the Phase 2 test). The rating for this joint is shown in Figure 4-33 to lie between good and excellent. The threaded coupling ring joint (Figure 4-1) is further noted to be more than a factor of 10 stiffer in rating than the continuous land ring joint (Figure 4-5). The explanation for this disparity is believed to lie in multiple versus single thread load path behavior.

The 5.0 inch diameter Marmon clamp joint compliance obtained during Phase 2 agrees well with the Phase 1 estimate, with a compliance difference of 22%. Here the original joint compliance estimate was selected from Alley's and Leadbetter's work (Reference 1) on the basis of engineering judgement and later confirmed in missile level tests. This joint also is seen to lie in the good to excellent range.

The 8.0 inch diameter shear bolt joint was not considered during the Phase 1 study; hence, no comparison can be made to the Phase 1 data. However an interesting relationship with the 13.5 inch diameter shear joint results is shown in Figure 4-34. Here the joint flexural compliances for both the 8.0 inch and 13.5 inch diameter joints (measured during Phase 2) have been multiplied by the joint diameter cubed and plotted versus the number of fasteners in the joint. The 8.0 inch diameter joint flexural compliance falls between the values obtained with six and nine fasteners for the 13.5 inch diameter shear bolt joint. The implication being that the number of fasteners, rather than structural details of the sections being joined, dominates the joint compliance characteristics.

The flexural compliance of the 13.5 inch diameter 18 fastener shear joint derived from the Phase 2 test data reveals a joint nearly five times as stiff as previously estimated, with a rating between good and excellent. Principal reasons for the inaccuracy of earlier estimates include joint location near the aft end of the missile airframe (response relatively insensitive to joint stiffness), previous test airframe complexity (many unknowns), and the lack of a systematic procedure for matching the theoretical and experimental modes.

The compliance of the continuous land ring joint also differs appreciably from earlier estimates, appearing to be nearly 80 percent more compliant than had been assumed in previous studies. Similarly, the pair of tension bolt joints judged in terms of net compliance (sum of individual contributions which are difficult to separate due to close proximity)

reveals nearly a 60 percent increase in compliance over earlier estimates.

When reasonably accurate estimates of mechanical joint compliance are required in design studies, a test approach based on placing the unknown joint at the midspan of well-defined uniform structure would appear to offer distinct advantages.

Table 4-1

13.5 INCH DIAMETER SHEAR BOLT JOINT
JOINT COMPLIANCES VS. NUMBER OF FASTENERS

NUMBER OF FASTENERS	EXPERIMENTAL JOINT COMPLIANCES			
	JOINT 1		JOINT 2	
	FLEXURAL RAD/IN-LB	SHEAR IN/LB	FLEXURAL RAD/IN-LB	SHEAR IN/LB
18	$.223(10)^{-8}$	$.554(10)^{-6}$	$.220(10)^{-8}$	$.531(10)^{-6}$
12*	$.394(10)^{-8}$	$.837(10)^{-6}$	$.464(10)^{-8}$	$.388(10)^{-6}$
9	$.590(10)^{-8}$	$.683(10)^{-6}$	$.598(10)^{-8}$	$.697(10)^{-6}$
6	$1.02(10)^{-8}$	$1.29(10)^{-6}$	$1.03(10)^{-8}$	$1.05(10)^{-6}$
3	$2.72(10)^{-8}$	$9.86(10)^{-6}$	$2.86(10)^{-8}$	$9.51(10)^{-6}$

*Non-uniform Spacing (See Fig. 4-15)

Table 4-2

COMPARISON OF FLEXURAL COMPLIANCES
WITH PHASE 1 DATA

TYPE OF JOINT	FIGURE NUMBER	JOINT COMPLIANCE – RAD/IN-LB	
		PREVIOUS ESTIMATE*	PHASE 2 DERIVED
2.75 Inch Diameter Threaded Coupling Ring	4-1	$2.0 \ (10)^{-7}$	$2.0 \ (10)^{-7}$
5.0 Inch Diameter Marmon Clamp	4-2	$5.0 \ (10)^{-8}$	$3.9 \ (10)^{-8}$
8.0 Inch Diameter Shear Bolt Joint (8 Fasteners)	4-3	——	$4.4 \ (10)^{-8}$
13.5 Inch Diameter Shear Bolt Joint (18 Fasteners)	4-4	$1.0 \ (10)^{-8}$	$0.22 \ (10)^{-8}$
13.5 Inch Diameter Continuous Land Ring	4-5	$1.5 \ (10)^{-8}$	$2.7 \ (10)^{-8}$
13.5 Inch Diameter 4 Tension Bolt Joint	4-6	$0.6 \ (10)^{-8}$	$<0.1 \ (10)^{-8}$
13.5 Inch Diameter 8 Tension Bolt Joint	4-7	$0.1 \ (10)^{-8}$	$1.1 \ (10)^{-8}$

*Reference 7

38

FIGURE 4-1

THREADED COUPLING RING JOINT

TITANIUM STRUCTURE

STEEL COUPLING NUT (L.H. & R.H. THREADS)

STEEL STRUCTURE

MISSILE

SPANNER HOLE
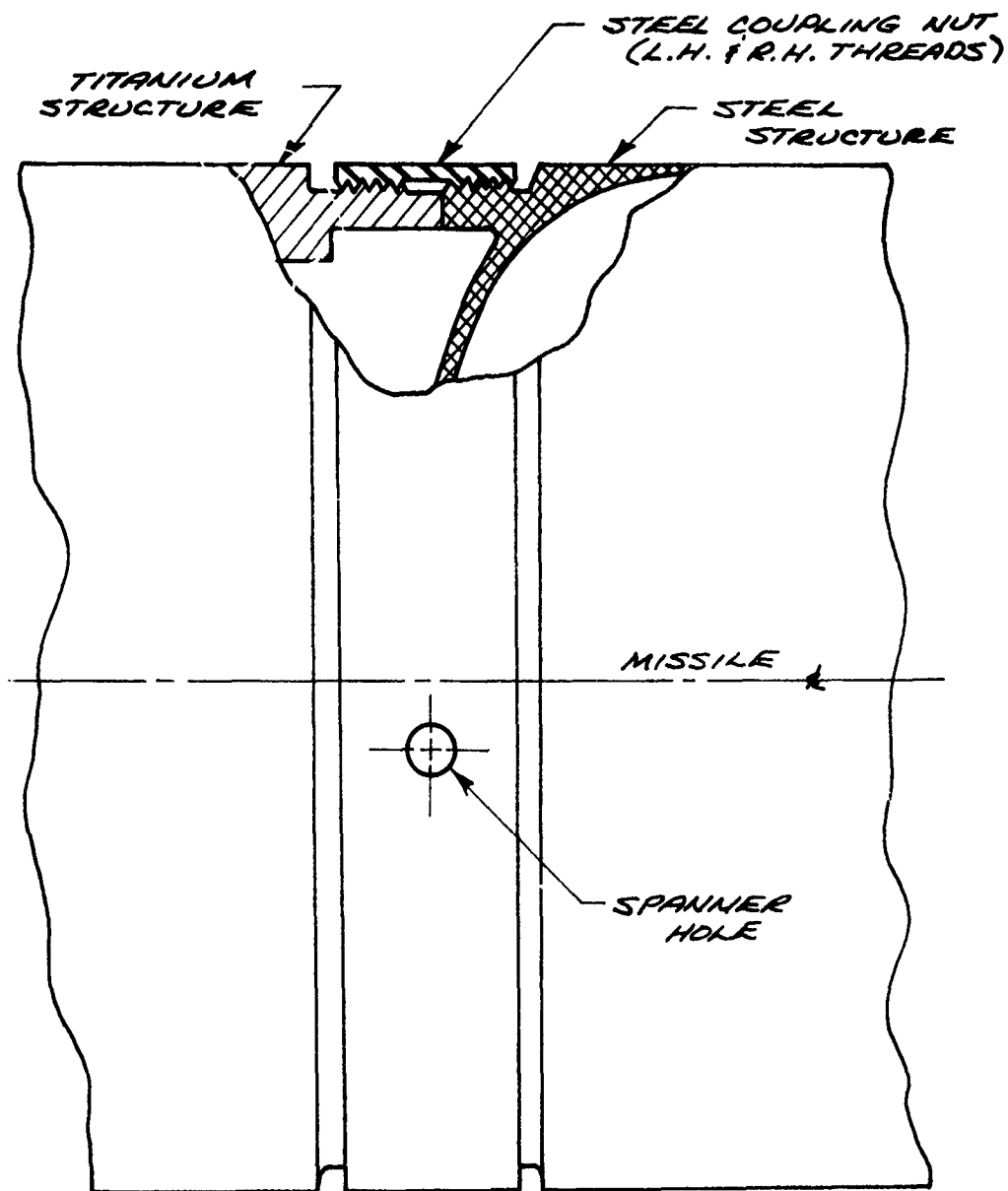
JOINT DIAMETER : 2.75 INCHES

SCALE : 2X

FIGURE 4-2

MARMON CLAMP JOINT

MARMON CLAMP

MISSILE

JOINT DIAMETER: 5.0 INCHES

SCALE : 2X

40
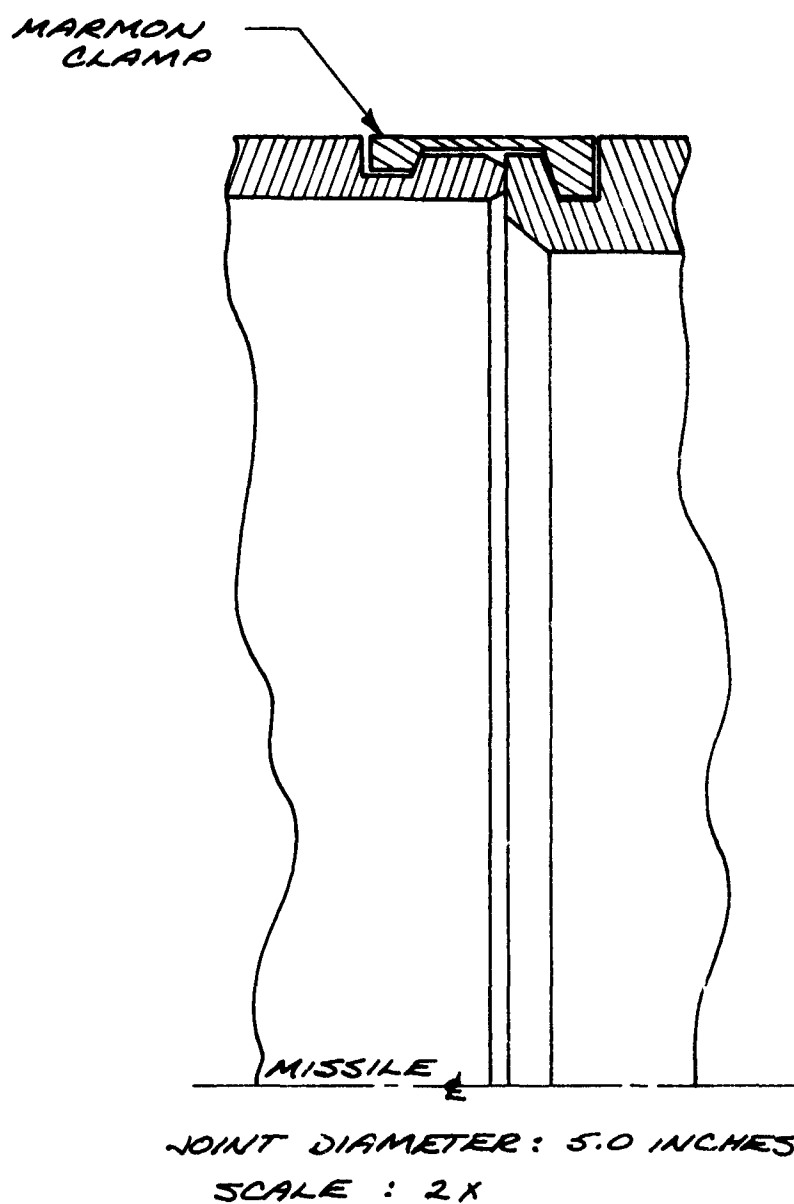
FIGURE 4-3

8.0 INCH DIAMETER SHEAR BOLT JOINT

SPECIMEN

JOINT DIAMETER: 8.0 INCHES

SCALE : 3/4 X

41
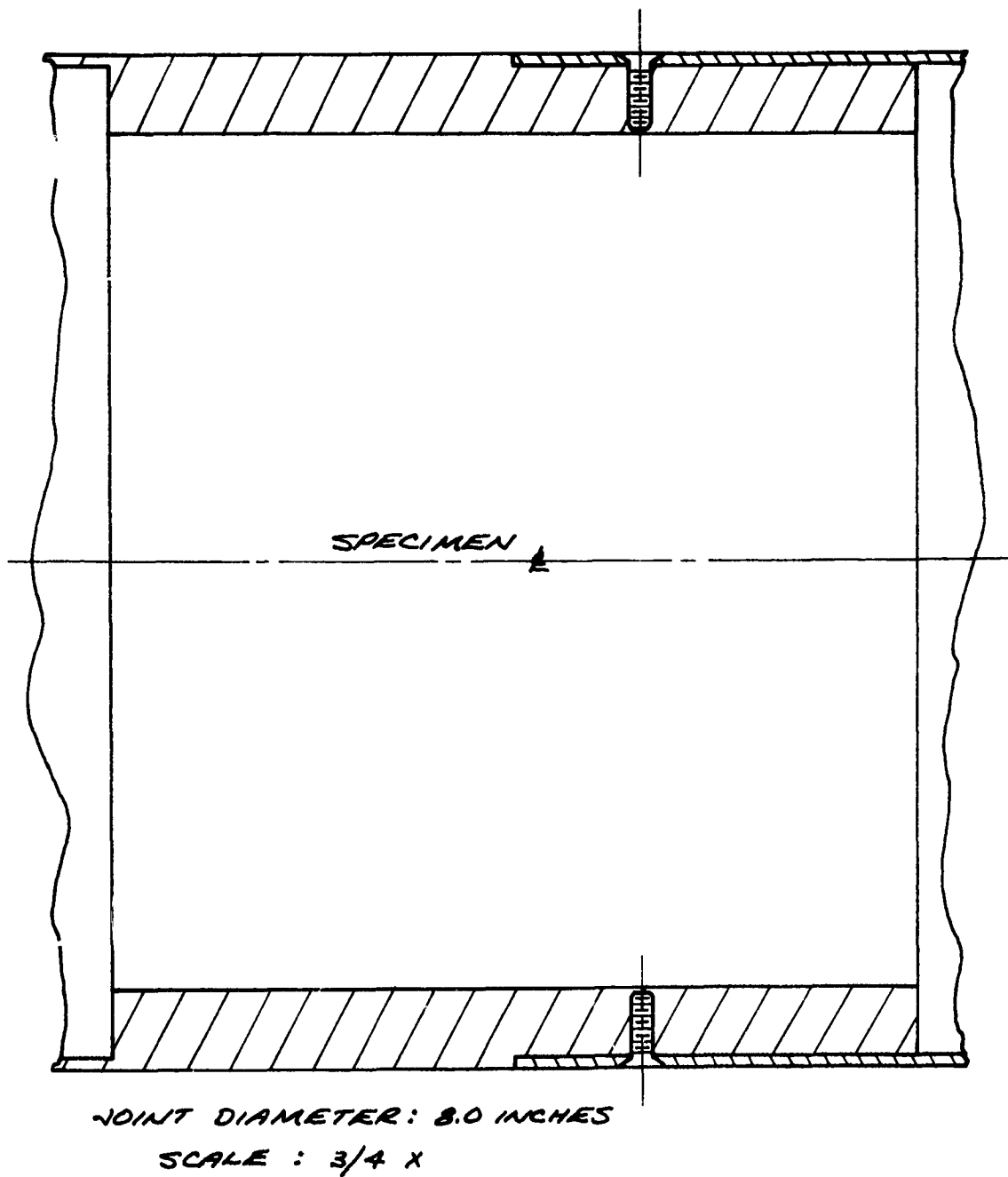
FIGURE 4-4

13.5 INCH DIAMETER SHEAR BOLT JOINT

STEEL
STRUCTURE

ALUMINUM
STRUCTURE

$\frac{1}{4}$ -28 SCREW
& DOME TYPE
NUT PLATE
18 LOCATIONS

MISSILE ₵

JOINT DIAMETER : 13.5 INCHES

SCALE : FULL

42
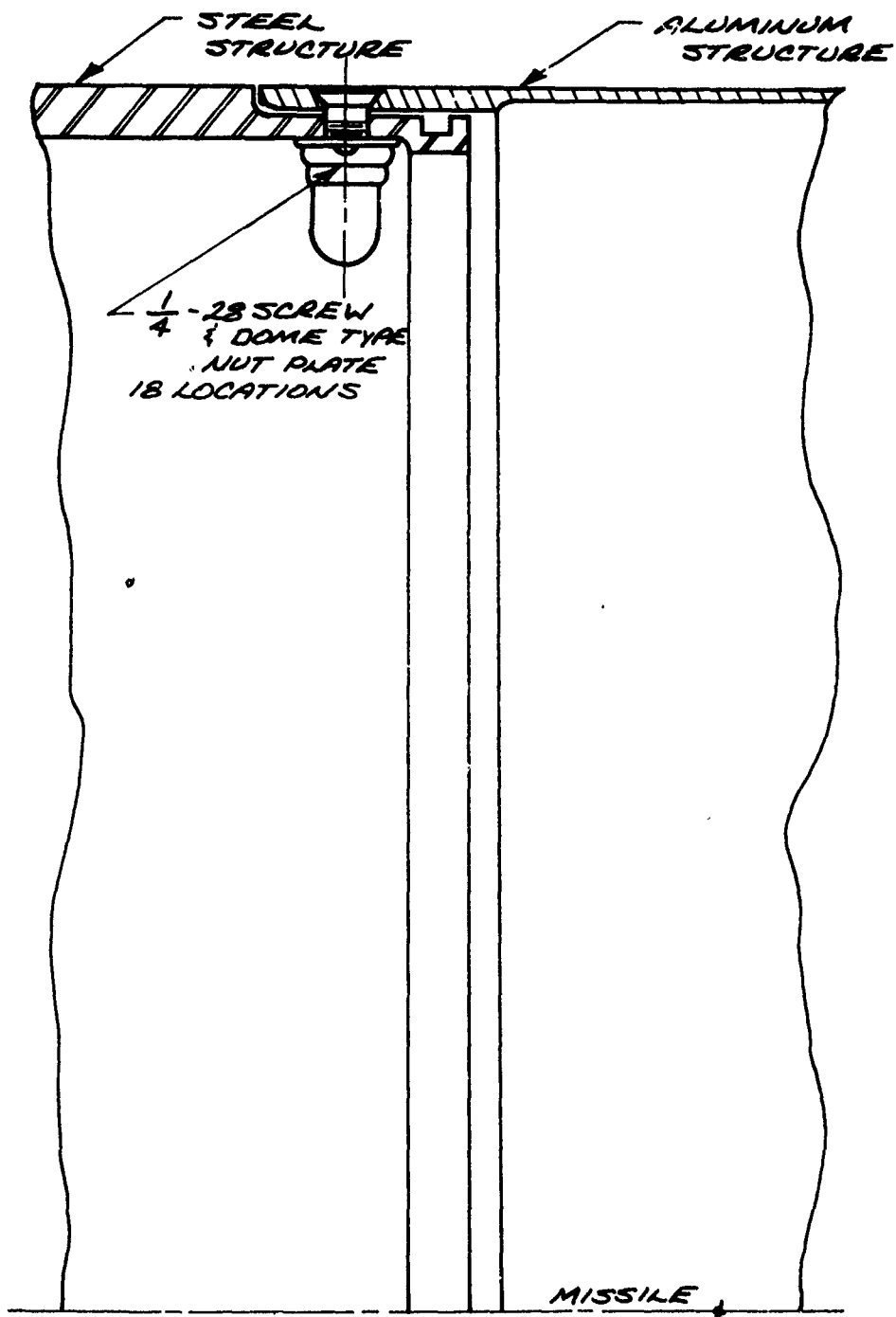
FIGURE 4-5

CONTINUOUS LAND RING JOINT

ALUMINUM STRUCTURE

STEEL COUPLING NUT (SPLIT)

ALUMINUM STRUCTURE

FIBERGLASS WRAP

FIBERGLASS WRAP

MISSILE

JOINT DIAMETER : 13.5 INCHES

SCALE : FULL

43
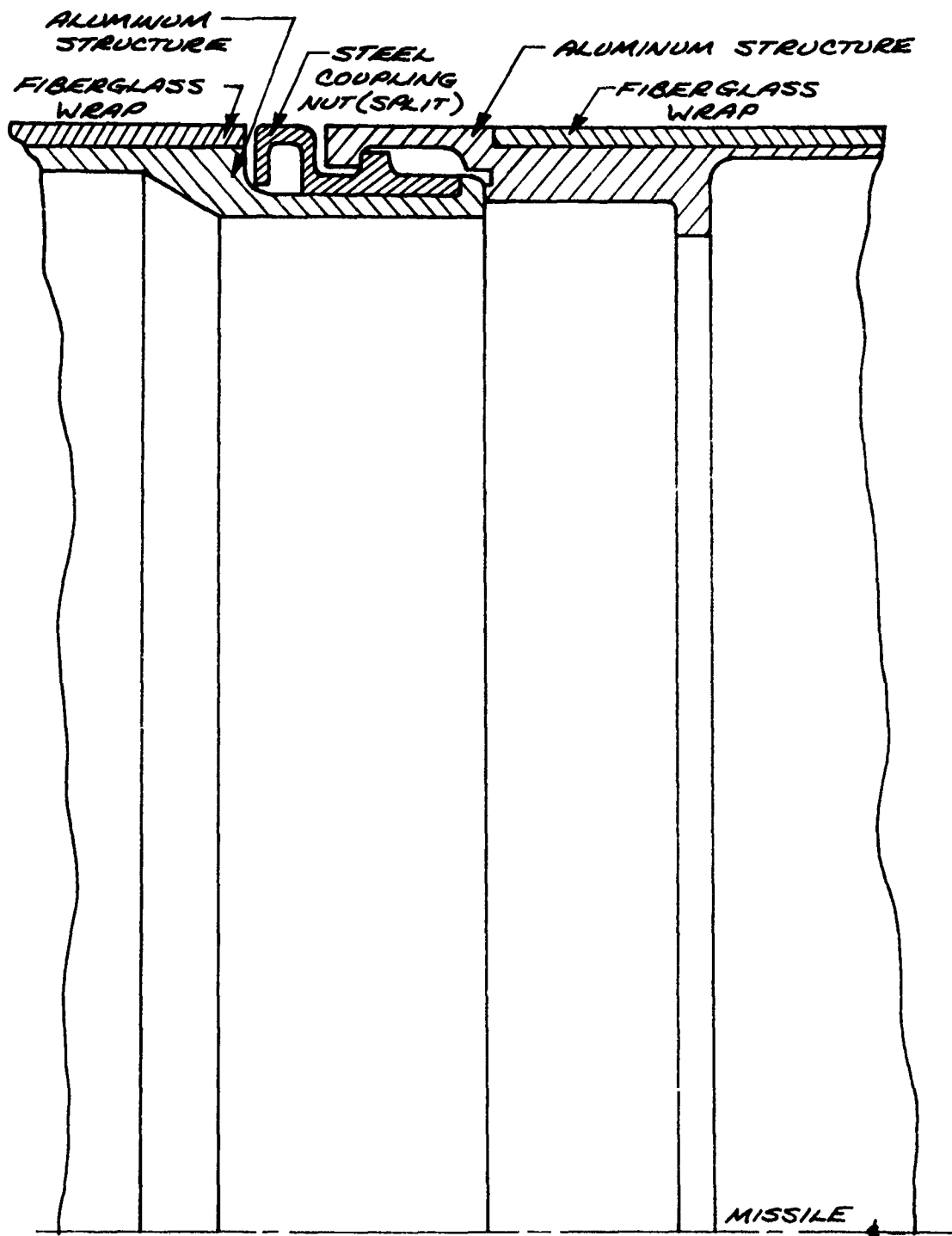
FIGURE 4-6

FOUR FASTENER TENSION BOLT JOINT

1/2" DIA. MS BOLT

THREADED INSERT

ALUMINUM STRUCTURE

ALUMINUM STRUCTURE

MISSILE

JOINT DIAMETER: 13.5 INCHES

SCALE : FULL

44
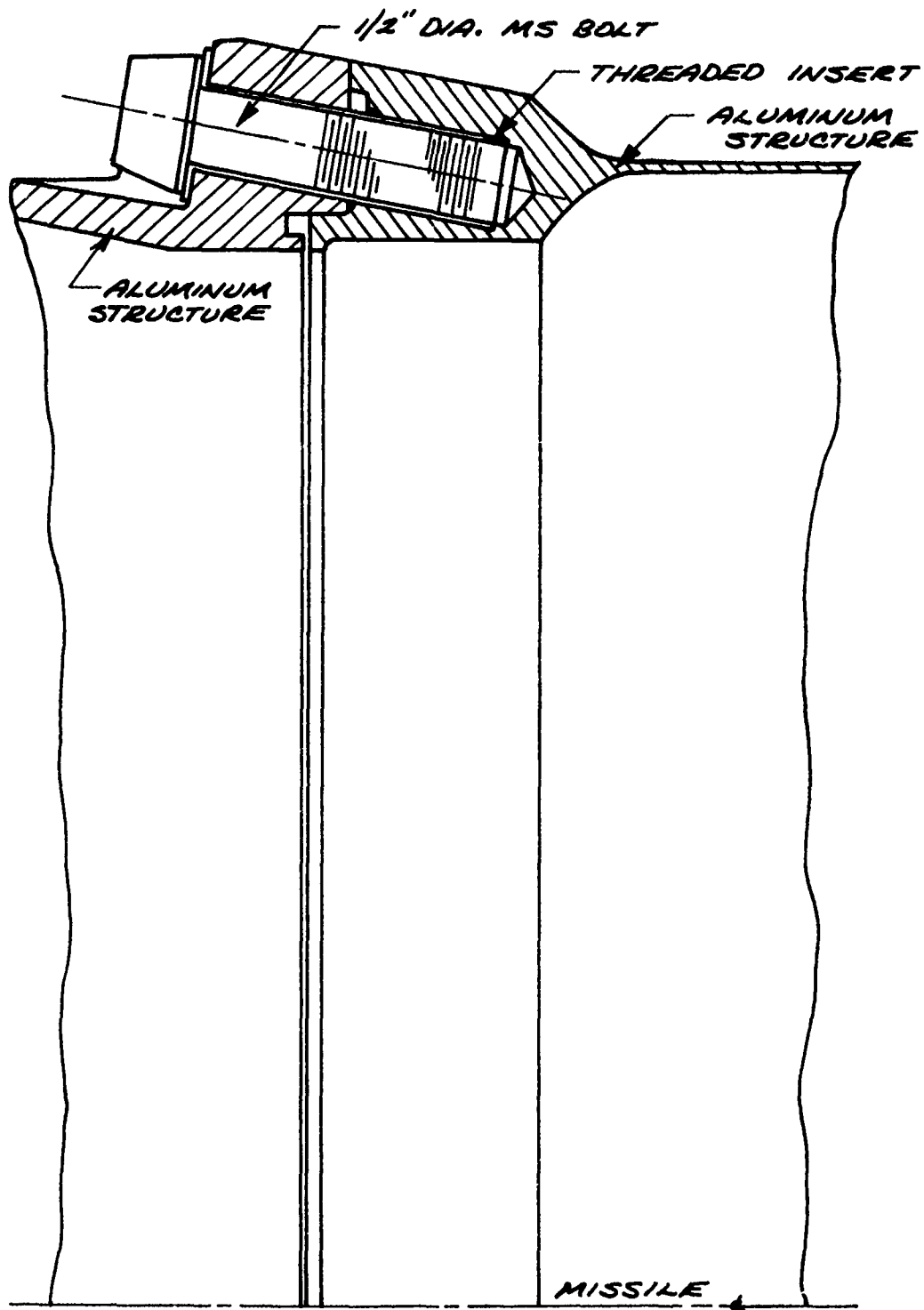
FIGURE 4-7
EIGHT FASTENER
TENSION BOLT JOINT

ALUMINUM STRUCTURE

TENSION STUD

STEEL STRUCTURE

MISSILE

JOINT DIAMETER: 13.5 INCHES

SCALE : FULL

45
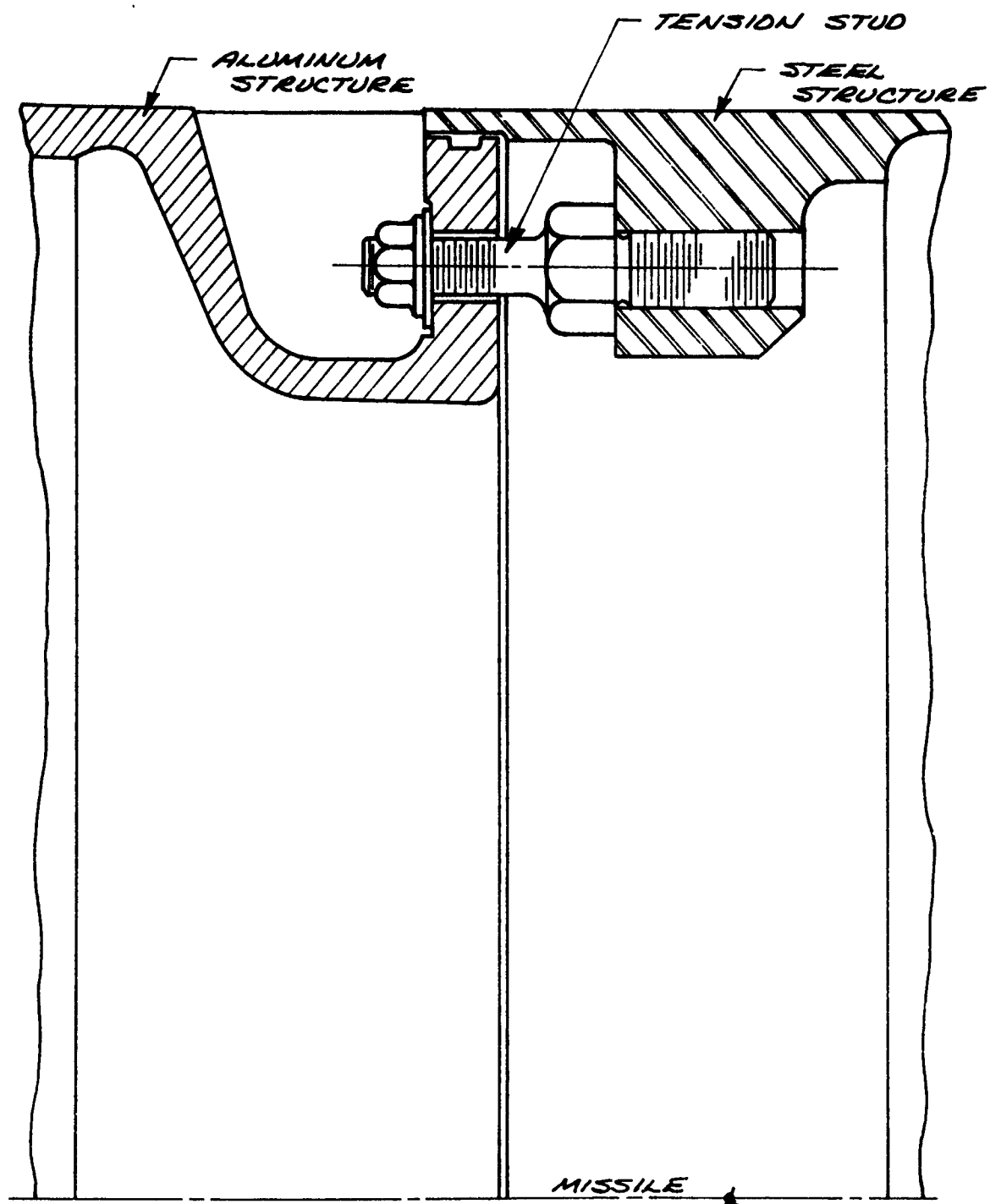
FIGURE 4-8

TYPICAL TEST CONFIGURATION
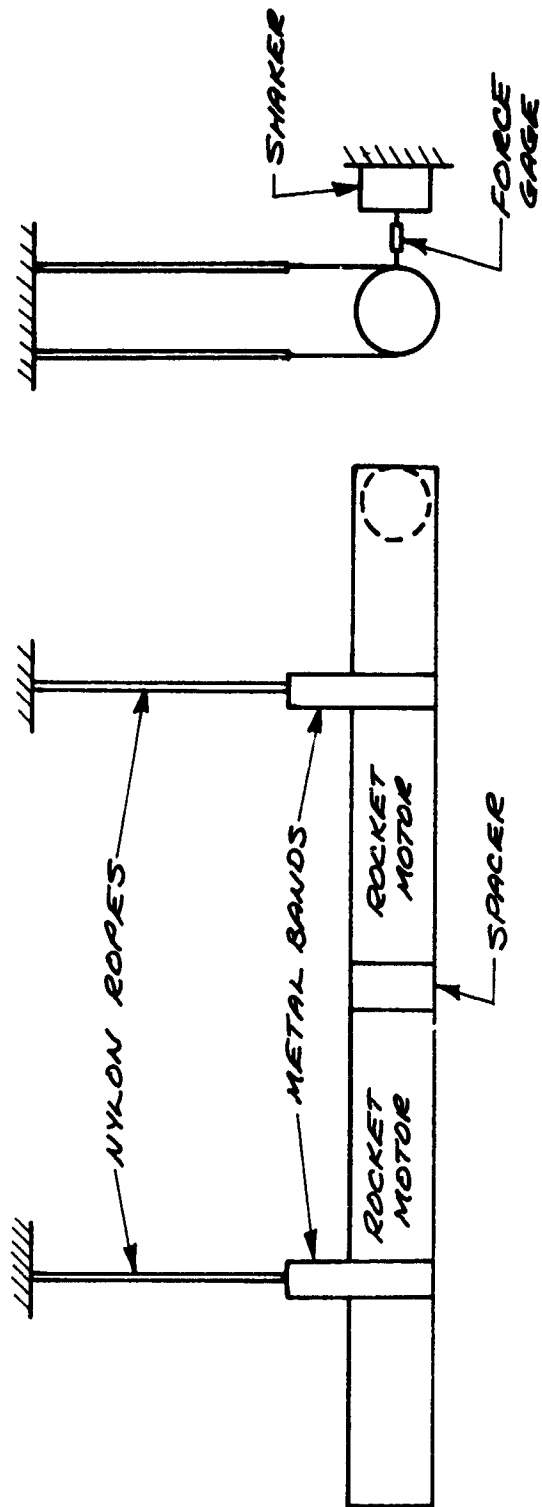
FIGURE 4-9

THREADED COUPLING RING

JOINT SPACER

DETAIL A

ALUMINUM TUBING

2.35

2.85

2.595

5.0

.375

.285

.100

DETAIL A

47
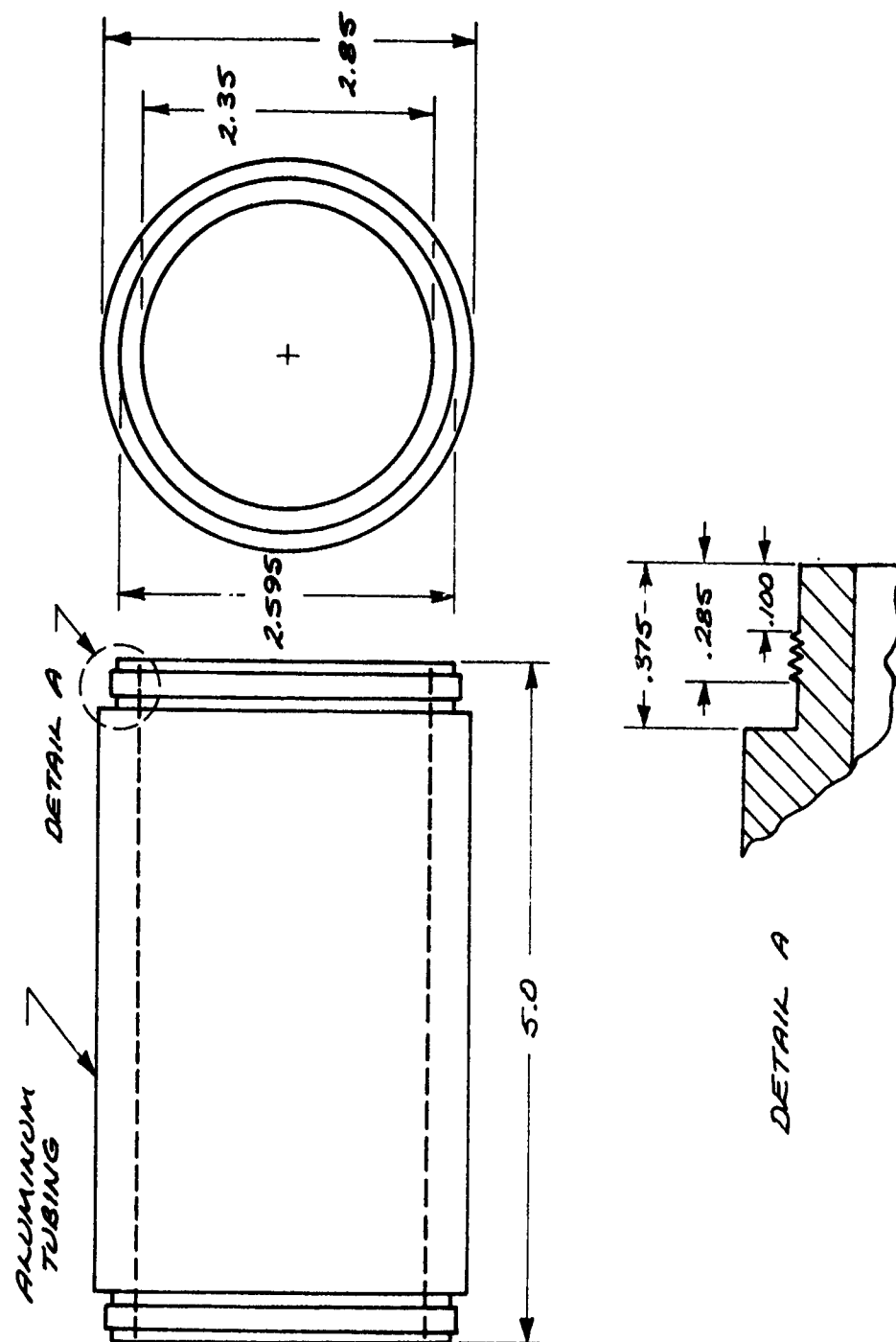
FIGURE 4-10
THREADED COUPLING RING JOINT
ANALYTICAL VS. EXPERIMENTAL MODES

O O EXPERIMENTAL - f_e = 186 Hz
—— THEORETICAL - f_t = 186 Hz

f_e = 574 Hz
f_t = 573 Hz

RELATIVE AMPLITUDE ~ IN/IN

BODY STATION ~ INCHES
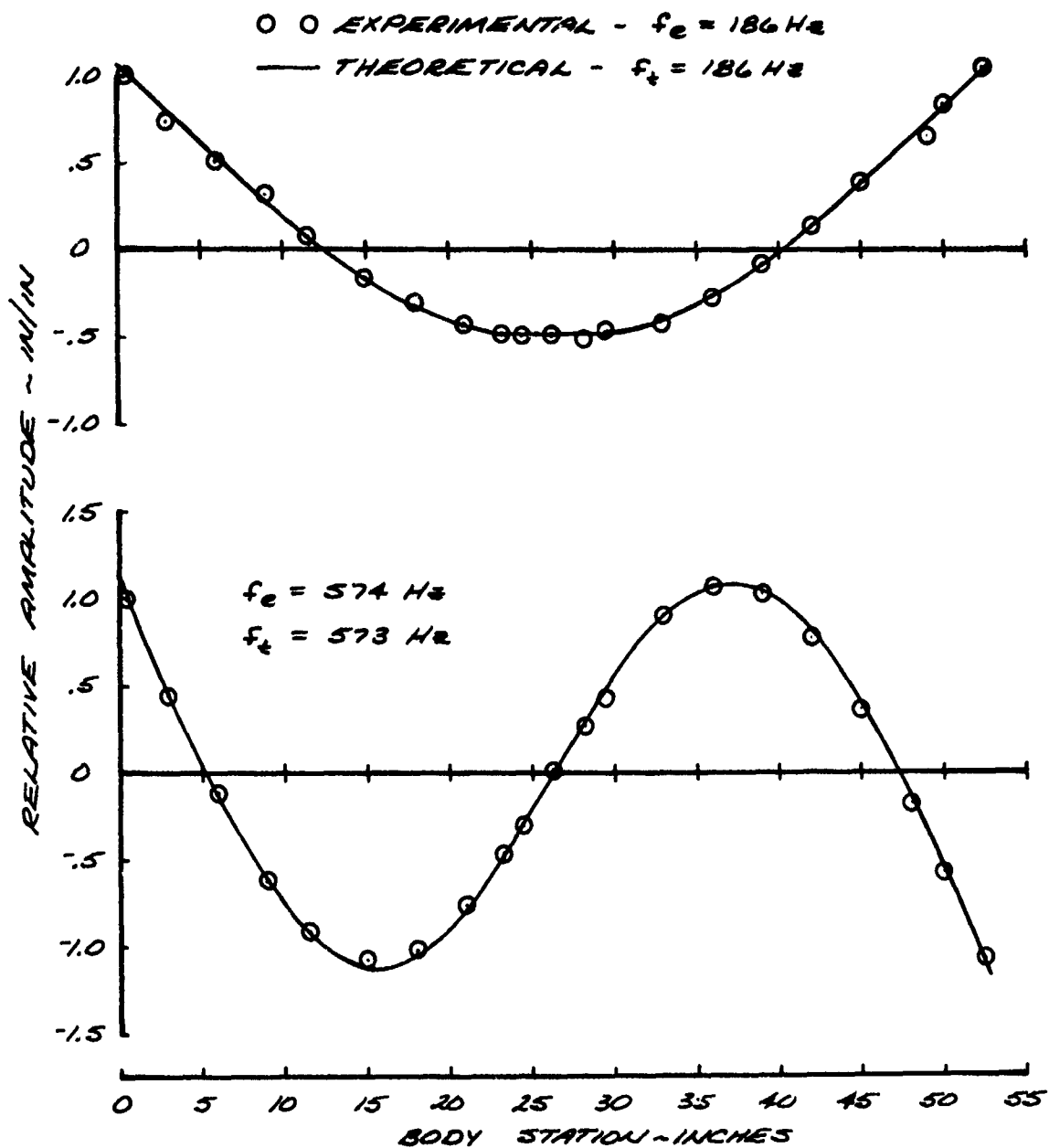
FIGURE 4-11

MARMON CLAMP JOINT
ANALYTICAL VS. EXPERIMENTAL MODES

O O $EXPERIMENTAL - f_e = 41.8 \, Hz$

—— $THEORETICAL - f_t = 41.6 \, Hz$

$f_e = 125 \, Hz$
$f_t = 129 \, Hz$

$f_e = 227 \, Hz$
$f_t = 234 \, Hz$

RELATIVE AMPLITUDE ~ IN/IN

BODY STATION ~ INCHES

49
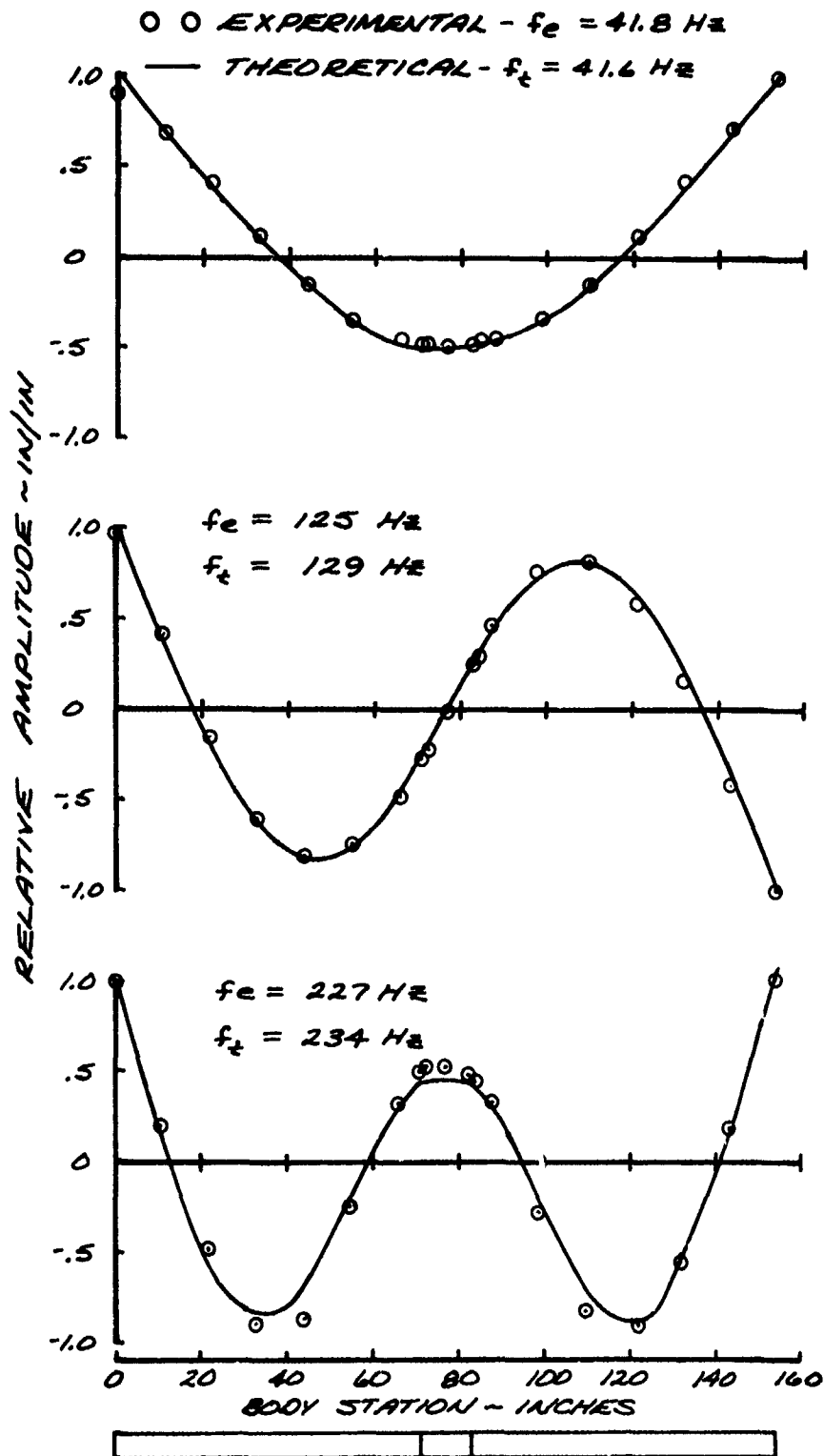
FIGURE 4-12

8.0 INCH DIAMETER SHEAR BOLT JOINT
TEST CONFIGURATION

JOINT

STEEL TUBE
(.083" THICK)

60

120

54

27.5

0.5

6 BULK HEADS LOCATED SYMMETRICALLY ABOUT
JOINT AS SHOWN (1/8" THICK STEEL)
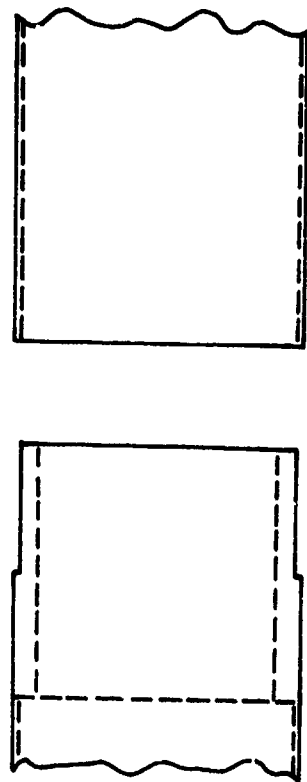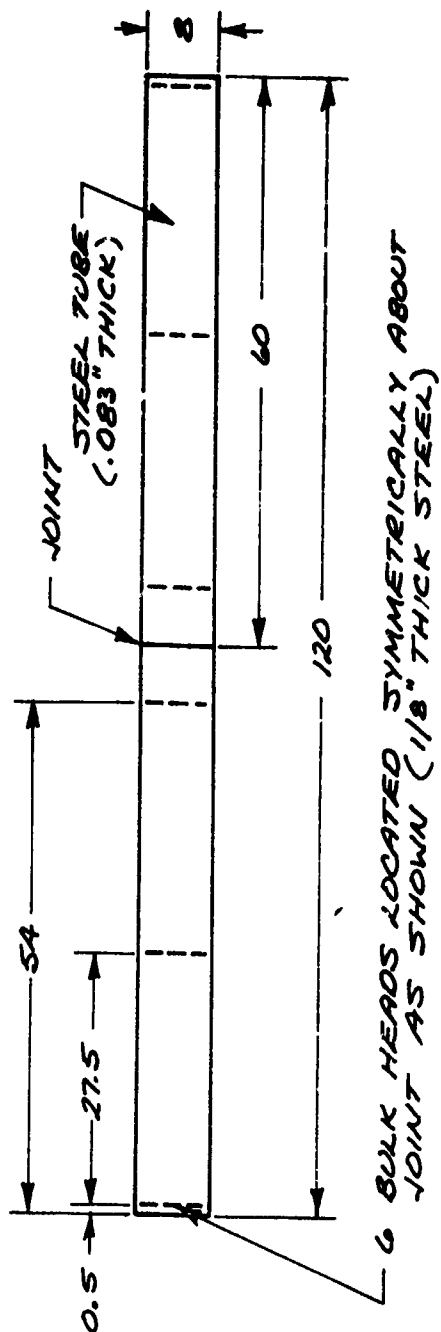
DETAIL OF MATING PARTS

FIGURE 4-13

8.0 INCH DIAMETER SHEAR BOLT JOINT

ANALYTICAL VS. EXPERIMENTAL MODES

O O EXPERIMENTAL - f_e = 86.9 Hz, 94. Hz *

— THEORETICAL - f_t = 89.6 Hz

f_e = 320. Hz

f_t = 321. Hz

f_e = 466. Hz, 476. Hz *

f_t = 465. Hz

RELATIVE AMPLITUDE ~ IN/IN

NON DIMENSIONAL LENGTH
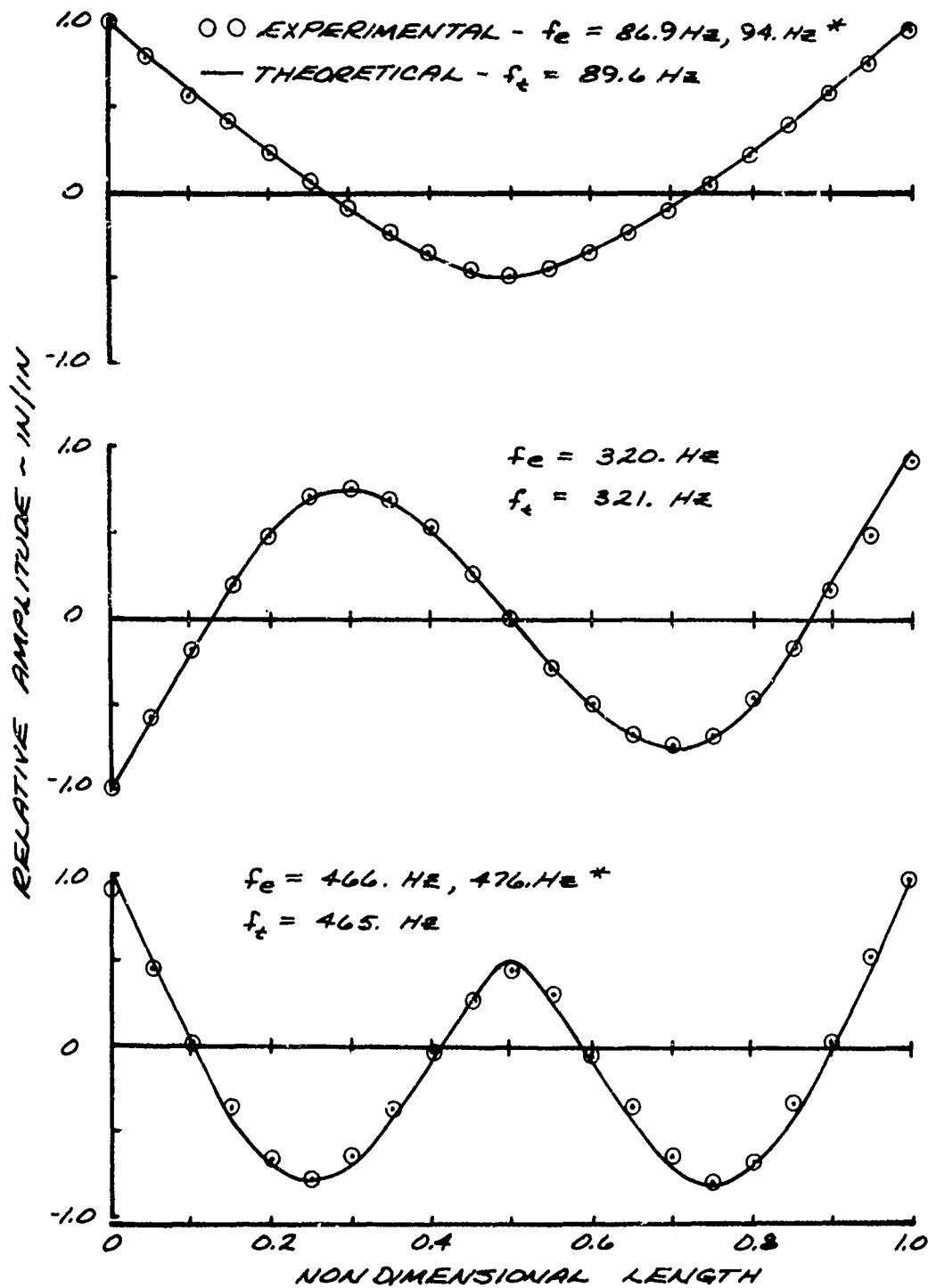
* DOUBLE PEAKED RESPONSES OCCURED NEAR THE FIRST AND THIRD MODES IN THE MEASURED FREQUENCY RESPONSE

FIGURE 4-14

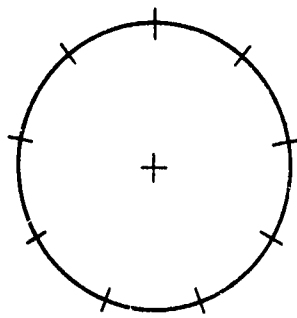13.5 INCH DIAMETER SHEAR BOLT JOINT
SPECIAL ALUMINUM SPACER

SCALE : 1" = 3"

SECTION A-A
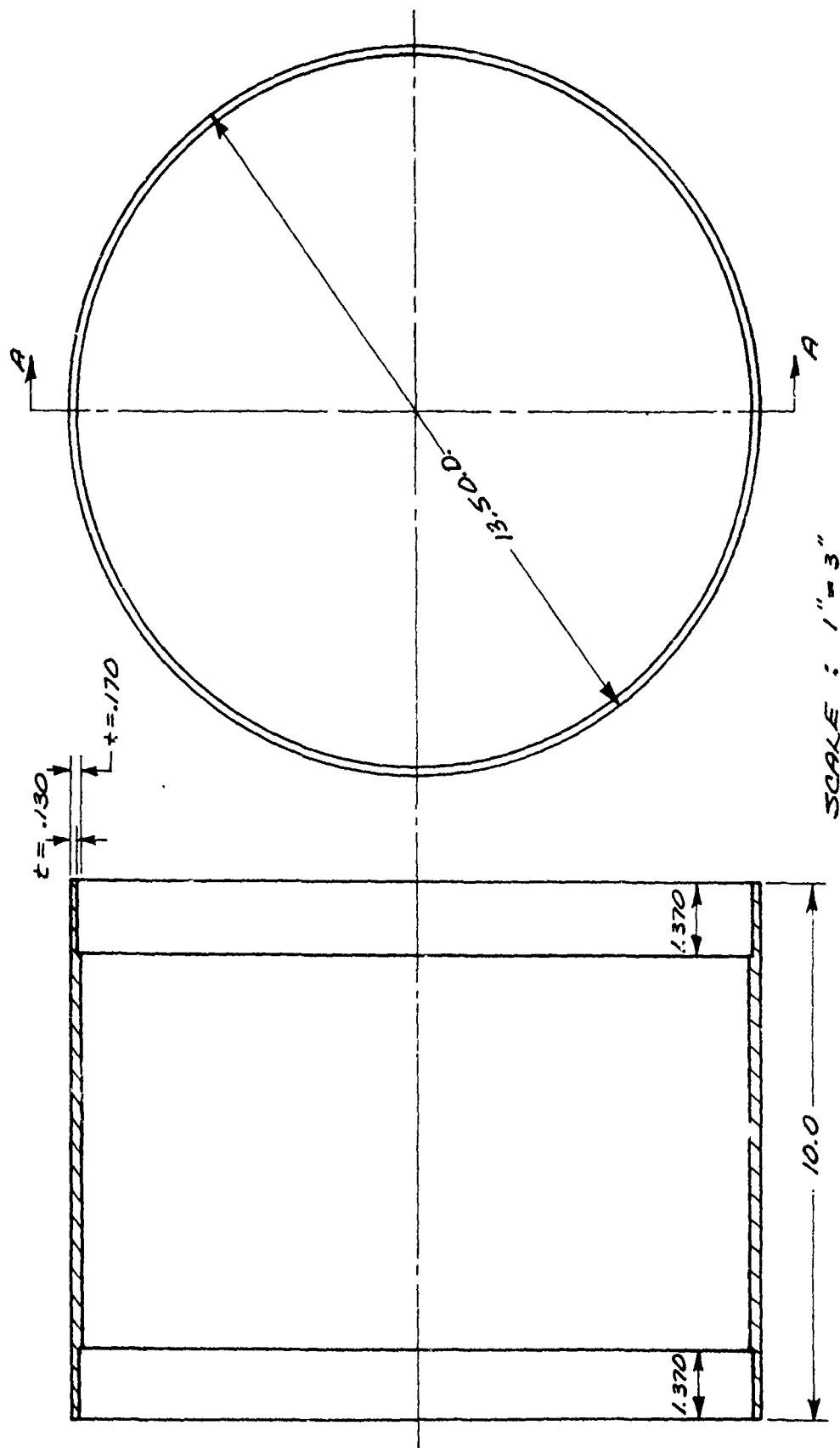
FIGURE 4-15

13.5 INCH DIAMETER SHEAR BOLT JOINT
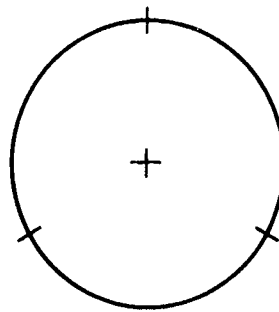FIVE FASTENER CONFIGURATIONS
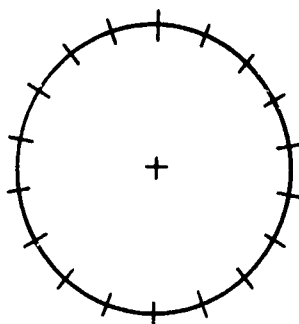
18 BOLTS
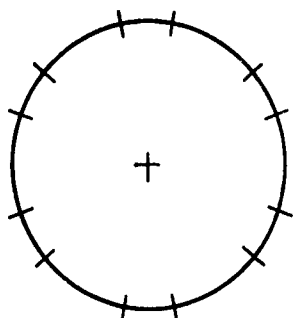
12 BOLTS
(NON- UNIFORM)

9 BOLTS

6 BOLTS

3 BOLTS

53
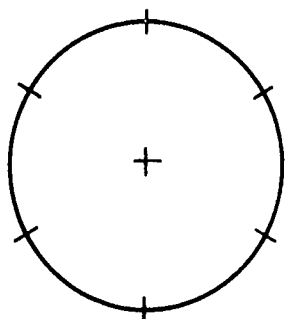
FIGURE 4-16

13.5 INCH DIAMETER SHEAR BOLT JOINT
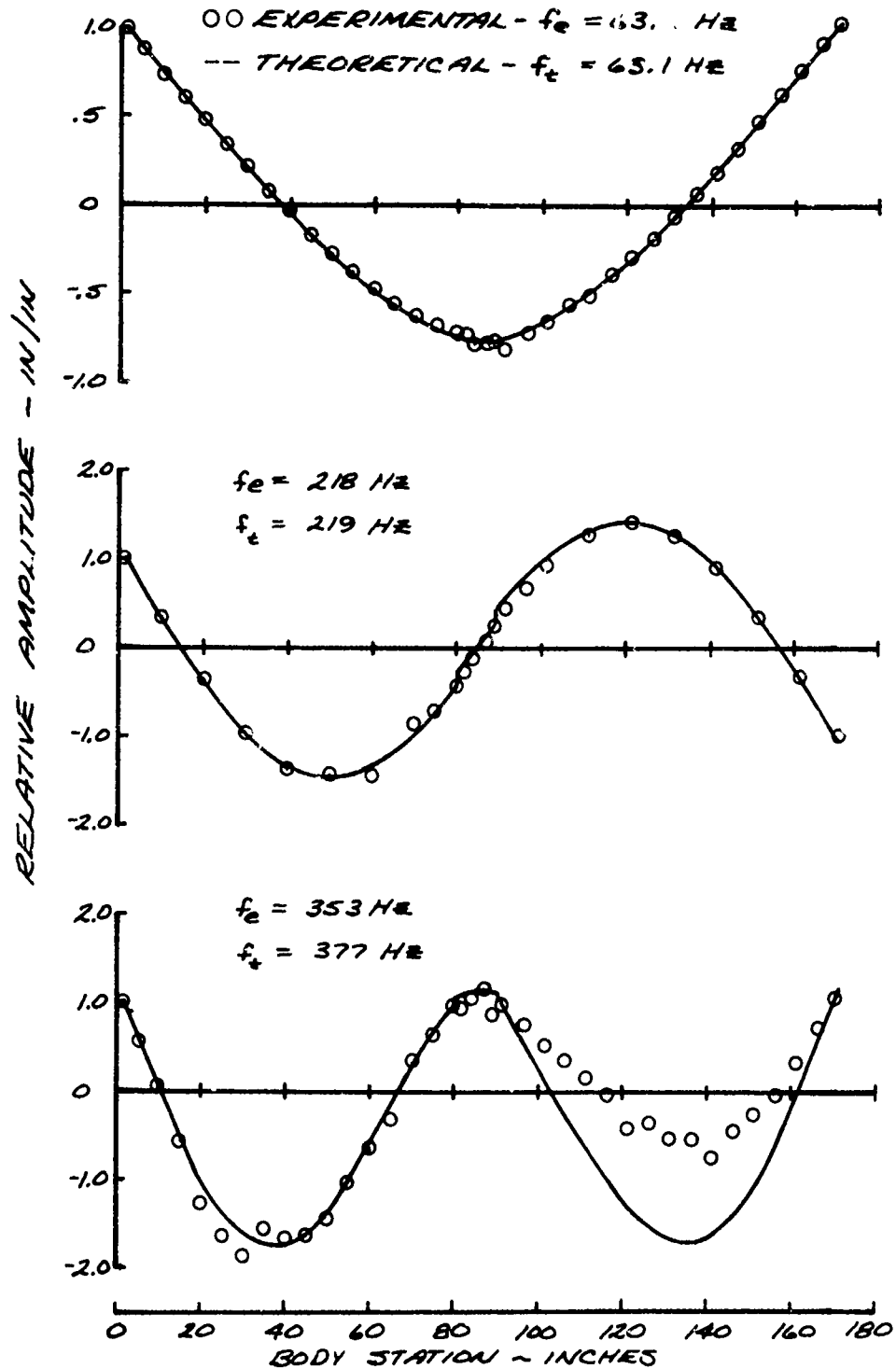EIGHTEEN FASTENER CONFIGURATION
ANALYTICAL VS. EXPERIMENTAL MODES

OO EXPERIMENTAL - f_e = 63. Hz
-- THEORETICAL - f_t = 65.1 Hz

f_e = 218 Hz
f_t = 219 Hz

f_e = 353 Hz
f_t = 377 Hz

RELATIVE AMPLITUDE ~ IN/IN

BODY STATION ~ INCHES

FIGURE 4-17

13.5 INCH DIAMETER SHEAR BOLT JOINT
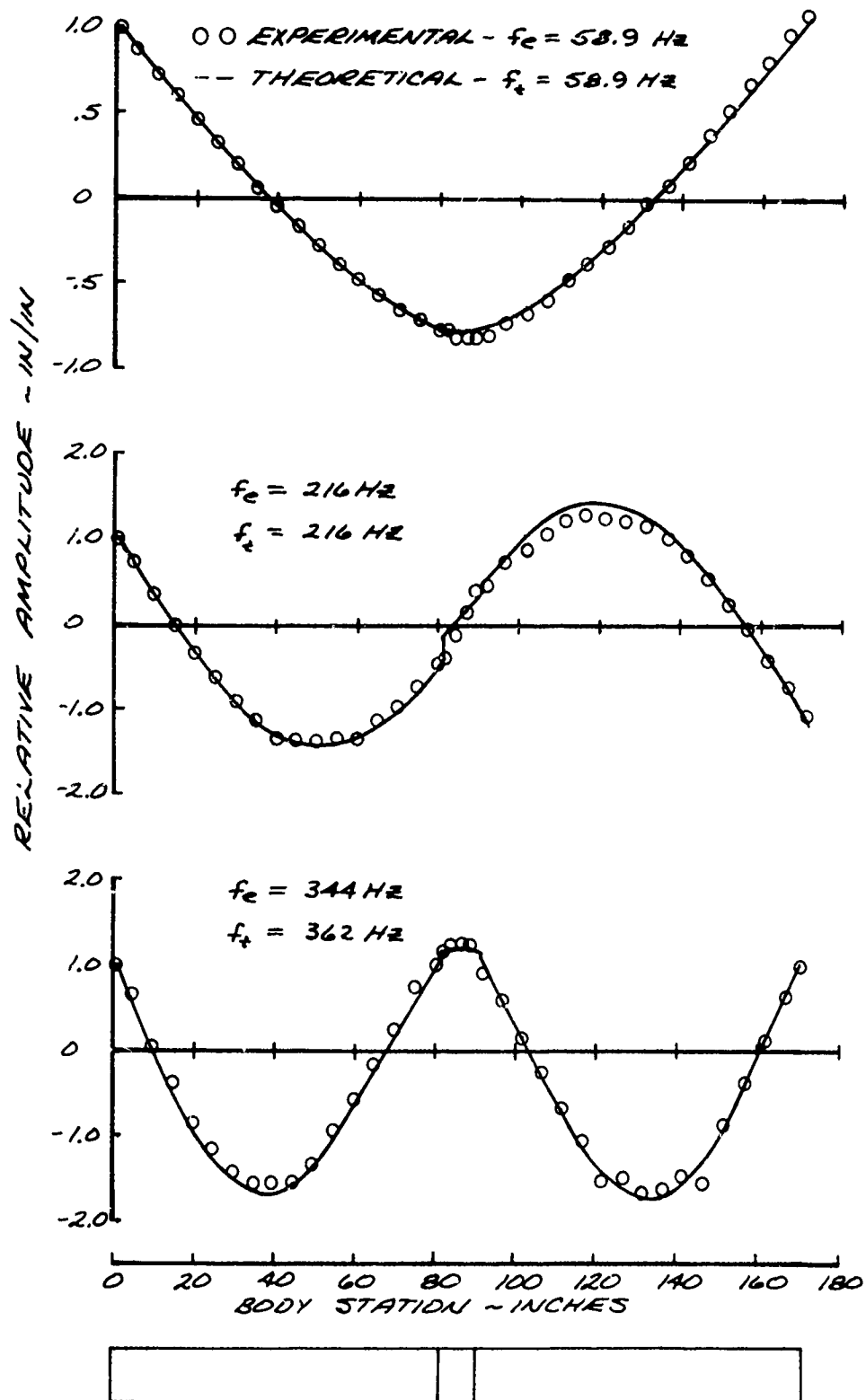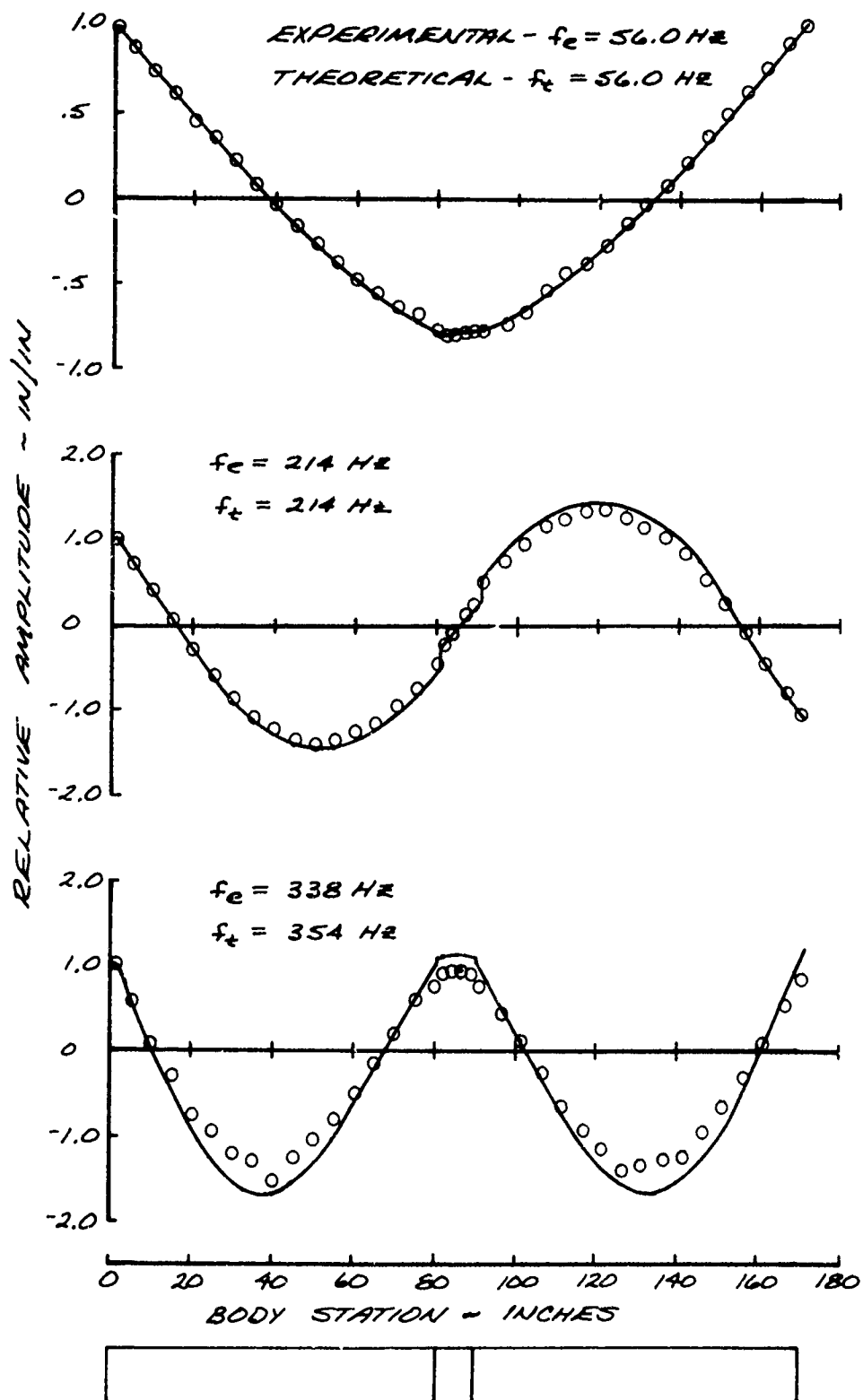TWELVE FASTENER CONFIGURATION
ANALYTICAL VS. EXPERIMENTAL MODES

O O EXPERIMENTAL - f_e = 58.9 Hz
-- THEORETICAL - f_t = 58.9 Hz

f_e = 216 Hz
f_t = 216 Hz

f_e = 344 Hz
f_t = 362 Hz

RELATIVE AMPLITUDE ~ IN/IN

BODY STATION ~ INCHES

FIGURE 4-18

13.5 INCH DIAMETER SHEAR BOLT JOINT
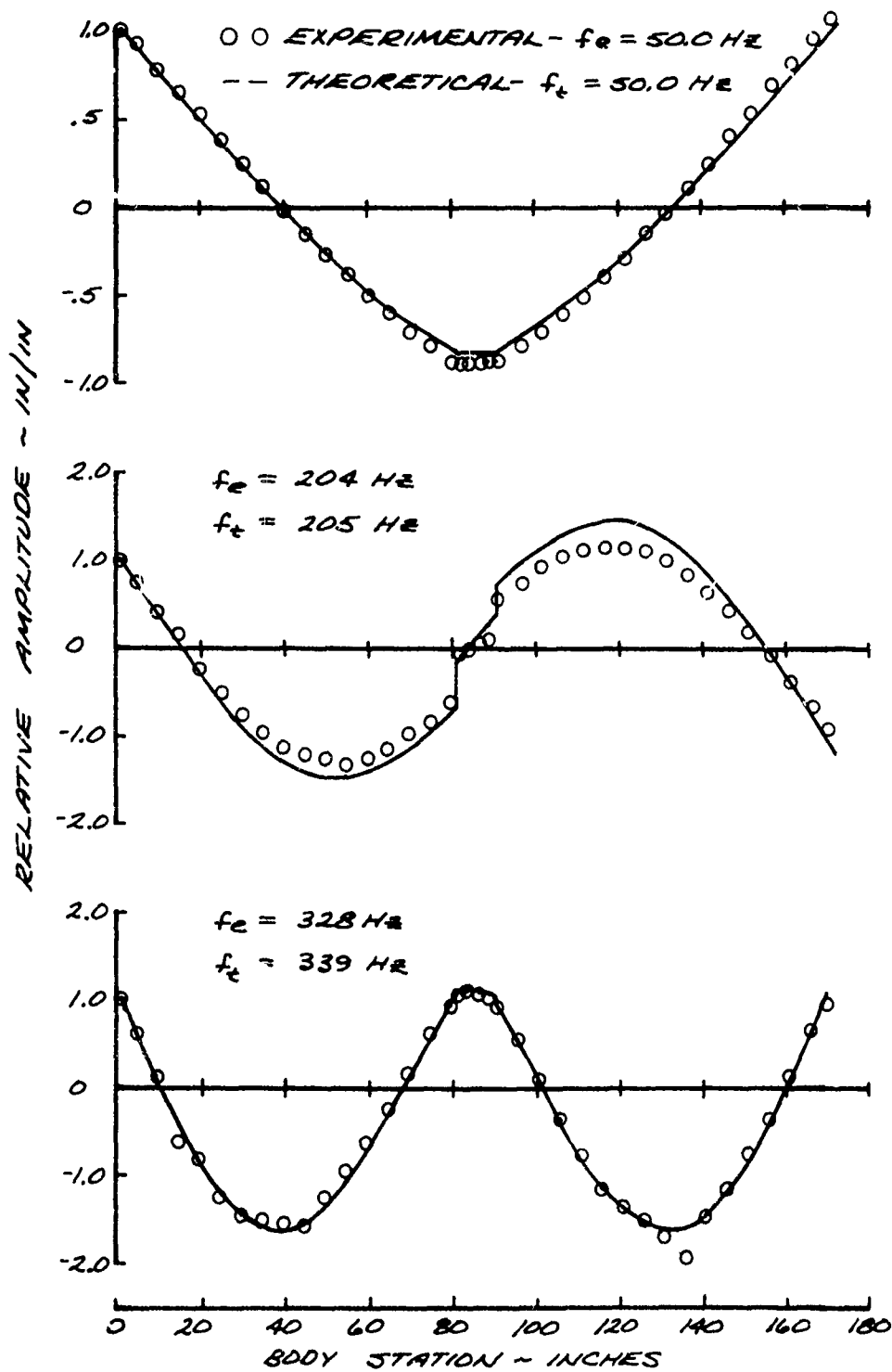NINE FASTENER CONFIGURATION
ANALYTICAL VS. EXPERIMENTAL MODES

EXPERIMENTAL - $f_e = 56.0$ Hz
THEORETICAL - $f_t = 56.0$ Hz

$f_e = 214$ Hz
$f_t = 214$ Hz

$f_e = 338$ Hz
$f_t = 354$ Hz

RELATIVE AMPLITUDE ~ IN/IN

BODY STATION ~ INCHES

56

FIGURE 4-19

13.5 INCH DIAMETER SHEAR BOLT JOINT

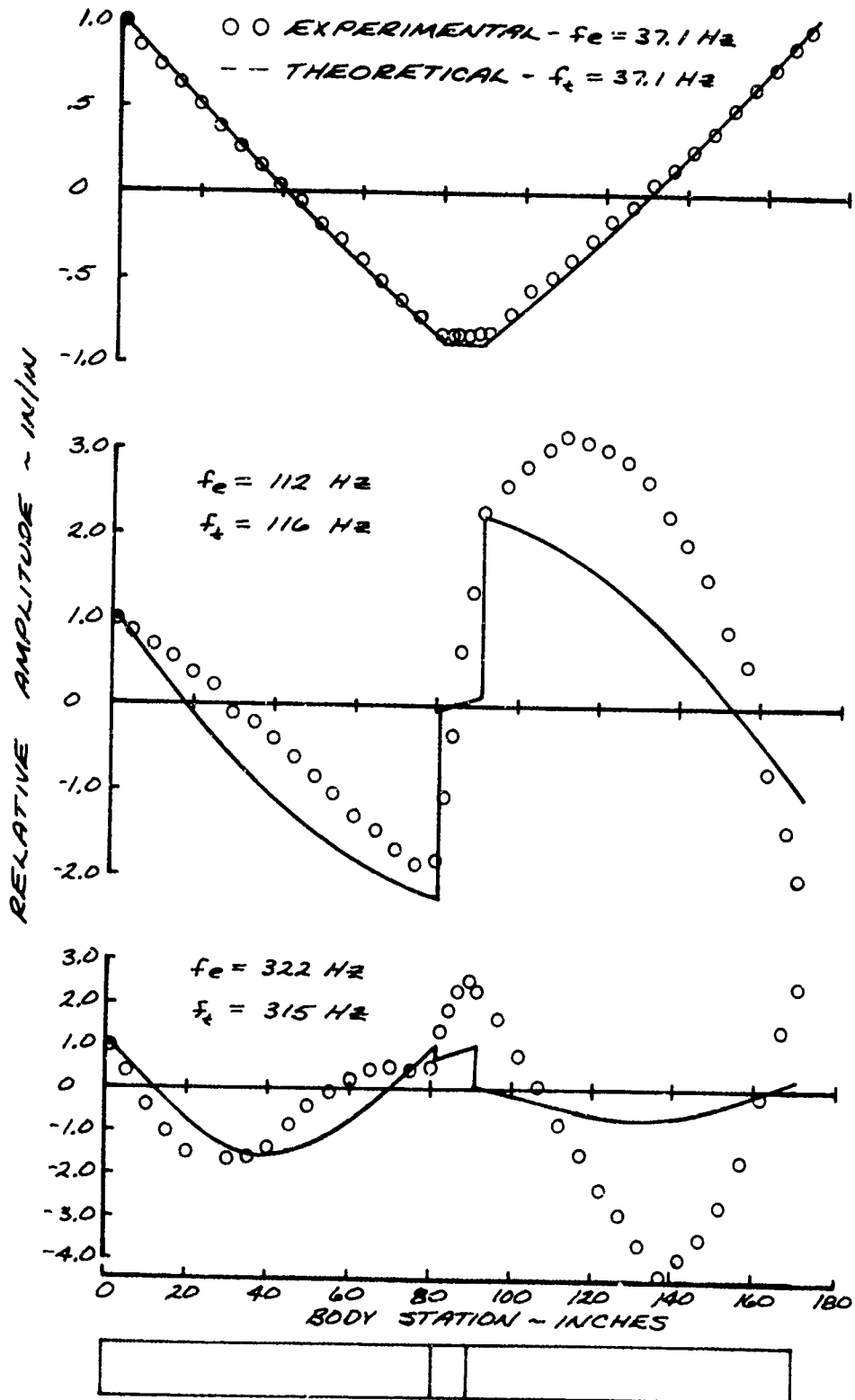SIX FASTENER CONFIGURATION

ANALYTICAL VS. EXPERIMENTAL MODES

O O EXPERIMENTAL - f_e = 50.0 Hz

— — THEORETICAL - f_t = 50.0 Hz

f_e = 204 Hz

f_t = 205 Hz

f_e = 328 Hz

f_t = 339 Hz

BODY STATION ~ INCHES

RELATIVE AMPLITUDE ~ IN/IN

57

FIGURE 4-20
13.5 INCH DIAMETER SHEAR BOLT JOINT
THREE FASTENER CONFIGURATION
ANALYTICAL VS. EXPERIMENTAL MODES

○ ○ EXPERIMENTAL - $f_e = 37.1\,Hz$
-- THEORETICAL - $f_t = 37.1\,Hz$

$f_e = 112\,Hz$
$f_t = 116\,Hz$

$f_e = 322\,Hz$
$f_t = 315\,Hz$

RELATIVE AMPLITUDE ~ IN/IN

BODY STATION ~ INCHES

FIGURE 4-21

13.5 INCH DIAMETER SHEAR BOLT JOINT

THREE FASTENER CONFIGURATION
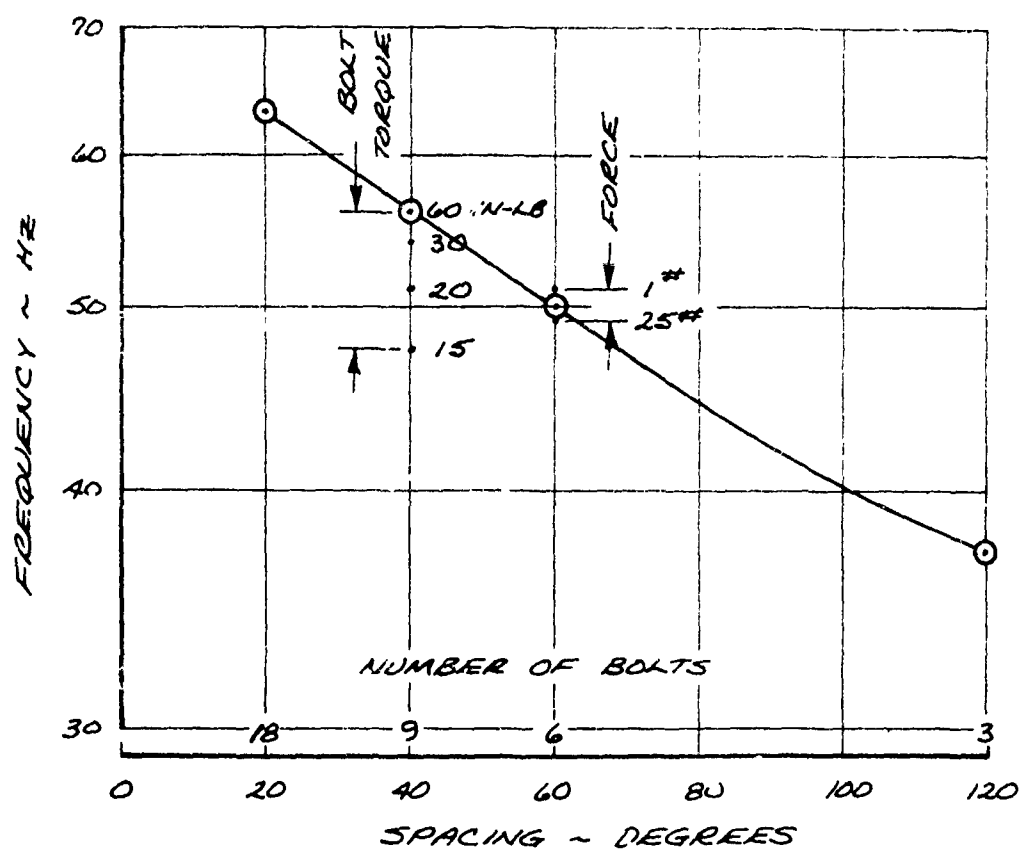
EXAMPLE OF FIRST MODE WAVE FORM DISTORTION
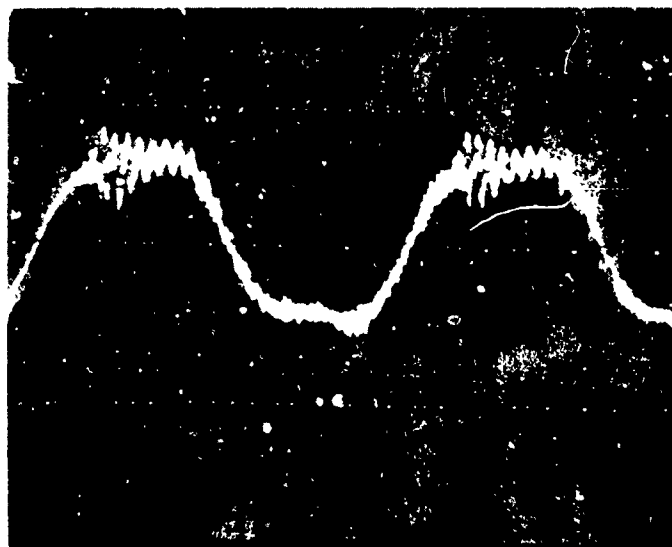
VERTICAL CALIBRATION : 1g / DIVISION

HORIZONTAL CALIBRATION : .005 SEC/DIVISION

FIGURE 4-22

13.5 INCH DIAMETER SHEAR BOLT JOINT
FIRST MODE FREQUENCY VS. NUMBER OF BOLTS

60

FIGURE 4-23

13.5 INCH DIAMETER SHEAR BOLT JOINT
FLEXURAL COMPLIANCE VS. NUMBER OF FASTENERS

⬡ JOINT 1 (STA. 81)
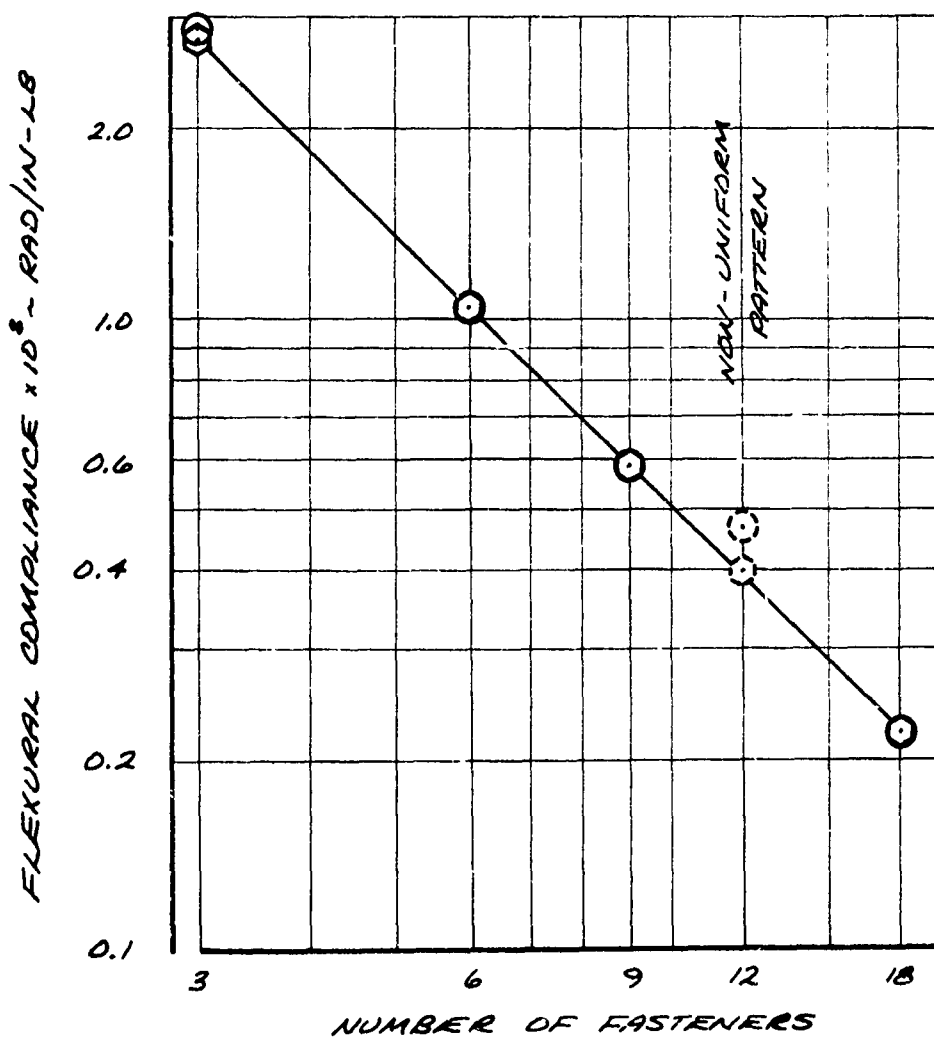◯ JOINT 2 (STA. 90)

FIGURE 4-24

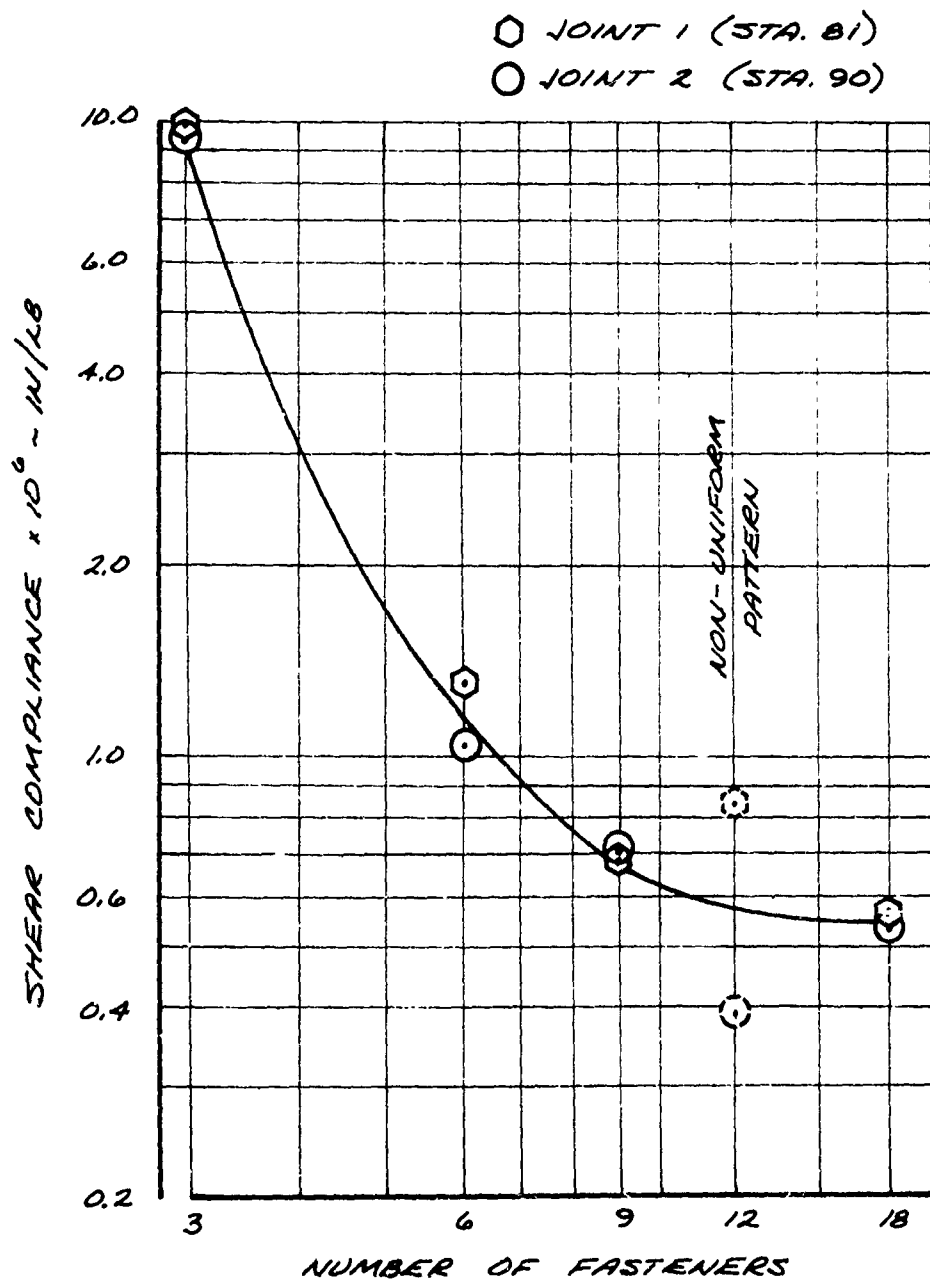13.5 INCH DIAMETER SHEAR BOLT JOINT
SHEAR COMPLIANCE VS. NUMBER OF FASTENERS

62

FIGURE 4-25

13.5 INCH DIAMETER SHEAR BOLT JOINT
SIX AND NINE BOLT CONFIGURATIONS
FLEXURAL COMPLIANCE VS. BOLT TORQUE
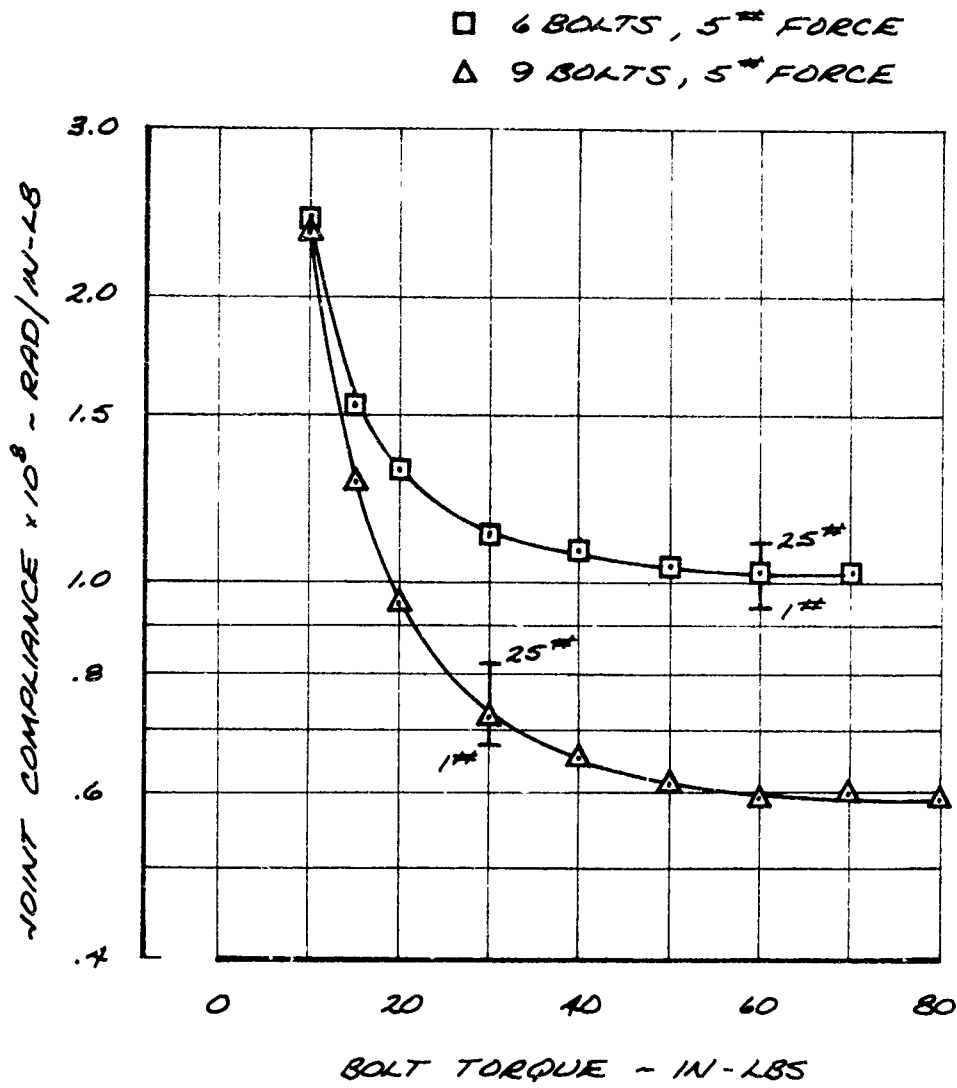
□ 6 BOLTS, 5# FORCE
△ 9 BOLTS, 5# FORCE

FIGURE 4-26

13.5 INCH DIAMETER SHEAR BOLT JOINT
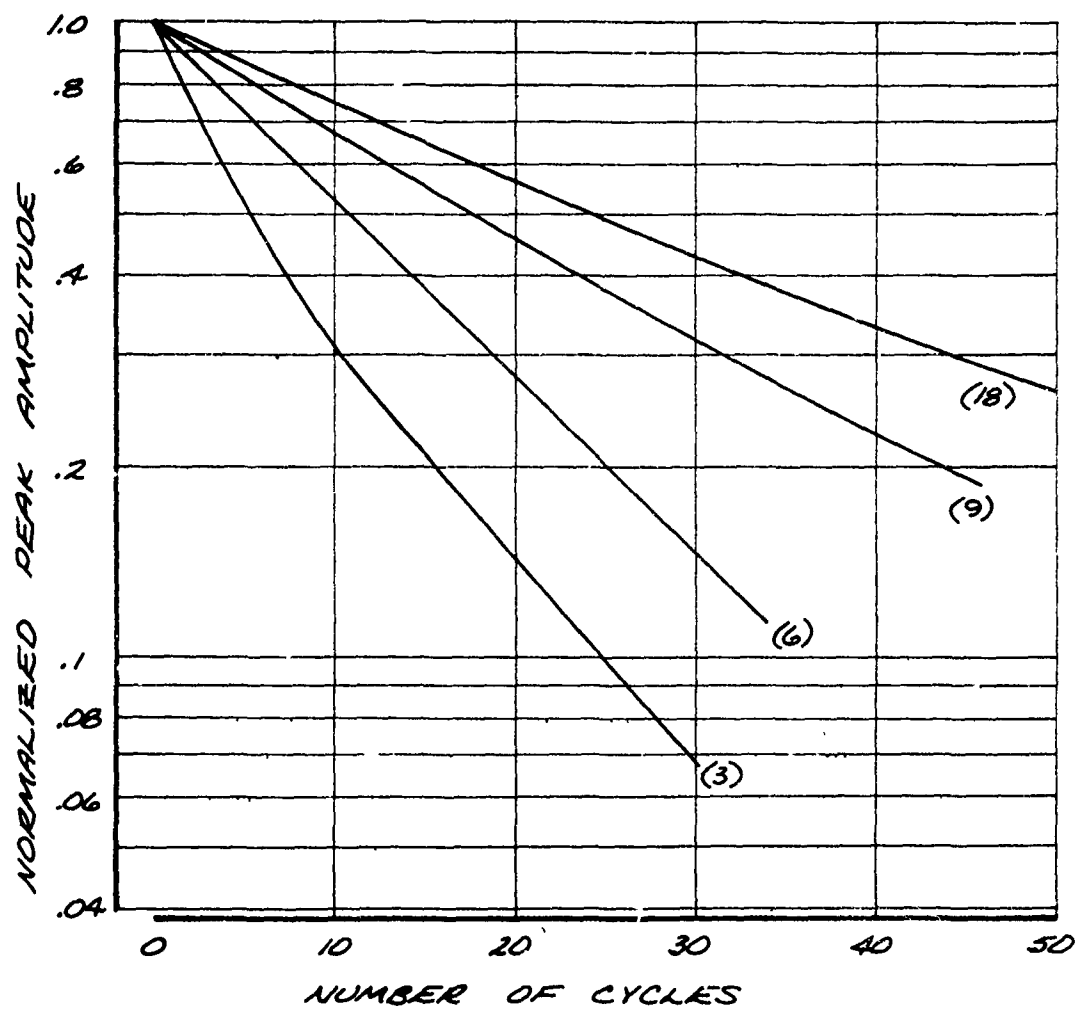NORMALIZED DECAYING PEAK RESPONSE
FOR VARIOUS BOLT PATTERNS

FIGURE 4-27

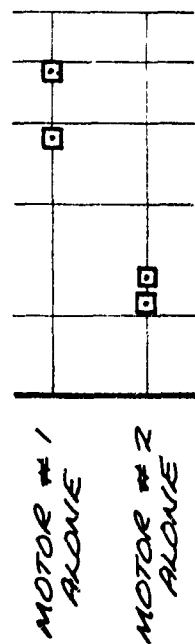13.5 INCH DIAMETER SHEAR BOLT JOINT
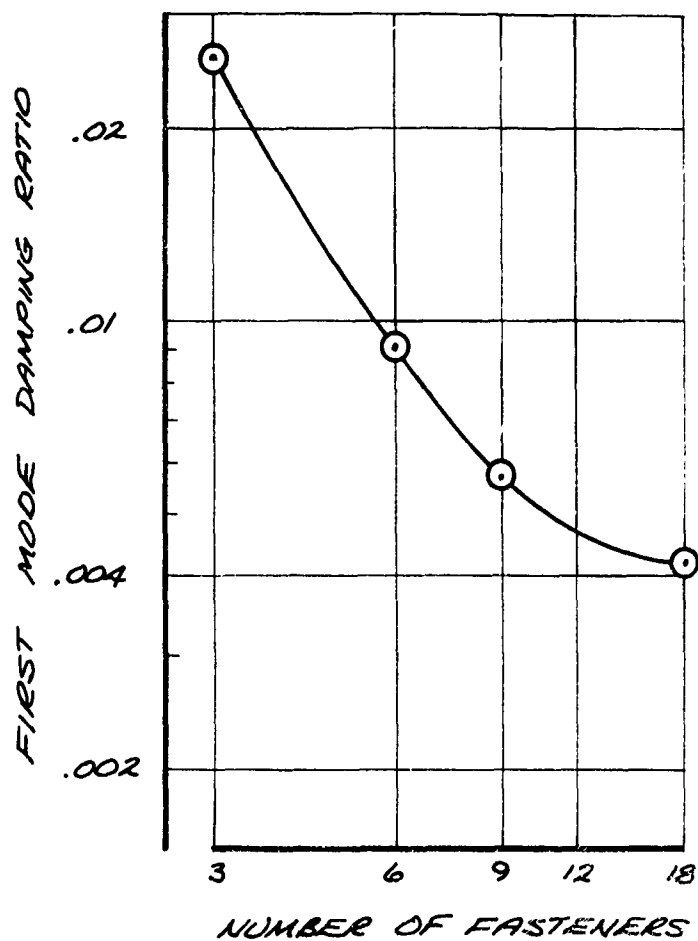DAMPING VS. NUMBER OF FASTENERS

FIGURE 4-28

13.5 INCH DIAMETER SHEAR BOLT JOINT
DAMPING VS. BOLT TORQUE
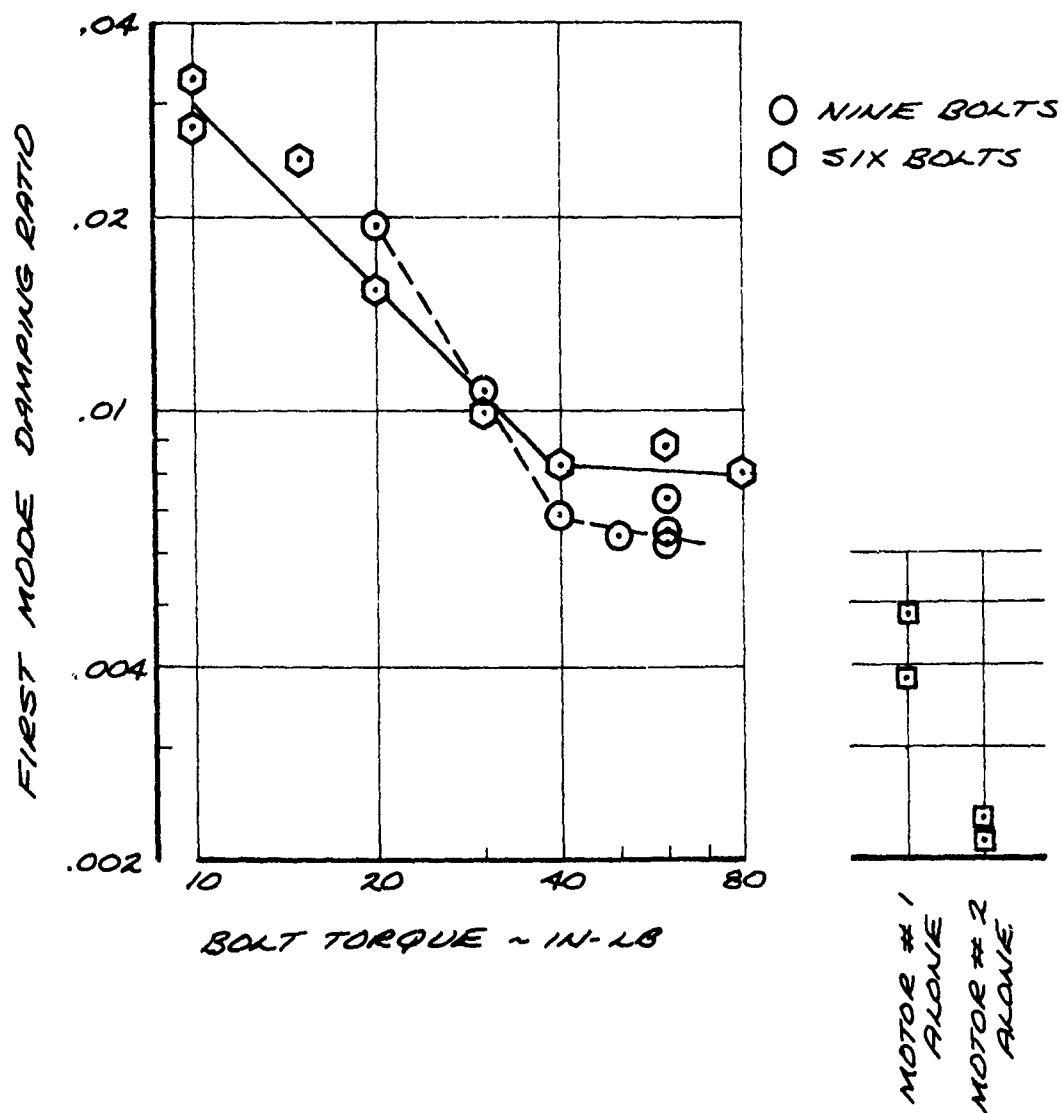
FIGURE 4-29

13.5 INCH DIAMETER SHEAR BOLT JOINT
FLEXURAL COMPLIANCE VS. NUMBER
OF FASTENERS FOR VARIOUS ANGULAR SPACINGS

O BASIC PATTERNS TESTED

△ SPECIAL PATTERNS TESTED
    (SEE FIGURE 4-30)
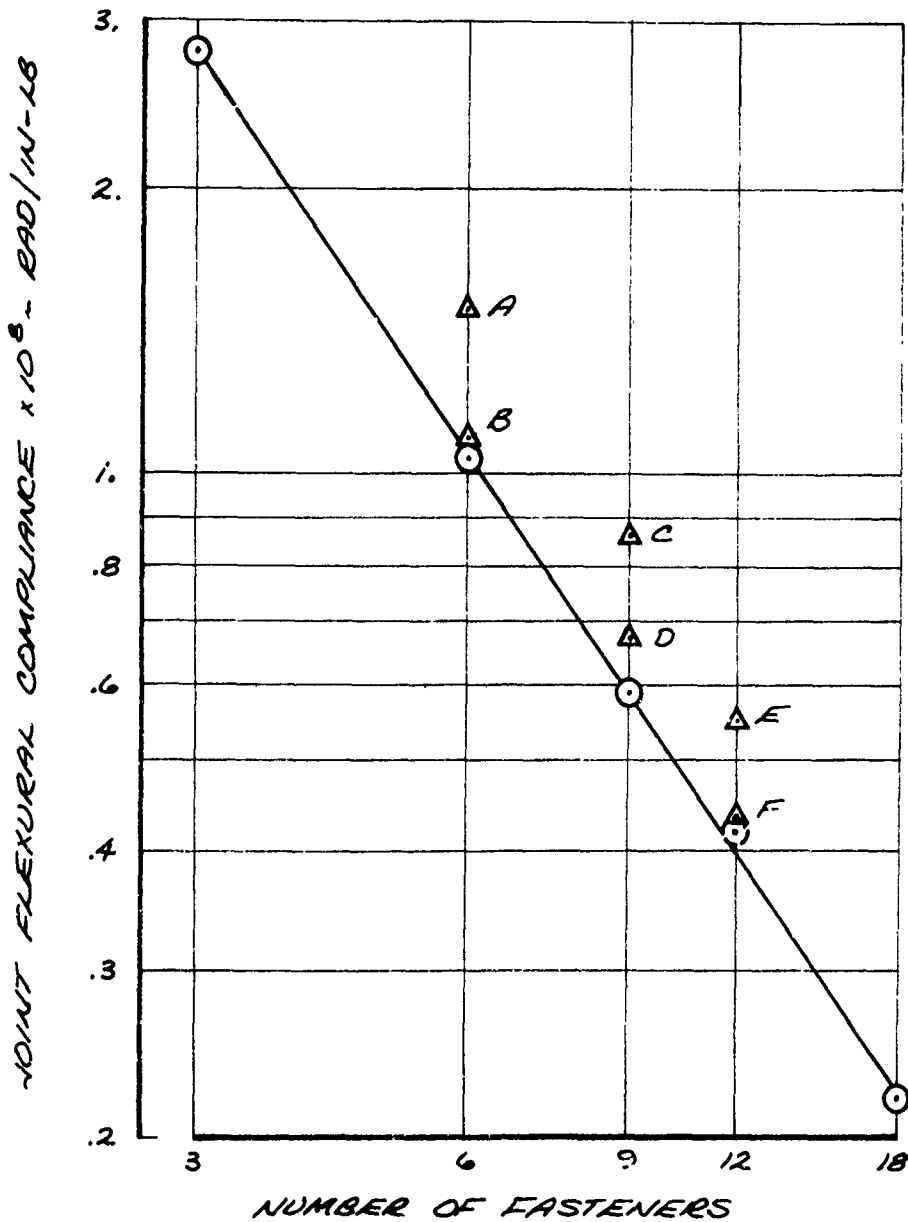
FIGURE 4-30

13.5 INCH DIAMETER SHEAR BOLT JOINT

SPECIAL BOLT PATTERNS

6 BOLTS	9 BOLTS	12 BOLTS
BASIC	BASIC	BASIC
A	C	E
B	D	F
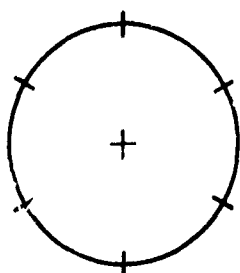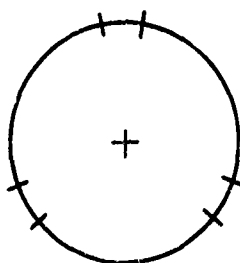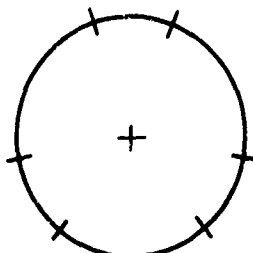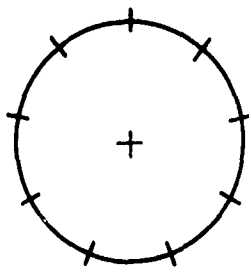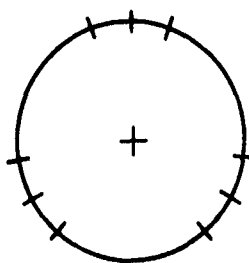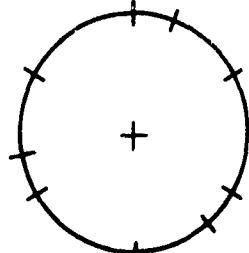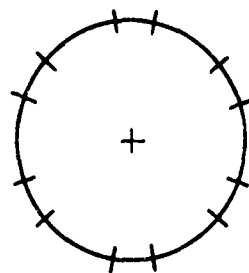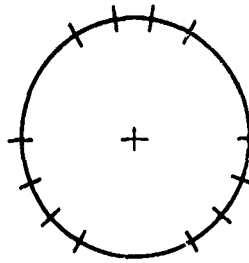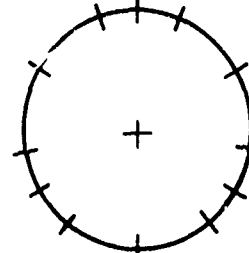
FIGURE 4-31

STANDARD MISSILE AIRFRAME
TEST ASSEMBLY
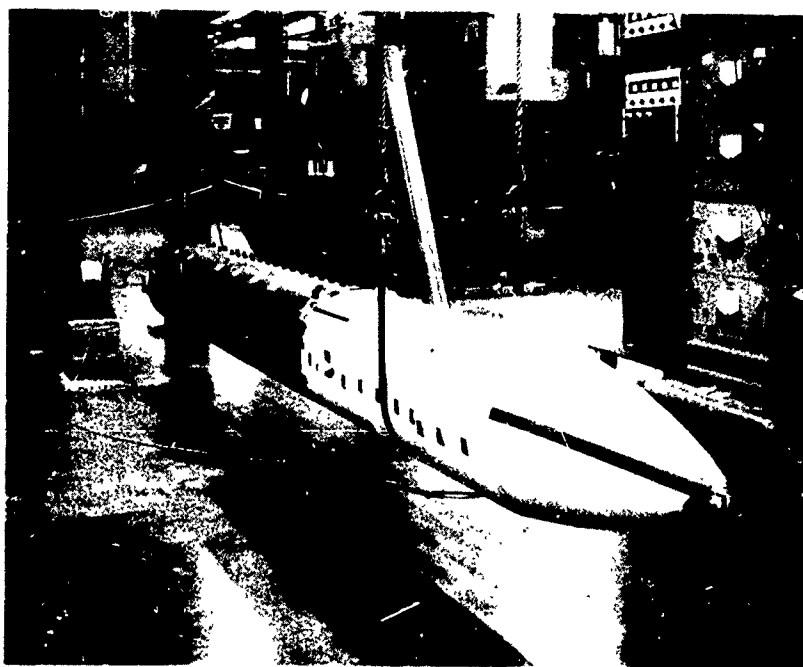
FIGURE 4-32
STANDARD MISSILE AIRFRAME
ANALYTICAL VS. EXPERIMENTAL MODES

OO EXPERIMENTAL - f_e = 80.0 Hz
THEORETICAL - f_t = 78.9 Hz

f_e = 224 Hz
f_t = 236 Hz

f_e = 357 Hz
f_t = 378 Hz

RELATIVE AMPLITUDE ~ IN/IN

MISSILE STATION ~ INCHES
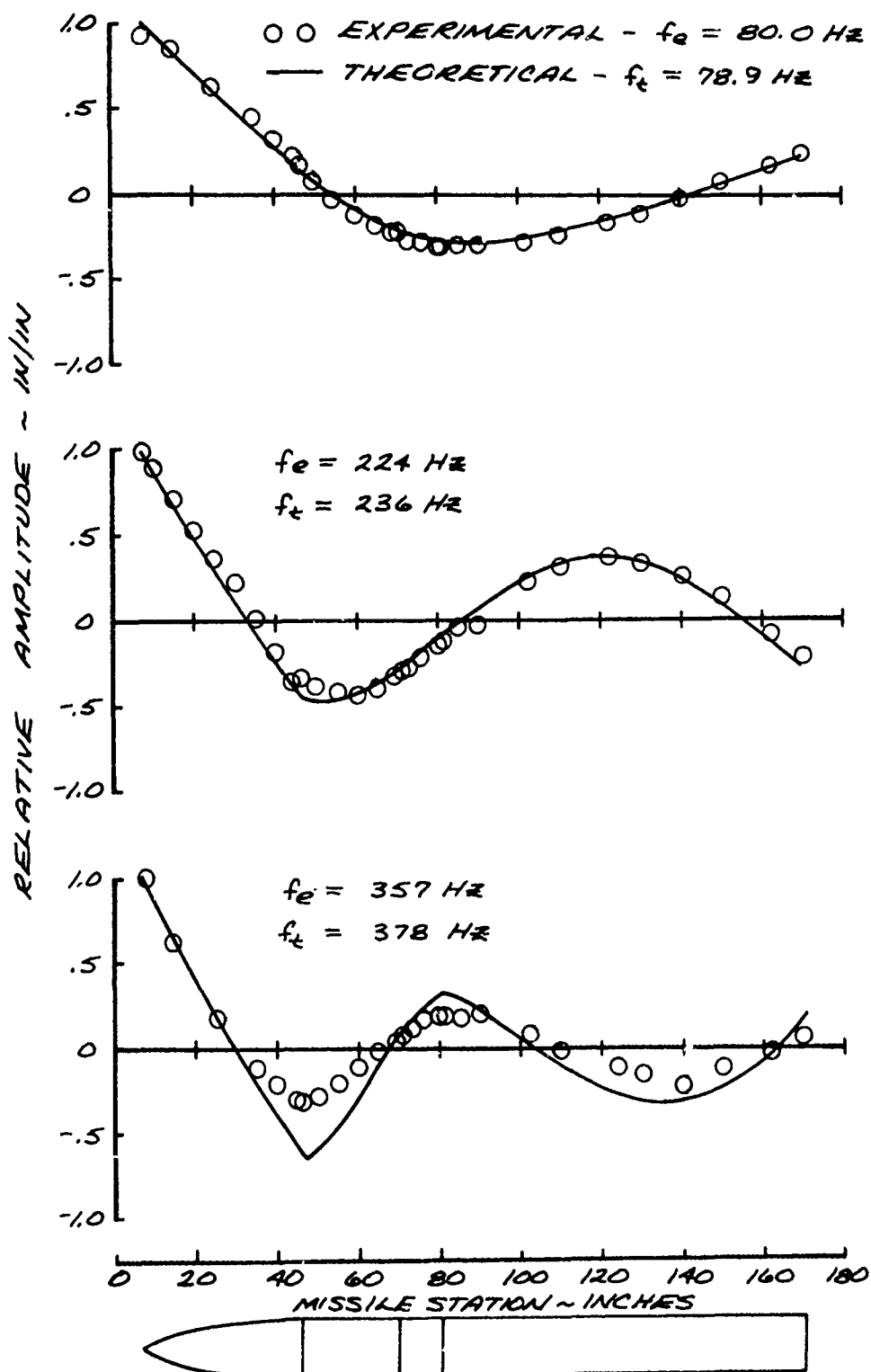
FIGURE 4-33

COMPARISON OF DERIVED FLEXURAL COMPLIANCES
WITH NASA RATING

△ THREADED COUPLING RING JOINT (FIG. 4-1)
□ MARMON CLAMP JOINT (FIG. 4-2)
○ EIGHT FASTENER SHEAR BOLT JOINT (FIG. 4-3)
● EIGHTEEN FASTENER SHEAR BOLT JOINT (FIG. 4-4)
■ CONTINUOUS LAND RING JOINT (FIG. 4-5)
⬡ FOUR FASTENER TENSION BOLT JOINT (FIG. 4-6)
▽ EIGHT FASTENER TENSION BOLT JOINT (FIG. 4-7)
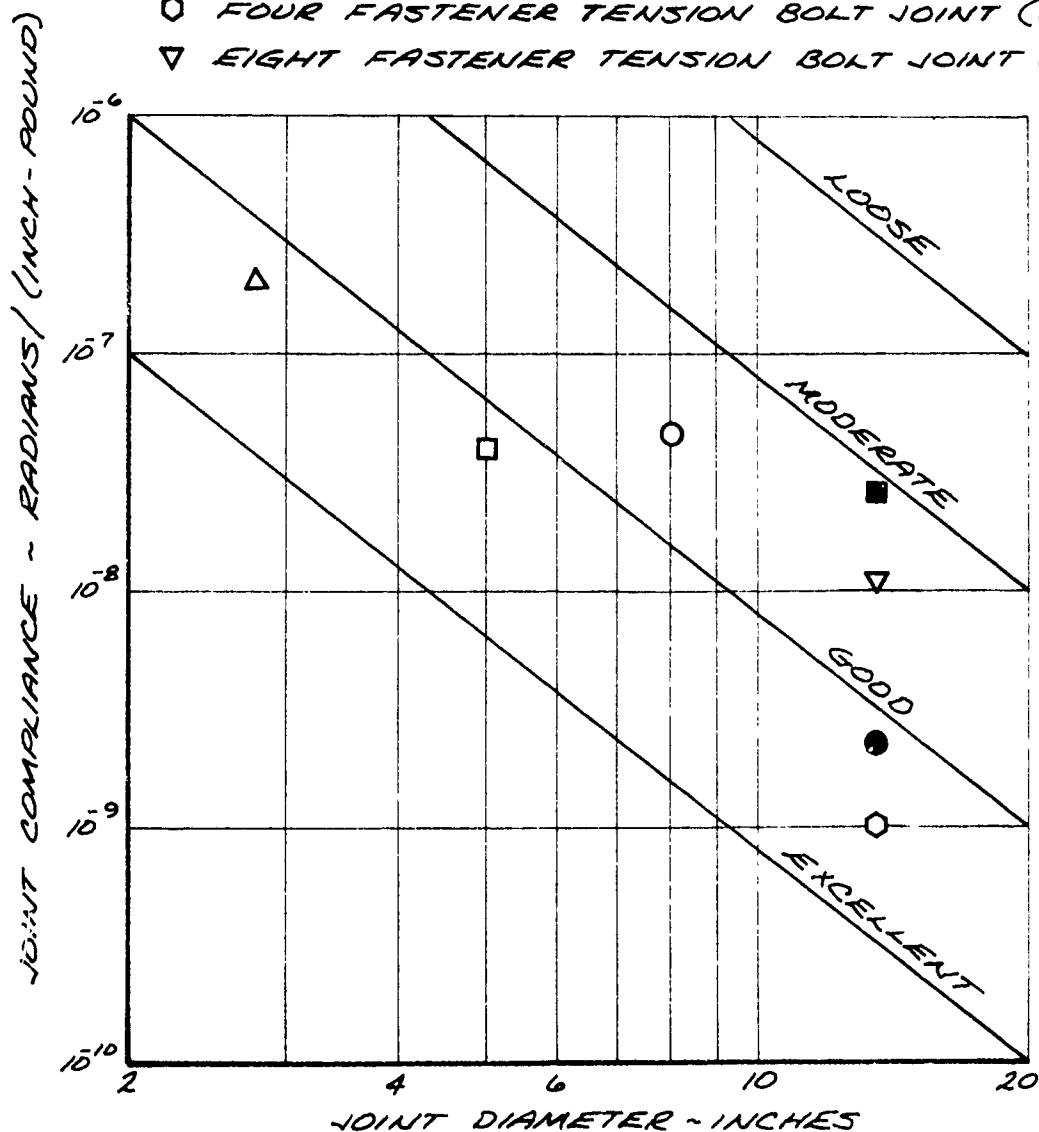
FIGURE 4-34

COMPARISON OF THE 8.0 INCH AND 13.5 INCH
DIAMETER SHEAR BOLT JOINT COMPLIANCES

⬡, ◯ 13.5 INCH DIAMETER TEST DATA
◼ 8.0 INCH DIAMETER TEST DATA

NUMBER OF FASTENERS
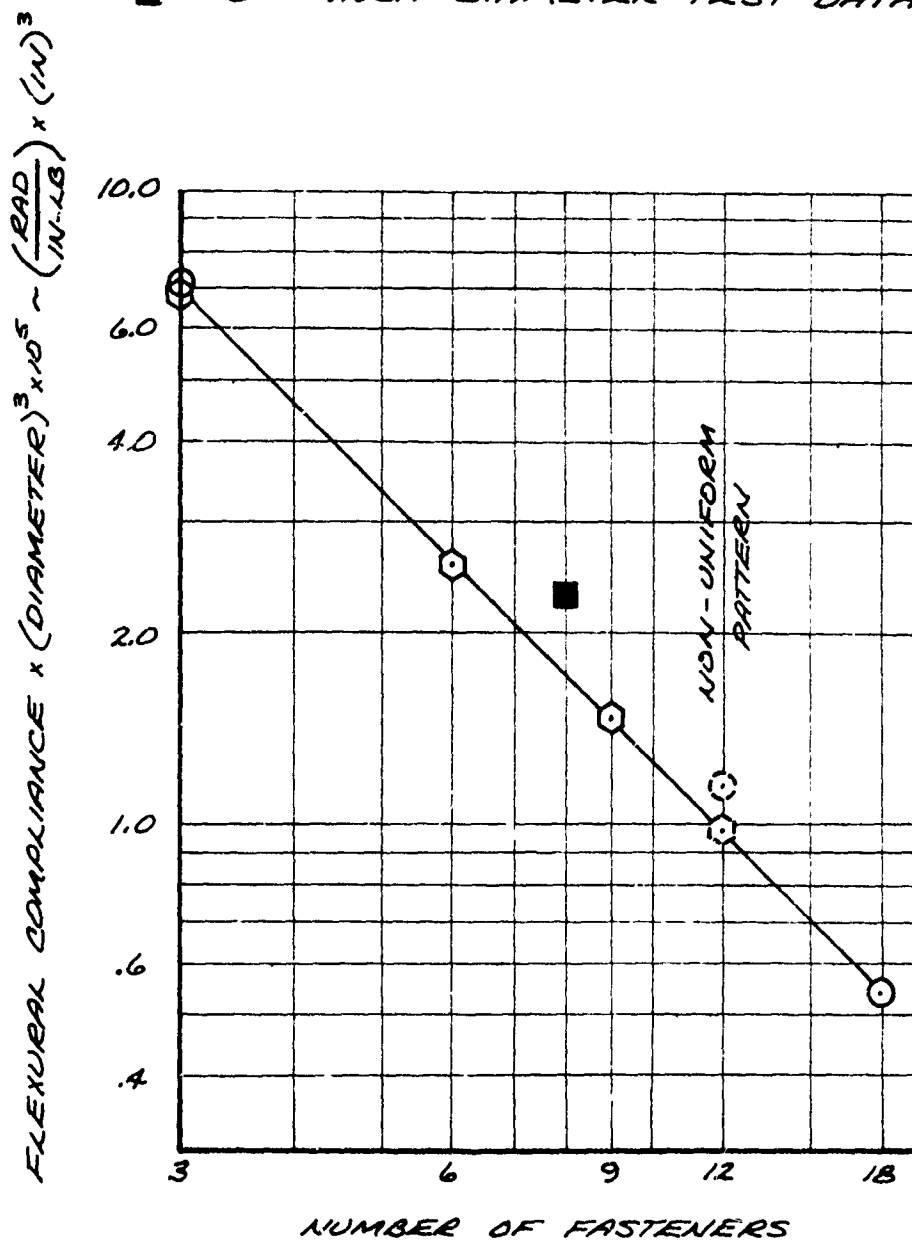
Section 5.0

FINITE ELEMENT ANALYSIS

In recent years many investigators have shown finite element methods to be very powerful tools in structural analysis. The intent of this section is to explore the application of these methods to the prediction of tactical missile mechanical joint properties. For this purpose, the 13.5 inch diameter shear bolt joint configuration described in section 4.2.4 was chosen to be analyzed using conical shell elements. The analysis was performed with the NASTRAN computer code (References 6 and 8), which utilizes the direct stiffness method of finite element analysis.

5.1 MODEL DEVELOPMENT

The structure which was analyzed consisted of two rocket motors connected by a specially fabricated spacer. This structure was deliberately made geometrically symmetric with respect to a plane passing through the center of the spacer and perpendicular to its centerline. Three variations of the shear bolt joint, located at the interface of the rocket motors and spacer, were considered in the analysis. These were the three, six, and nine bolt configurations shown in Figure 5-1. The bolt placements of each joint had geometric symmetry with respect to plane A-A, which contains the centerline of the structure.

Portions of the structure which are greater than approximately one diameter away from the shear bolt joint are uniform, thin shells. When the structure is subjected to mechanical loads, the deformational behavior of this region essentially satisfies the Kirchoff-Love assumptions of thin elastic shell theory. These assumptions are:

1. The thickness of the shell is small compared to the smallest radius of curvature of the shell.

2. Deflections of the shell are small.

3. Transverse normal stress is negligible.

4. Normals to the reference surface of the shell remain normal to it during deformation.

Based upon these assumptions, the stress distribution across the thickness of the structure in this region is linear. The portion of the structure in the vicinity of the joint does not satisfy the Kirchoff-Love assumptions, however. This is due to the complicated geometry of the structure in this region. There are abrupt changes in the thickness of the

73

structure, and the load paths between the spacer and the rocket motor are significantly altered by the bolts in the joint. The resulting stress distribution in the structure near the joint, therefore, varies nonlinearly across the thickness of the structure.

In order to predict the bending compliance of the shear bolt joint due to an applied bending moment in the A-A plane at each rocket motor end, a finite element idealization of the structure was made. Conical shell elements were considered to be best suited for the structural idealization in this non-axisymmetric elasticity problem since Fourier series are used to describe he displacement and rotation fields. Therefore, the model of the structure consisted of conical shell elements to represent the rocket motors and spacer, with provisions for discrete springs to represent the bolts of the joint. Because the structure had geometric and applied load symmetry with respect to a plane perpendicular to the structure centerline and passing through the middle of the spacer, only one-half of the structure needed to be idealized. Since the bending moment is constant at each cross section of the structure, only a three diameter length of the half structure was idealized. A ten inch long section of the structure modeled is shown in Figure 5-2. The bending moment was applied at the end of the modeled structure and was far enough removed from the shear bolt joint to be in the region of linear stress variation at the cross-section of the structure.

Since the force-deflection properties of the conical shell elements result in a linear stress distribution across their thickness, the structural idealization using these elements would not be representative of the force-deflection characteristics of the structure in the region of the joint. This difficulty was compensated for, however, by considering the following auxiliary problem. Let the ten inch long portion of the structure in Figure 5-2 be subjected to an enforced axial displacement of 0.010 inch at station ten. Assume the structure to be continuous at the shear bolt joint, i.e., the discrete bolts are replaced by an axisymmetric connector between the rocket motor and spacer. Since this structure and the loading are axisymmetric, it can be idealized with finite elements in two ways. The structure can be represented by triangular and trapezoidal solid of revolution elements, and also, it can be represented by conical shell elements. The representation of this structure by solid of revolution elements has the advantage of being able to closely approximate the nonlinear stress distribution which occurs due to the complicated geometry in the region of the joint. This is due to the fact that many of these finite elements can be placed across the thickness of the structure, resulting in a good piecewise approximation to the nonlinear stress distribution. By comparing the deformations predicted using the solid of revolution element model and the conical shell element model of this structure, the latter model can be adjusted to give essentially the same structural deformations as the solid of revolution element model. These adjustments consist of changes in the thickness of the elements, and also

slight changes in the node ring geometry which establishes the middle surfaces of the conical shell elements.

Proceeding in this manner, a 328 element solid of revolution model, and a 28 conical shell element model were developed for the continuous structure. They are shown in Figures 5-6 and 5-3, respectively. Figures 5-4 and 5-5 compare the predicted axial and radial displacements of the final conical shell element model and the solid of revolution model. As can be seen, the conical shell element model adequately represents the deformation of the structure in the region of the joint. Figure 5-6 shows the undeformed solid of revolution model, the deformed shape due to the .010 inch enforced axial displacement, and an overlay of the deformed shape on the undeformed shape. Figure 5-7 shows this deformed configuration to an enlarged scale.

Having used the auxiliary problem to establish a conical shell element model which was representative of the structure in the region of the joint, this model was then extended to the desired three body diameters by adding four additional conical shell elements. These elements were located in the uniform shell region of the structure where the stress varies linearly across the thickness of the structure. Hence the model was still representative of the structure.

The conical shell element model was further extended to include provisions for representing the bolts connecting the spacer to the rocket motor. Since the bolts in the real structure are preloaded, the interface region of the bolts has a high localized stress in the radial direction, and can develop potentially large friction forces influencing the local relative motion of the rocket motor and spacer in the circumferential and axial directions. Explicit simulation of these effects is considered to be a difficult modeling task beyond the scope of this exploratory analysis. It was handled by removing the axisymmetric connector at node rings 13 and 14 of the model (cf. Figure 5-3) and representing the bolt and interface contact stiffness by discrete springs located at the circumferential locations of the bolts. These springs constrain corresponding points on node rings 13 and 14 in the radial, circumferential and axial directions. The localized contact between the spacer and rocket motor of the real structure caused by bolt preloads is not expected to be broken when the structure is deformed. Therefore, the spring rates were given arbitrarily large values, which in effect constrain the points of spring attachment on node rings 13 and 14 to move together.

Generally, when using conical shell elements, the resulting stiffness matrix is structured so that the coefficients of one harmonic are uncoupled from those of all other harmonics. This enables each harmonic to be solved for independently of all other harmonics. However, in the case of the radial shear joint, the introduction of the discrete attachment points results in coupling of the various harmonics. This plays an

important part in the investigation of solution convergence. The individual contributions of the non-zero harmonics change with the number of the highest order contributing harmonic considered in the analysis. Therefore, one can not consider an appropriate subset of the larger set of harmonics to determine how much of the solution is attributable to this subset. The solution must be computed separately for the subset to establish its contribution to the solution.

5.2 CORRELATION ANALYSIS

The bending compliances of the three, six, and nine bolt configurations were predicted for comparison with compliances determined from dynamic tests of the structure (cf Section 4). The analysis procedure was as follows. The deflection and slope due to a unit bending moment at station ten of the structure were first predicted using classical Bernoulli-Euler beam theory. In this case, the beam representing the structure is considered continuous at the joint location. The EI distribution of the ten inch long portion of the structure is shown in Figure 5-8. Following this, the corresponding deflections and slopes of the continuous fastener structure and the three, six, and nine bolt shear joint structure were predicted from the appropriate conical shell element models. In these cases, a unit bending moment was applied at the rocket motor end of the model. The number of degrees of freedom for each structural model representing the various shear bolt joint configurations varies with the number of Fourier series harmonics used in the analysis. Table 5-1 summarizes the degrees of freedom of the structural models representing the various bolt configurations analyzed. Figures 5-9 through 5-12 compare the computed deflections over the first ten inches of the finite element and classical beam models. The effective joint compliance for representation as a discrete rotational spring is the difference between the beam theory predicted slope and the finite element predicted slope at station 10. The compliance was therefore, computed by the expression:

$$ C_\theta = \left(\frac{\theta}{M}\right)_f - \left(\frac{\theta}{M}\right)_b $$

where

θ/M = structure slope at station 10 per unit applied bending moment

and subscripts f and b denote finite element analysis and beam analysis, respectively.

Since the structural deformations predicted by the finite element models depend on the number of Fourier series harmonics used in the analysis, the question of solution convergence becomes an important considera-

76

tion. Desirably, sufficient harmonics would be used to assure reasonable convergence. The three bolt shear joint model was used as a basis for exploring solution convergence characteristics. Joint compliance was predicted for this configuration using one, four, seven, and ten harmonics in the solution. The number of non-zero harmonics contributing to the solution for the joint compliance in these cases were one, three, five, and seven respectively. This information is summarized in Table 5-1, which includes similar data on the six and nine bolt fastener analyses. The graph of Figure 5-13 shows the behavior of the predicted bending compliance versus the number of harmonics used in the analysis. On first inspection, the solution appears to be converging to a reasonably close approximation (within 10%) of the compliance value determined for the test data in Section 4.0. In order to obtain more than a qualitative judgement on solution convergence, however, many additional harmonics would have to be included. An unfortunate shortcoming of the present NASTRAN code in using conical shell elements makes convergence testing very costly in computer time particularly as the number of joint fasteners increases.

If N is the order of the highest Fourier series harmonic of interest in the analysis, NASTRAN constructs the element stiffness matrix using all N harmonics. This consumes a large amount of computer time when N is large. Often, however, only certain of the harmonics contribute to the solution. In the case of the 18 fastener joint, for example, a solution comparable to that for the three fastener case involving seven participating harmonics would require 55 total harmonics in the present method of analysis. A considerable savings in computer operating expense could be realized if individual harmonics could be selected for use in constructing the stiffness matrix.

A second aspect of the present modeling approach introduces an additional problem in judging solution convergence. If one were able to consider an infinite number of harmonics in the analysis, the assumption of point loads associated with the joint fasteners would result in infinite stresses and displacements at their points of application. The predicted joint compliance would, therefore, diverge as the number of harmonics approaches infinity. More realistically, the model should incorporate attachment forces distributed over a small area. This area would represent the area of the localized normal and frictional forces developed at the joint interface due to the bolt preloads. This would avoid infinite displacements, and result in a convergence value for the predicted compliance when an infinite number of harmonics is considered. From a practical viewpoint, however, one can only consider a finite number of harmonics in the analysis. The resulting truncated Fourier series representations of the concentrated spring forces is in effect spread over some finite area, as it is in reality. It is probable that there is a large interval of harmonics, beyond some minimal order harmonic, in which the predicted joint compliance undergoes only slight changes in values. Beyond this interval, the predicted joint compliance would tend

to diverge. Within this interval, the predicted joint compliance would be expected to provide a reasonable approximation of the joint compliance. Additional study of predicted compliance versus number of harmonics would be required to establish this interval of pseudo convergence.

For the six and nine bolt configurations, seven and ten harmonics, respectively, were used in the analysis, providing only three participating harmonics in each case. The predicted bending compliances were 45% and 37%, respectively, below the average measured values. In these instances, more harmonics are clearly required to improve the answers. These data are summarized in Table 5-2 and Figure 5-14. Using the three bolt case as a guideline for these configurations, at least 19 and 28 harmonics, respectively, would have to be used in the analyses to expect a reasonable approximation. This estimate would give seven contributing harmonics for each configuration.

Aside from the question of convergence (which can be more realistically addressed after making some refinements in both the mathematical model and the analysis code), the important point to be made is that the predicted compliances are sufficiently close (even when only three contributing harmonics are used) to illustrate the power of finite element techniques in coping with grossly distorted load paths through airframe joints. The three fastener configuration in fact is believed to represent the most severe test of this modeling approach. Further study will hopefully show that refinements in representing the local interface contact region constitute second order considerations and therefore will not demand more precise analysis.

Table 5-1

NUMBER OF HARMONICS AND DEGREES OF FREEDOM
FOR THE SHELL ELEMENT MODELS

Number of Fasteners	Highest Harmonic Used	Contributing Harmonics	Degrees of Freedom
3	1	1	167
3	4	1, 2, 4	501
3	7	1, 2, 4, 5, 7	835
3	10	1, 2, 4, 5, 7, 8, 10	1169
6	7	1, 5, 7	501
9	10	1, 8, 10	501

Table 5-2

SUMMARY OF EXPERIMENTAL AND PREDICTED
JOINT COMPLIANCES

Number of Bolts	Avg. Measured Compliance $\times 10^8$, Rad/In-Lb	Predicted Compliance $\times 10^8$, Rad/In-Lb Participating Harmonics Considered		
		3	5	7
3	2.79	1.73	2.27	2.54
6	1.03	0.562	- -	- -
9	0.594	0.377	- -	- -

FIGURE 5-1

SHEAR BOLT JOINT

BOLT PATTERNS ANALYZED WITH FINITE ELEMENTS

A-A IS A PLANE OF SYMMETRY

3 BOLTS
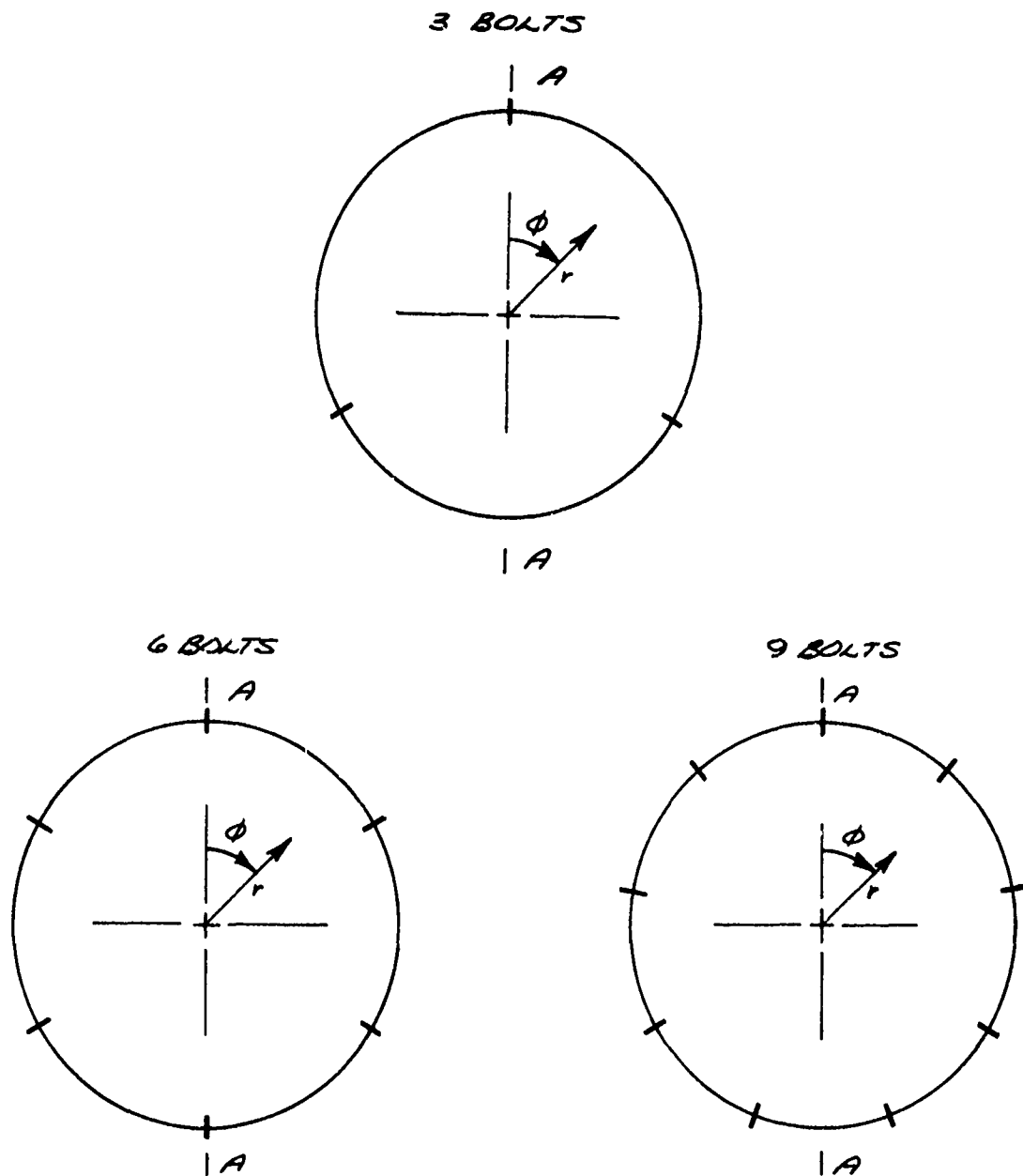

6 BOLTS

9 BOLTS

FIGURE 5-2

SHEAR BOLT JOINT

TEST SPECIMEN AND SECTION MODELED USING FINITE ELEMENTS
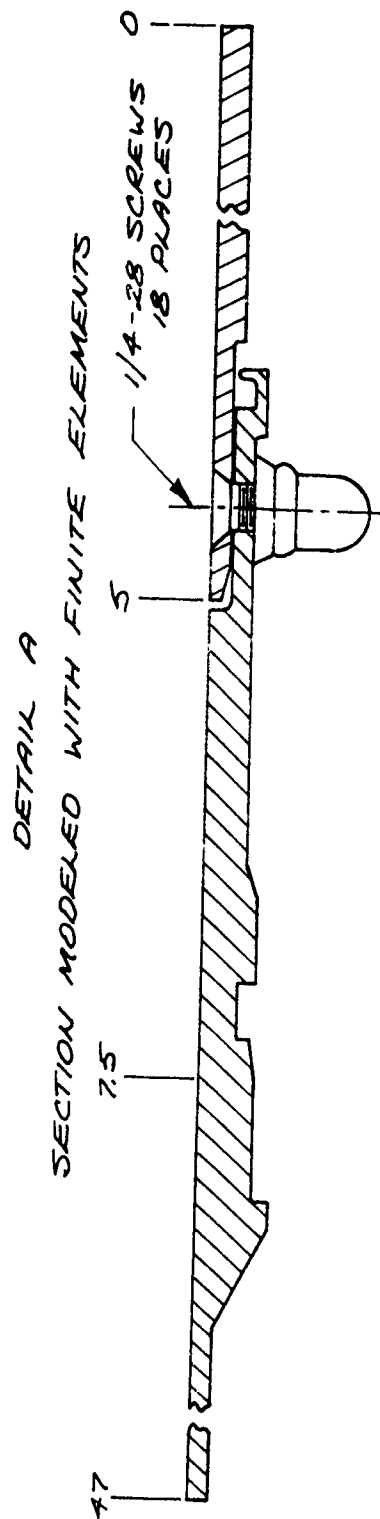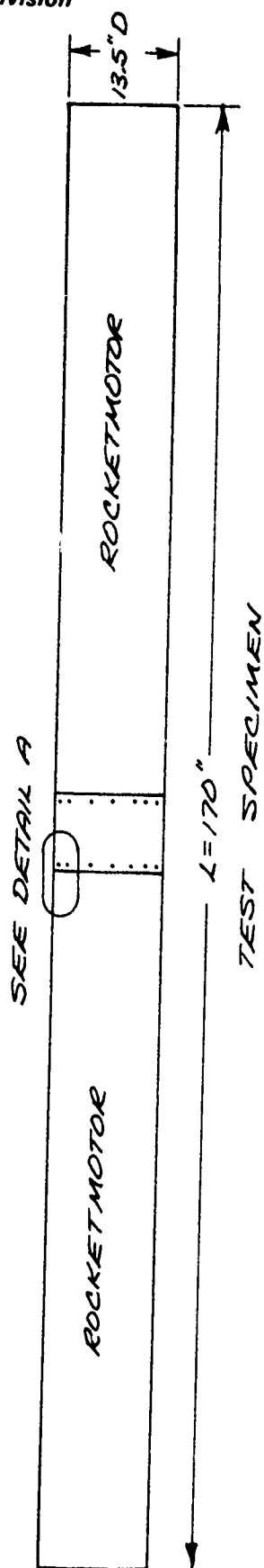
FIGURE 5-3

SHELL ELEMENT MODEL IN THE REGION OF THE
SHEAR BOLT JOINT

82
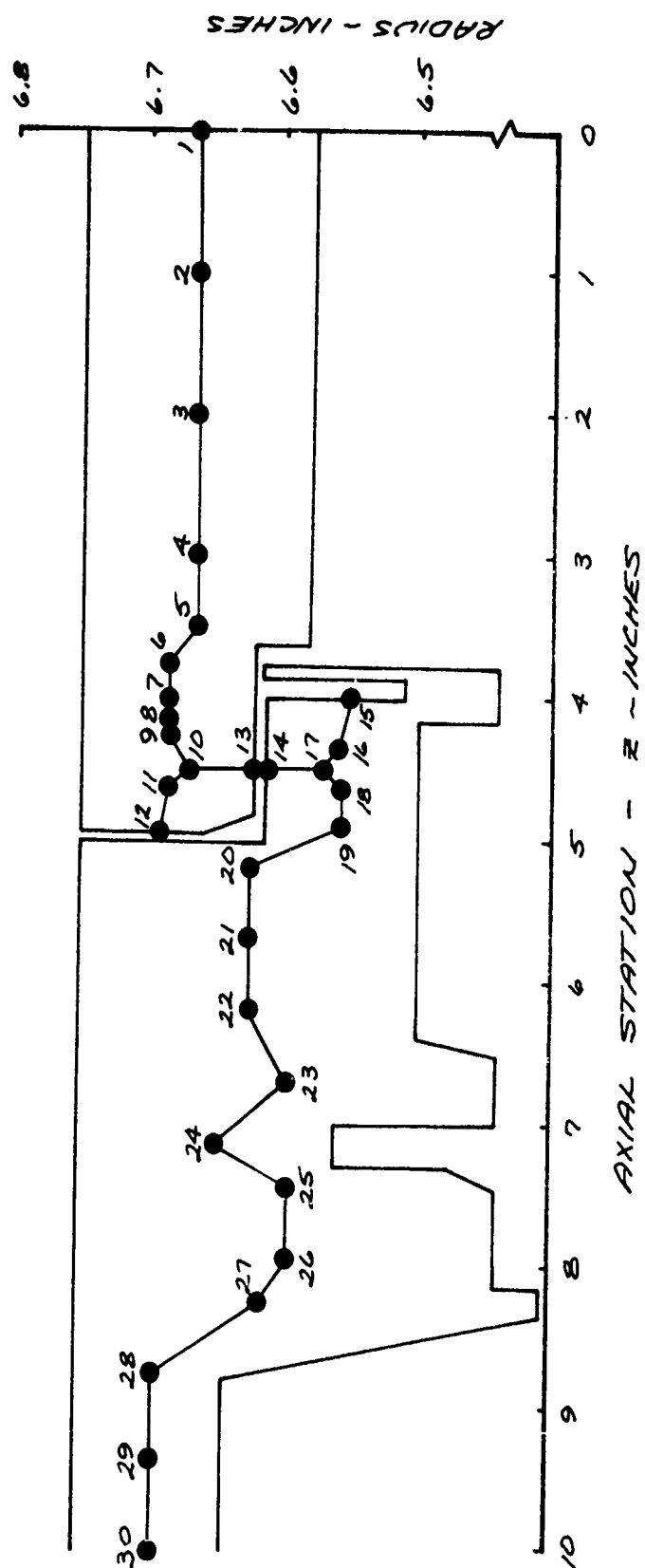
FIGURE 5-4

COMPARISON OF AXIAL DEFLECTIONS
FOR AN ENFORCED AXIAL DISPLACEMENT AT STATION 10
FOR THE SOLID AND SHELL ELEMENT MODELS
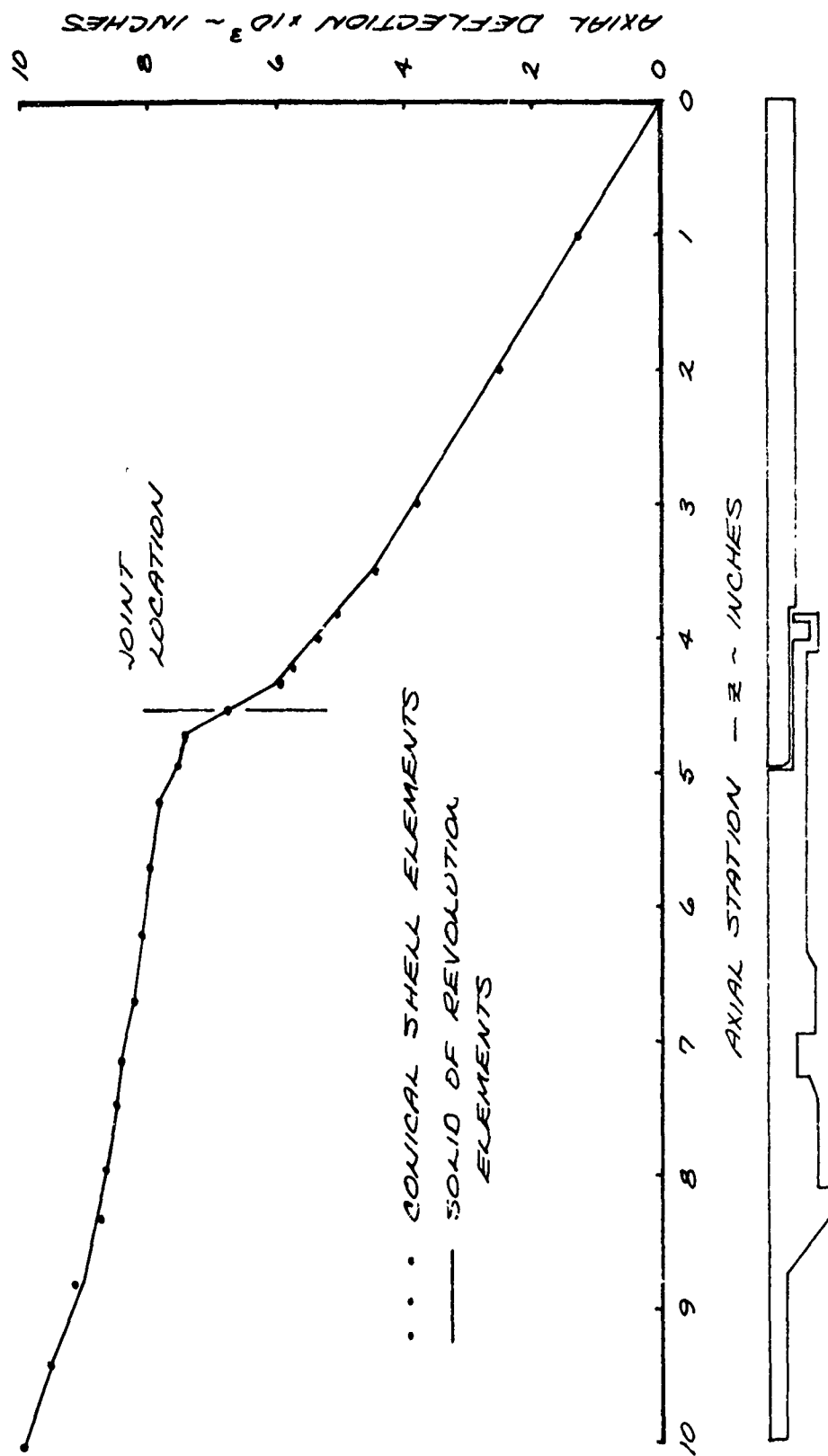
FIGURE 5-5

COMPARISON OF RADIAL DEFLECTIONS
FOR AN ENFORCED AXIAL DISPLACEMENT AT STATION 10
FOR THE SOLID AND SHELL ELEMENT MODELS
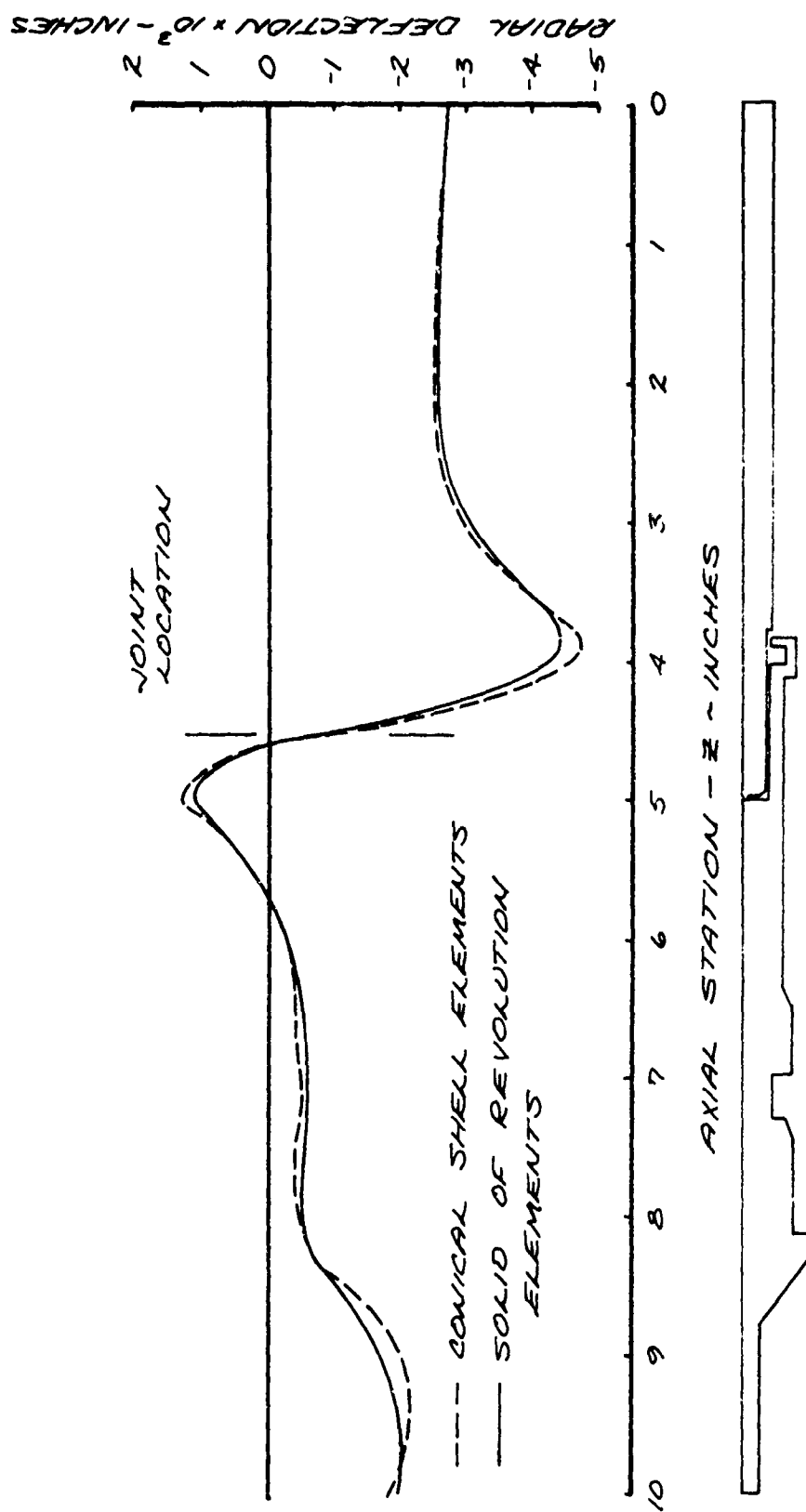
FIGURE 5-6

PLOTS OF THE

TOTAL SOLID ELEMENT MODEL

UNDEFORMED

DEFORMED

DEFORMED
PLUS
UNDEFORMED

85

FIGURE 5-7

PLOTS OF PORTIONS OF THE SOLID ELEMENT MODEL

FIGURE 5-7 (CONT.)

STA. 6.5

STA. 8.3

STA. 8.3

STA. 10.0

87
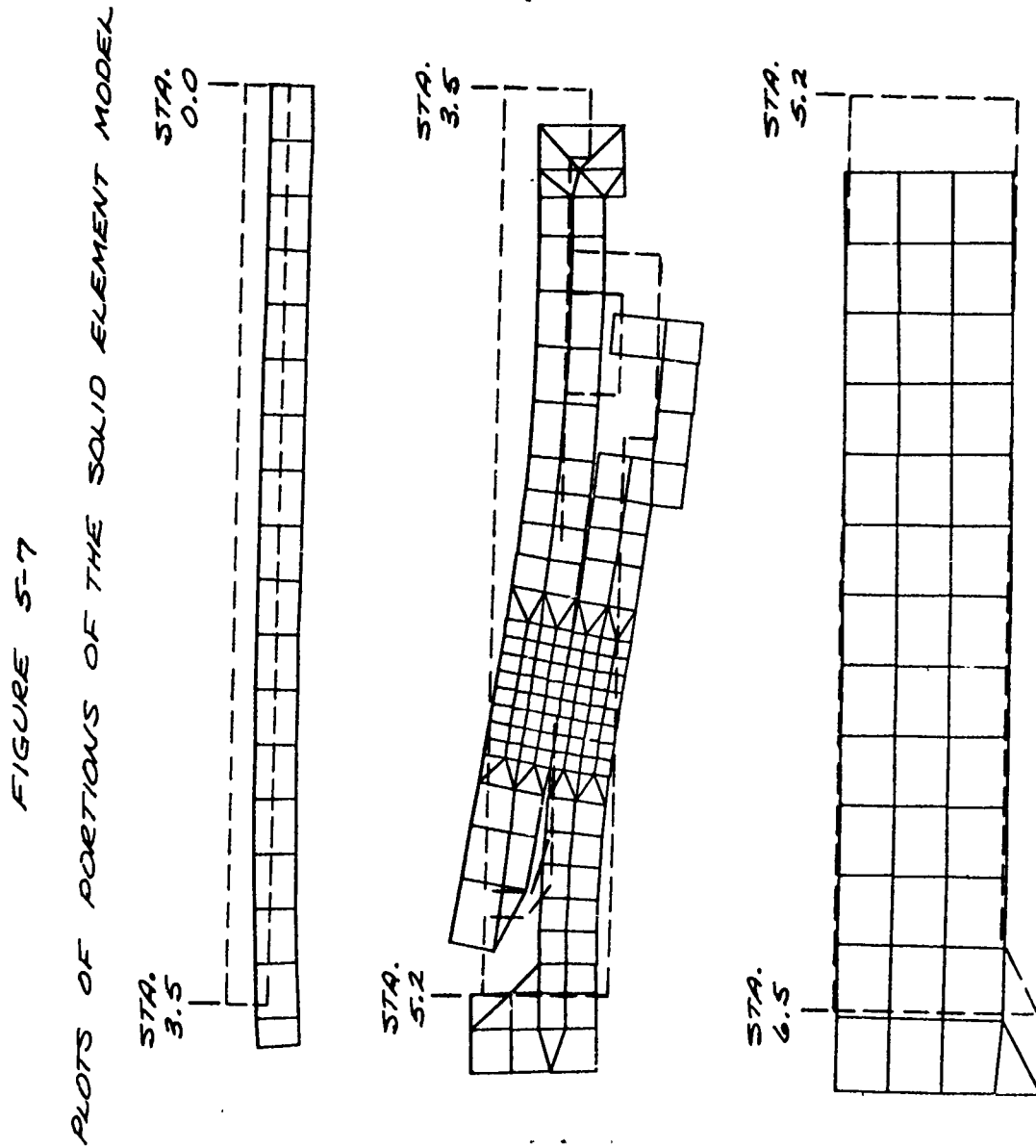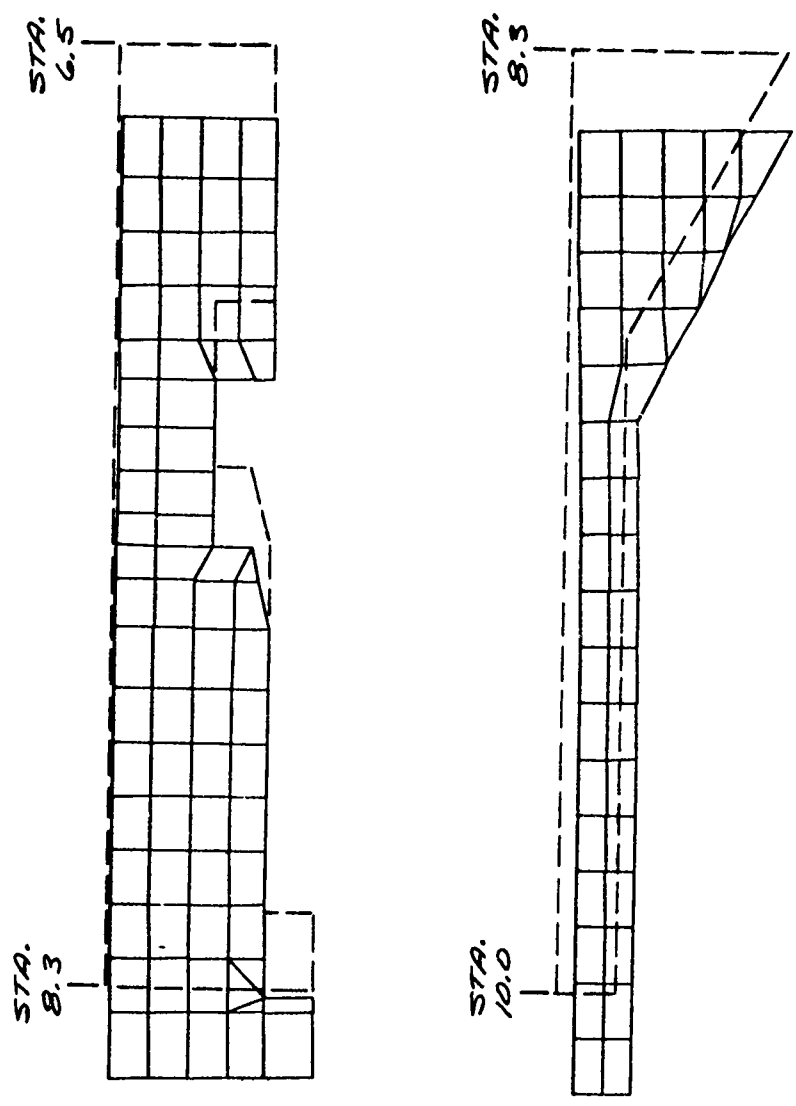
FIGURE 5-8

BEAM REPRESENTATION OF STRUCTURE
NEAR THE SHEAR BOLT JOINT

AXIAL STATION - Z ~ INCHES
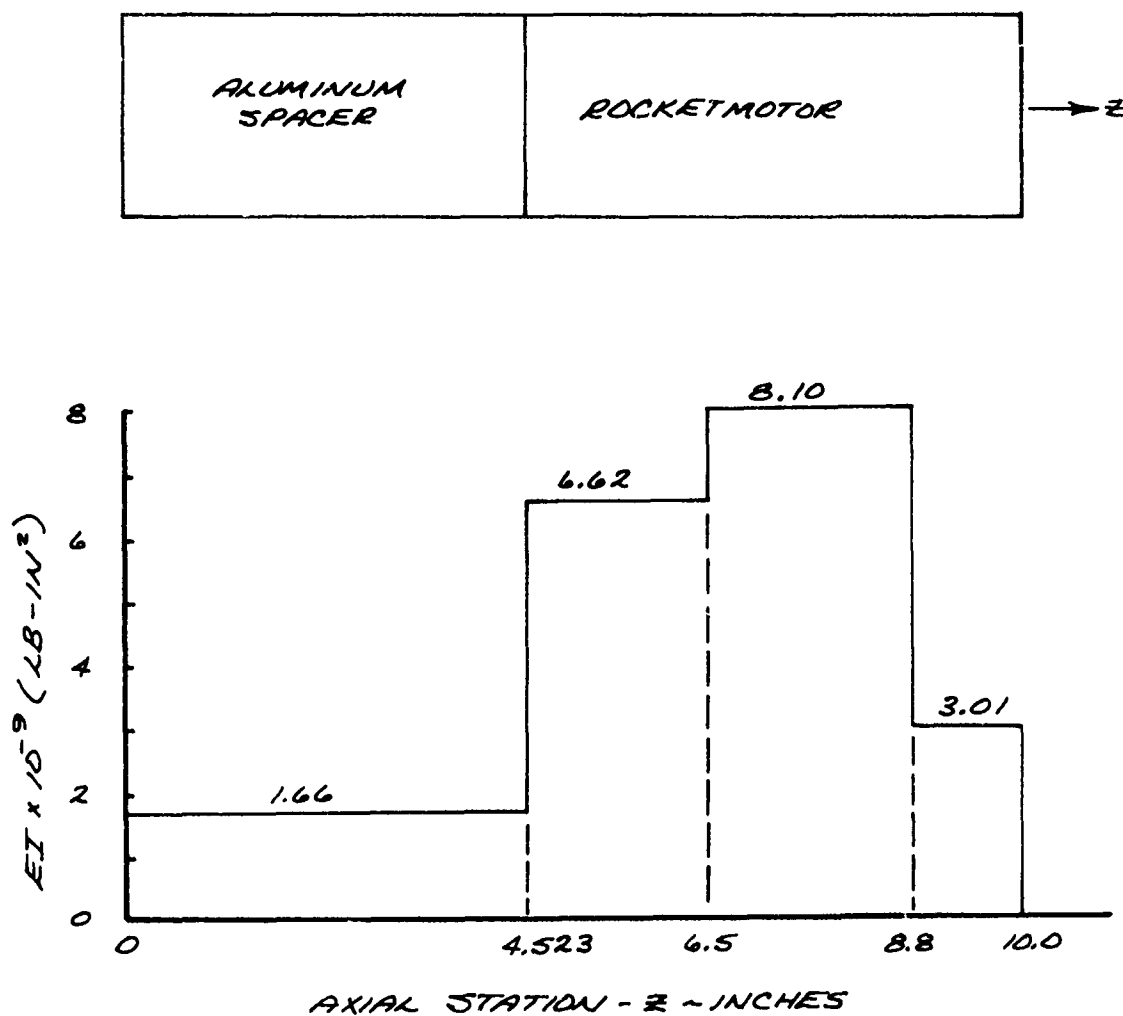
FIGURE 5-9

CONTINUOUS STRUCTURE SHEAR BOLT JOINT
FINITE ELEMENT MODEL VS. BEAM THEORY
BENDING DEFLECTIONS

$C_\phi = 0.070 \times 10^{-8}$ RAD/IN-LB

FINITE ELEMENT MODEL

BEAM THEORY

TANGENTIAL DEFLECTION AT $\phi = 90°$ PER UNIT MOMENT $\times 10^8 \sim$ IN/IN-LB

AXIAL STATION - Z ~ INCHES

89
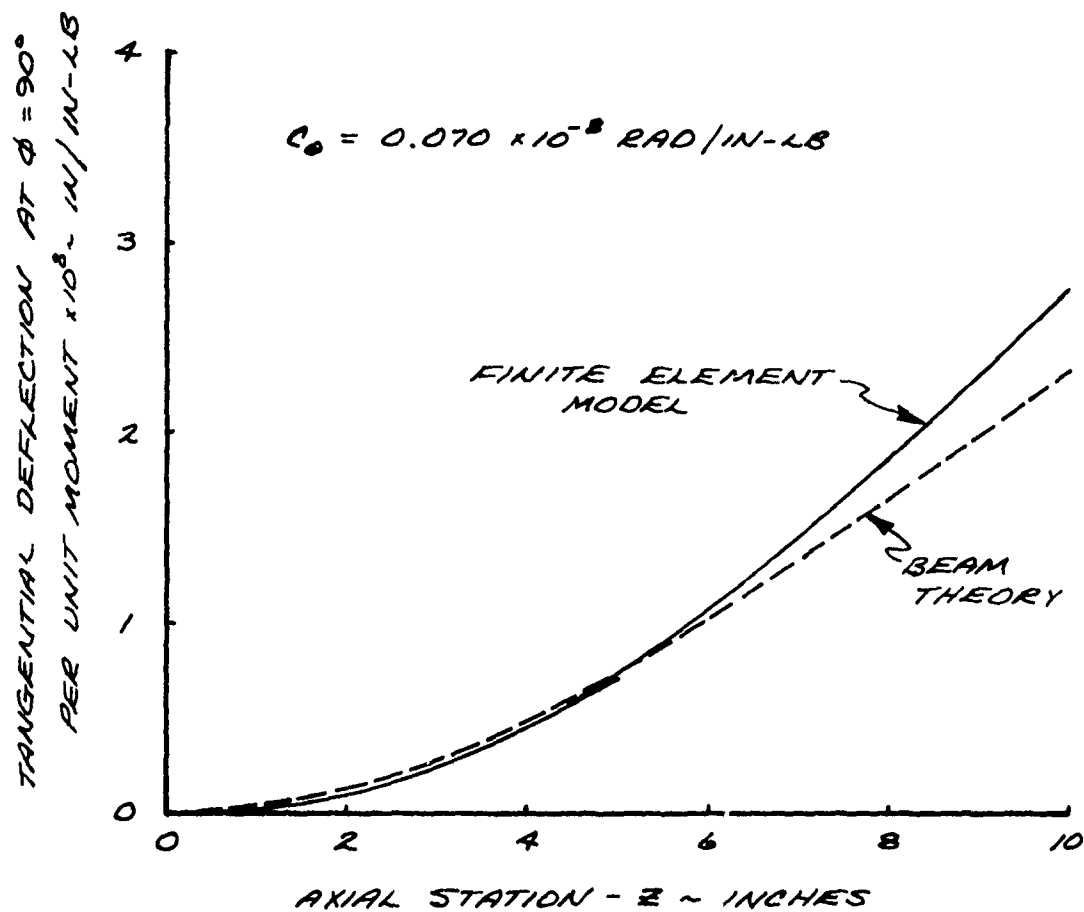
FIGURE 5-10

NINE FASTENER SHEAR BOLT JOINT
FINITE ELEMENT MODEL VS. BEAM THEORY
BENDING DEFLECTIONS

$$C_\theta = 0.377 (10)^{-3} \; RAD/IN\text{-}LB$$

FINITE ELEMENT
MODEL

BEAM
THEORY
(NO JOINT)

(Y-axis) TANGENTIAL DEFLECTION AT $\phi = 90°$ PER UNIT MOMENT $\times 10^8$ ~ IN/IN-LB

(X-axis) AXIAL STATION - Z ~ INCHES

90
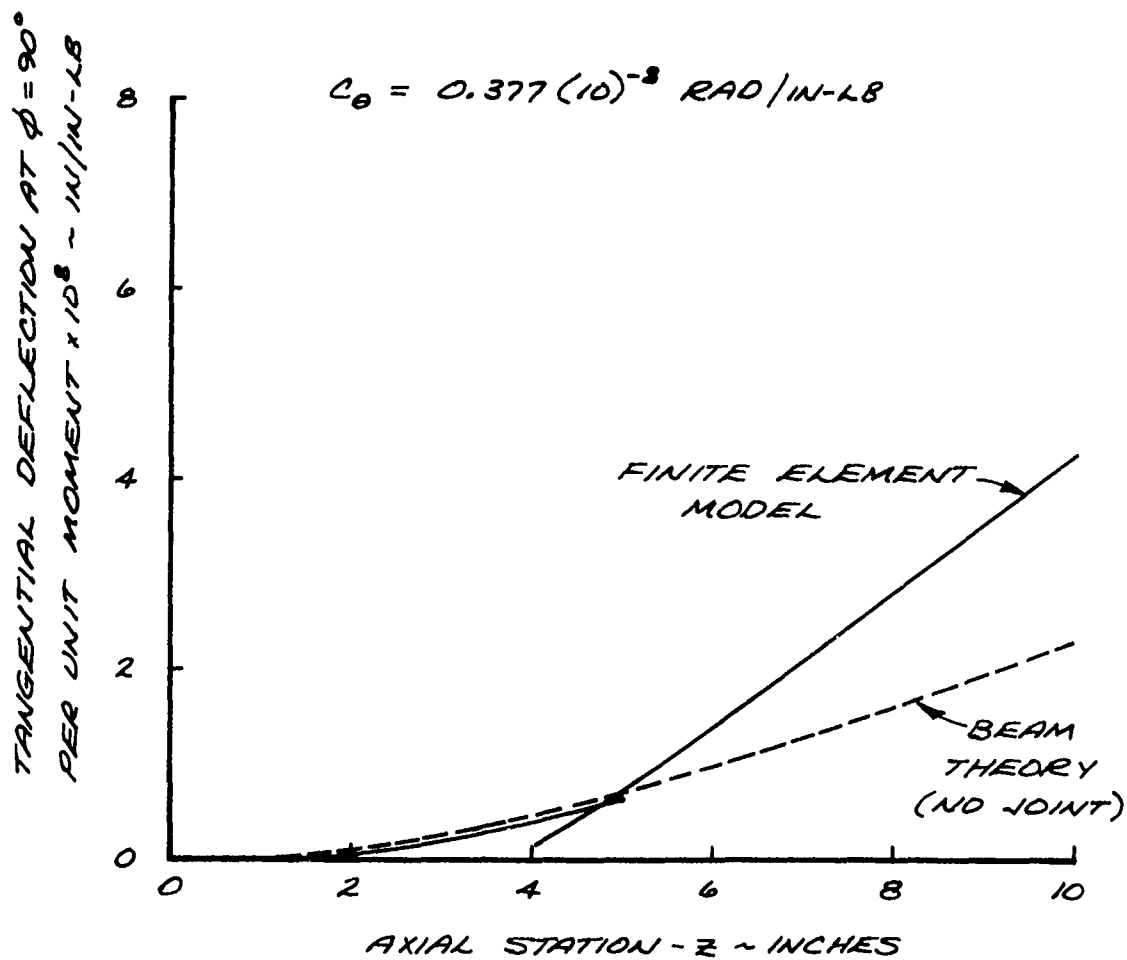
FIGURE 5-11

SIX FASTENER SHEAR BOLT JOINT
FINITE ELEMENT MODEL VS. BEAM THEORY
BENDING DEFLECTIONS

$$C_\theta = 0.562(10)^{-8} \ RAD/IN\text{-}LB$$

91
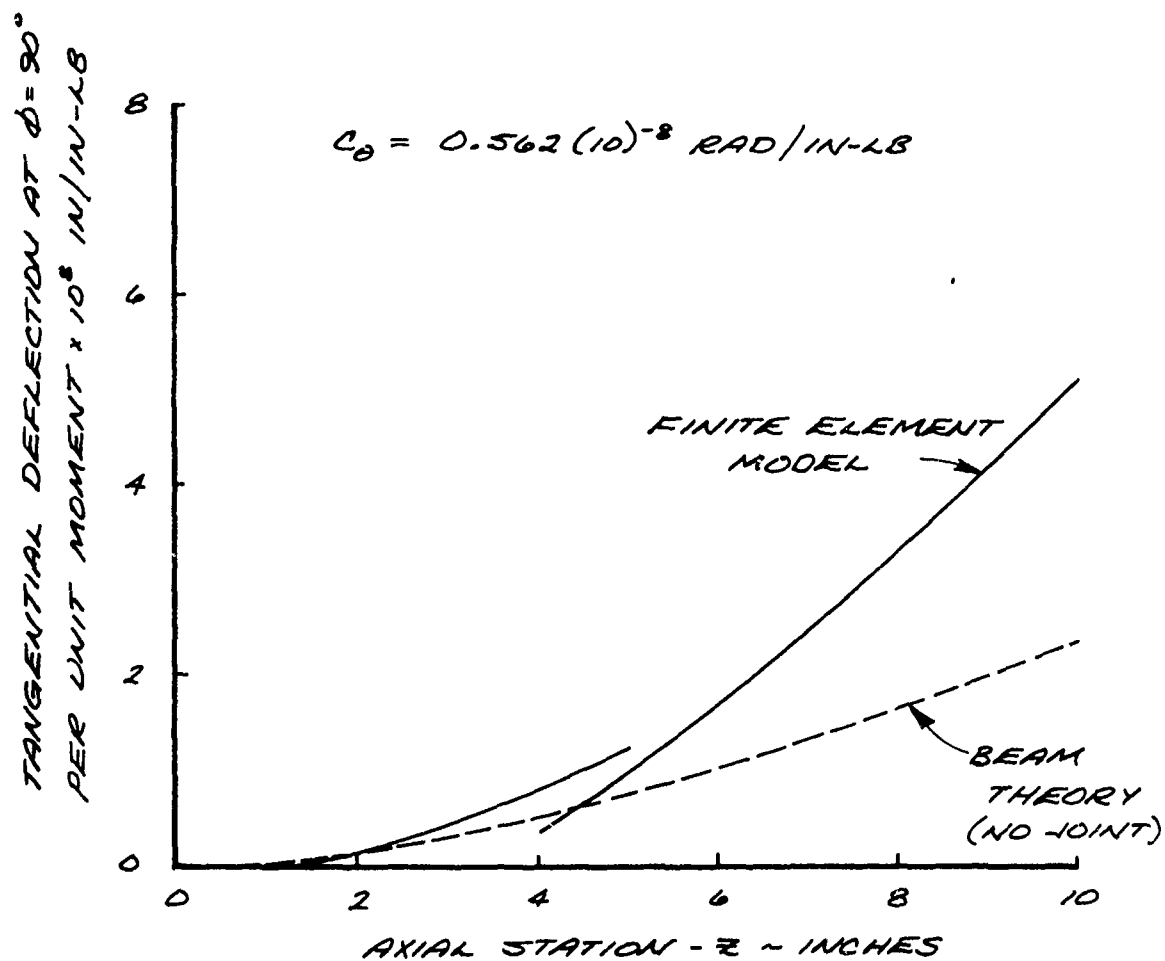
FIGURE 5-12

THREE FASTENER SHEAR BOLT JOINT
FINITE ELEMENT MODEL VS. BEAM THEORY
BENDING DEFLECTIONS

$$C_\theta = 2.54 (10)^{-8} \text{ RAD}/\text{IN-LB}$$

FINITE ELEMENT MODEL

BEAM THEORY (NO JOINT)

92
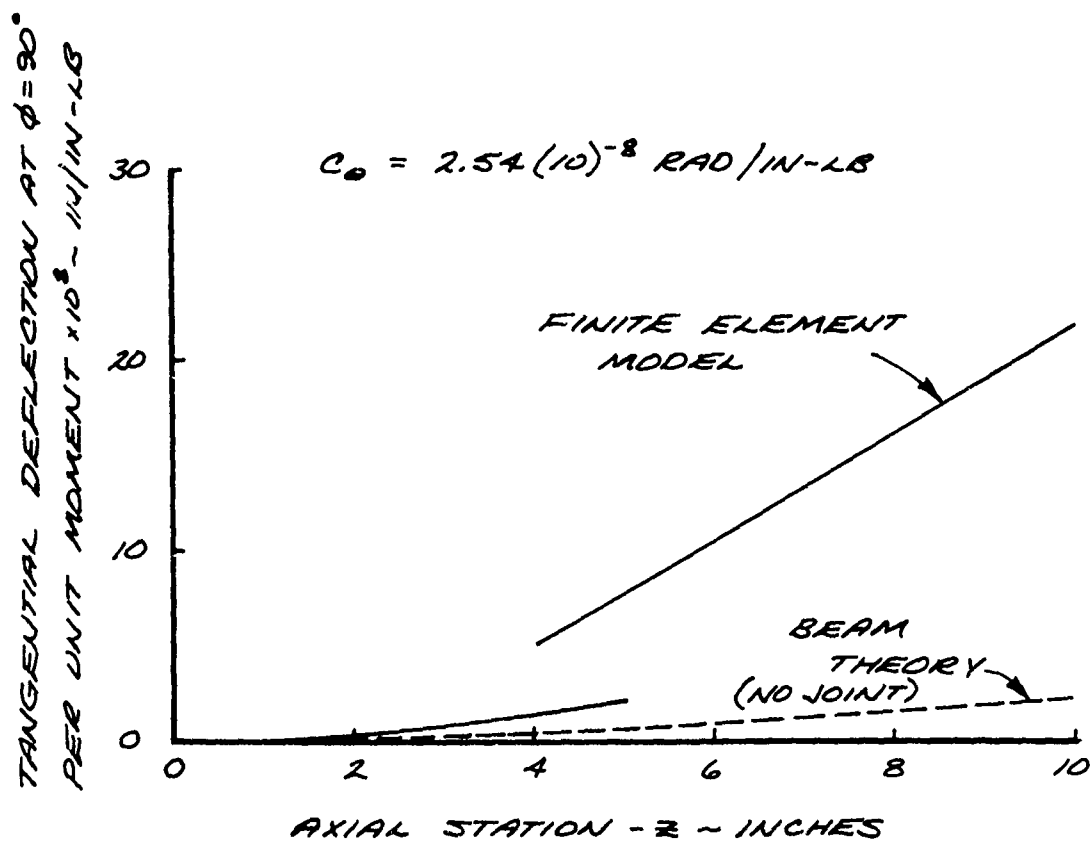
FIGURE 5-13

JOINT COMPLIANCE CONVERGENCE FOR THREE BOLT
FINITE ELEMENT MODEL
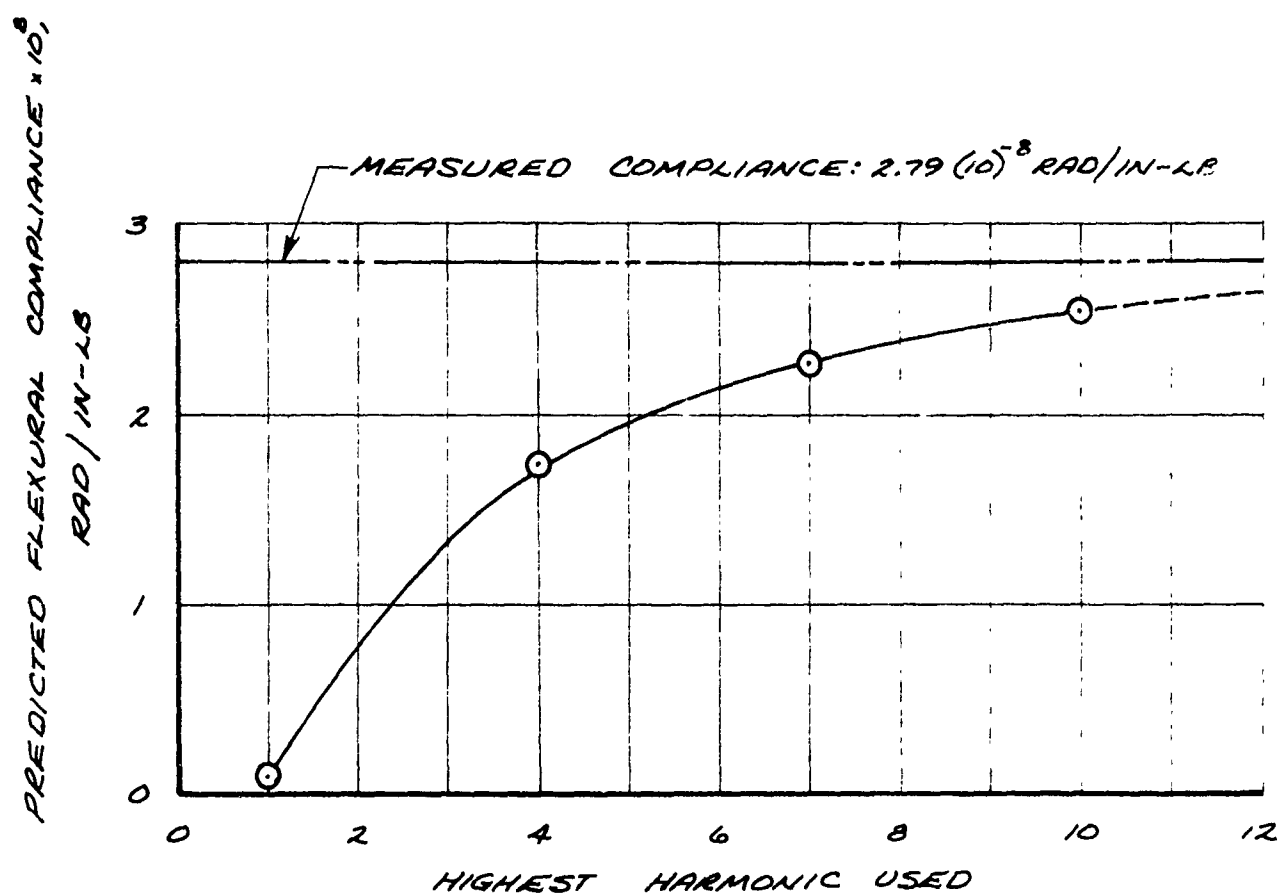
FIGURE 5-14

COMPARISON OF EXPERIMENTAL AND PREDICTED JOINT COMPLIANCES

O   TEST DATA

$\square_i$ FINITE ELEMENT ANALYSIS

i NUMBER OF PARTICIPATING HARMONICS

Section 6.0

CONCLUSIONS

In reviewing the results of Phase 2, the Data Acquisition and Analysis Extension Phase", the major points are the following.

(1) The joint compliance extraction technique, which has been extended using the formulation of Reference 3, is now a powerful and versatile elastic mode data reduction tool. All of the significant restrictions and limitations of the original method have now been removed.

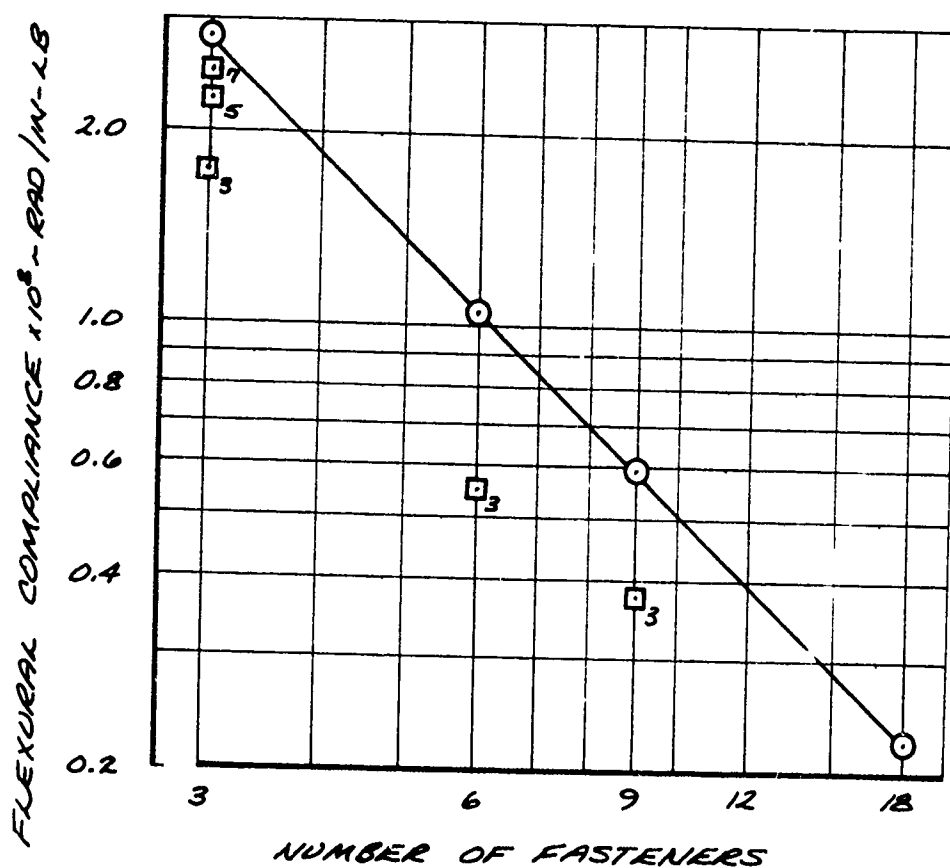(2) A test method designed to isolate the structural dynamic characteristics of joints using full scale actual missile joint hardware has been designed and implemented. Th. test method increases the resolutions of the desired data by minimizing the uncertainties.

(3) Empirically derived flexural joint compliances are determined for seven different tactical missile joints and for five variations of one of the joints using the joint compliance extraction technique.

(4) Comparison of the empirically derived flexural joint compliances with the estimates obtained in the Phase 1 study (Reference 7) show good agreement for the threaded coupling and Marmon clamp joints and significant differe ces for the shear bolt, continuous land ring and tension b it joints.

(5) An exploratory analysis has shown that finite element methods can be useful in predicting compliance values for missile airframe joints.

(6) The finite element analysis has demonstrated analytically that the number of load paths and their spacing around the periphery of the joint are the determining parameters in joint compliance.

The next phase of this study, identified as "Phase 3, Methods Confirmation and Documentation Phase" is directed at accomplishing the following objectives.

(1) Extend the finite element modeling techniques developed during Phases 1 and 2 to model joints in a more cost effective manner.

95

(2) Perform modifications to the joint compliance extraction technique digital computer code to improve its convergence characteristics and to facilitate its application to experimental data.

(3) Prepare a user's manual for tne joint compliance extraction code to facilitate its distribution to and application by interested government and industry users.

(4) Model the joint interface impact phenomena which acts as a vibration source under certain conditions, develop an approach to reducing the vibration source and illustrate the approach in a limited laboratory evaluation program.

(5) Develop a rating system for the structural dynamic properties of commonly used tactical missile airframe joints and integrate the ratings into overall system requirements.

(6) Prepare a final report which will summarize the findings of the Phase 3 study and also provide an overview of the Phase 1, 2 and 3 studies.

REFERENCES

1. Alley, Jr., V. L. and Leadbetter, S. A., "The Prediction and Measurement of Natural Vibrations on Multistage Launch Vehicles", American Rocket Society Launch Vehicles: Structures and Materials Conference Report, April 1962.

2. Fox, R. L. and Kapoor, M. P., "Rates of Change of Eigenvalues and Eigenvectors", AIAA Journal, Vol. 6, Number 12, December 1968, p. 2426.

3. Hall, B. M., Calkin, E. D. and Sholar, M. S., "Linear Estimation of Structural Parameters from Dynamic Test Data", AIAA/ASME 11th Structures, Structural Dynamics, and Materials Conference, Denver, Colorado, April 22-24, 1970.

4. Householder, A. S., Principles of Numerical Analysis, McGraw-Hill; New York, 1953.

5. Jeter, E. L., "A Dynamic Study of the Sidewinder and Chaparral Motor Joint", Naval Weapons Center, China Lake, California, TN 4062-57, February 1971.

6. MacNeal, R. H., The NASTRAN Theoretical Manual, NASA, Washington D. C., 1970.

7. Maloney, J. G., Shelton, M. T., and Underhill, D. A., "Structural Dynamic Properties of Tactical Missile Joints - Phase I", General Dynamics, Pomona Division Report No. CR-6-348-945-001, June 1970.

8. McCormick, C. W., The NASTRAN User's Manual, NASA, Washington D. C., 1970.

9. McIntyre, K. L., "Modified Holzer-Myklestad Modal Analysis Final Report - CWA 245", General Dynamics/Pomona TM-348-15.1-3, July 24, 1961.

DISTRIBUTION

Naval Air Systems Command
Department of the Navy   2 copies
Washington, D. C.   20360
Code AIR-530214

Naval Air Systems Command
Department of the Navy   1 copy
Washington, D. C.   20360
Code AIR-53042B

Naval Air Systems Command
Department of the Navy   1 co,
Washington, D. C.   20360
Code AIR-320B

Naval Air Systems Command
Department of the Navy   14 copies
Washington, D. C.   20360
Code AIR-6041A

Commanding Officer
Naval Air Development Center   1 copy
Aeromechanics Department, Code AMFC
Warminster, Pennsylvania   18974

Commander, Naval Weapons Center
Aeromechanics Division, Code 4062   1 copy
China Lake, California   93555

Applied Physics Laboratory
The Johns Hopkins University   1 copy
8621 Georgia Avenue
Silver Spring, Maryland   20910
Attn: Mr. A. J. Bell

Bell Aerosystems Corporation
P. O. Box 1   1 copy
Buffalo, New York   14240
Attn: Mr. G. C. C. Smith

The Martin Company
Space Programs Division   1 copy
Baltimore, Maryland   21203
Attn: Mr. J. M. Hedgepeth

DISTRIBUTION - Cont'd.

North American Rockwell Corporation   1 copy
4300 E. Fifth Avenue
Columbus, Ohio 43219
Attn: Mr. L. Kazmerzak

Fairchild-Hiller Corporation   1 copy
Republic Aviation Division
Farmingdale, Long Island, New York 11735
Attn: Mr. S. Rabinowitz

National Aeronautics and Space Administration 1 copy
Langley Research Center
Hampton, Virginia 23365
Attn: Mr. I. E. Garrick

National Aeronautics and Space Administration 1 copy
George C. Marshall Space Flight Center
Huntsville, Alabama 35812

Air Force Flight Dynamics Laboratory   1 copy
Air Force Systems Command
Wright-Patterson Air Force Base, Ohio 45433

Chief, Office of Naval Research   1 copy
Washington, D. C. 20360

Commanding Officer   1 copy
Naval Ordnance Laboratory
White Oak, Silver Spring, Maryland 20903

Aerospace Corporation   1 copy
2400 E. El Segundo Blvd.
El Segundo, California 90245
Attn: Dr. E Fleming

Aeronutronic Division, Philco-Ford   1 copy
Ford Road
Newport Beach, California 92705
Attn: Mr. H. M. Marshall

Grumman Aerospace Corporation   1 copy
Bethpage, New York 11714
Attn: Mr. E. F. Baird

DISTRIBUTION - Cont'd.

Vought Aeronautics Division   1 copy
LTV Aerospace Corporation
P. O. Box 5907
Dallas, Texas 75222
Attn: Mr. A. L. Head, Jr.

General Dynamics Corporation   1 copy
P. O. Box 748
Fort Worth, Texas 76101
Attn: Mr. L. E. Wilson

Lockheed-Georgia Company   1 copy
Marietta, Georgia 30060
Attn: Mr. L. A. Tolve

The Boeing Company   1 copy
P. O. Box 707
Renton, Washington 98055
Attn: Mr. L. J. Topp

McDonnell Douglas Astronautics Corporation   1 copy
Western Division
Santa Monica, California 90406
Attn: Mr. B. M. Hall

Federal Aviation Agency   1 copy
800 Independence Avenue, S.W.
Washington, D. C. 20590
Attn: Mr. R. Rosenbaum

Martin Marietta   1 copy
P. O. Box 179
Denver, Colorado 80201
Attn: Mr. G. Morosow

Lockheed-California Company   1 copy
P. O. Box 551
Burbank, California 91503
Attn: Mr. H. J. Hassig

McDonnell Douglas Corporation   1 copy
McDonnell Company
P. O. Box 516
St. Louis, Missouri 63166
Attn: Mr. C. H. Perisho

DISTRIBUTION—Cont'd.

Stanford University Menlo Park, California 94025 Attn: Mr. Holt Ashly	1 copy
McDonnell Douglas Corporation Douglas Airplane Division Long Beach, California 90801 Attn: Mr. R. Stringham	1 copy
General Dynamics Corporation CONVAIR Division San Diego, California 92112 Attn: Mr. R. E. Martin	1 copy
Lockheed-California Company P. O. Box 551 Burbank, California 91503 Attn: Mr. A. Messina	1 copy
Martin Marietta Corporation P. O. Box 5837 Orlando, Florida 32805 Attn: Mr. G. Fotieo	1 copy
Sikorsky Aircraft Division United Aircraft Corporation Stratford, Connecticut 06602	1 copy
Vertol Division The Boeing Company P. O. Box 16858 Philadelphia, Pennsylvania 19142	1 copy
Bell Helicopter Company P. O. Box 482 Fort Worth, Texas 76101	1 copy
Kaman Aircraft Division Kaman Corporation Old Windsor Road Bloomfield, Connecticut 06002	1 copy

101

DISTRIBUTION—Cont'd

Hughes Aircraft Company   1 copy
Missile Systems Division, Aerospace Group
Canoga Park, California   91304
Attn: Mr. R. Oedy

Raytheon Company   1 copy
Missile Systems Division, Lowell Plant
P. O. Box 740
Lowell, Massachusetts   01853

DOCUMENT CONTROL DATA - R & D

Security classification of title, body of abstract and indexing annotation must be entered when the overall report is classified

1. ORIGINATING ACTIVITY (Corporate author)	2a. REPORT SECURITY CLASSIFICATION
Electro Dynamic Division of General Dynamics Inc.	UNCLASSIFIED
1675 W. Mission Boulevard	2b. GROUP
Pomona, California 91766	

3. REPORT TITLE

Structural Dynamic Properties of Tactical Missile Joints - Phase 2

4. DESCRIPTIVE NOTES (Type of report and inclusive dates)

Final (June 1970 thru August 1971)

5. AUTHOR(S) (First name, middle initial, last name)

John G. Shelton

6. REPORT DATE	7a. TOTAL NO. OF PAGES	7b. NO. OF REFS
September 1971	112	9

8a. CONTRACT OR GRANT NO.	9a. ORIGINATOR'S REPORT NUMBER(S)
N00019-70-C-0296	CR-6-348-945-002
b. PROJECT NO	
c.	9b. OTHER REPORT NO(S) (Any other numbers that may be assigned this report)
d.	AIR-5306 14

10. DISTRIBUTION STATEMENT

Approved for public release, distribution unlimited

11. SUPPLEMENTARY NOTES	12. SPONSORING MILITARY ACTIVITY
	Naval Air Systems Command
	Department of the Navy
	Washington, D. C. 20360

13. ABSTRACT

The work performed and the results accomplished during the second phase of a study of the structural dynamic properties of tactical missile joints are presented in this report. The method of extracting joint compliances from missile dynamic test data evaluated in the Phase 1 study (CR-6-348-945-001) was extended and the major restrictions were overcome during the Phase 2 effort. A vibration test program was performed to determine structural dynamic characteristics of several actual tactical missile joints, with the unknowns in the test being minimized to improve the quality of the data obtained. The joint compliance extraction technique was then used to obtain joint compliance information from the measured modal data. Also an investigation was performed which demonstrates the possibility of predicting mechanical joint properties using finite element methods. In addition, the finite element analyses also demonstrated analytically that the number of load paths and their spacing around the circumference of a joint are major factors in determining joint compliance.

KEY WORDS	LINK A		LINK B		LINK C	
	ROLE	WT	ROLE	WT	ROLE	WT
Tactical Missile Joints						
Dynamics of Joints						
Joint Compliance						
Joint Damping						
Joint Stiffness						
Finite Element Applications						